Volume 7 No 1, June 2024

CHEESA

Chemical Engineering Research Articles

a scientific journal that publishes articles in the field of Chemical Engineering, and Chemistry

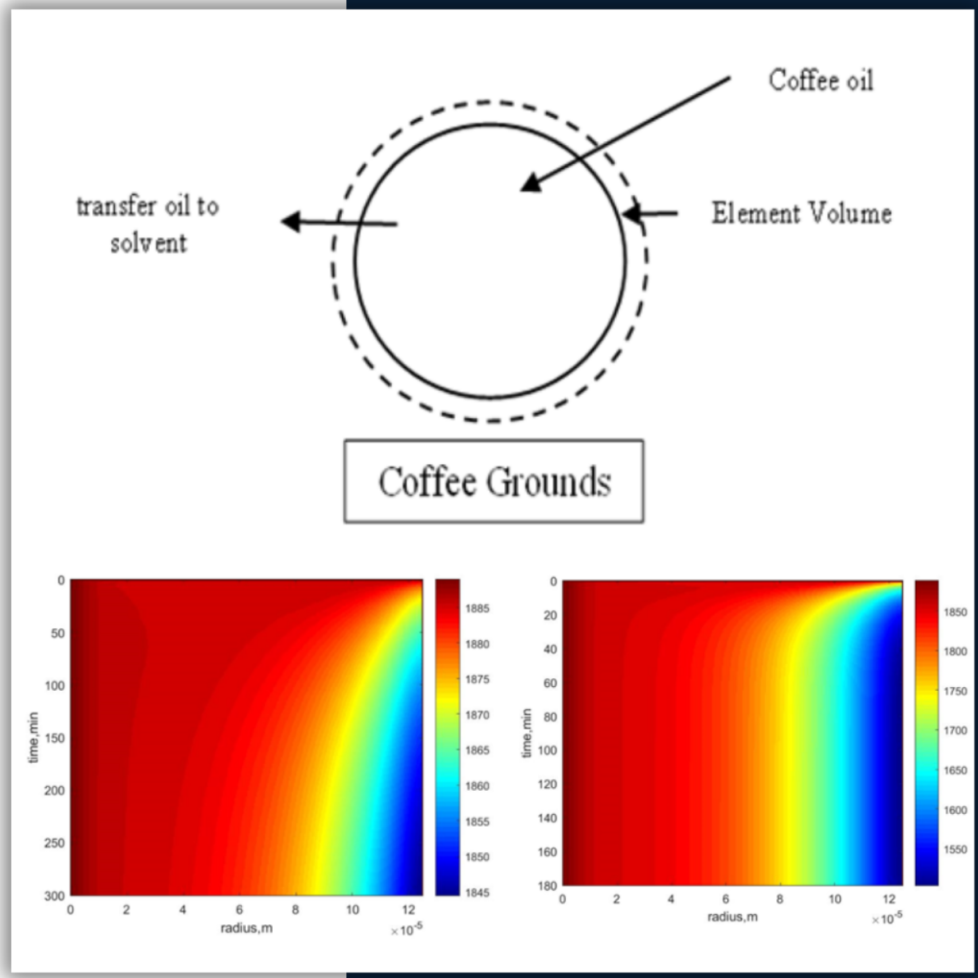

Coffee Oil Extraction (Mustikaningrum, et al)

E-ISSN: 2615-2347
P-ISSN: 2614-8757

EDITORIAL BOARD

CHEESA: Chemical Engineering Research Articles

Volume 7 No 1, 2024

ISSN 2614-8757 (Print), ISSN 2615-2347 (Online)

Available online at: http://e-journal.unipma.ac.id/index.php/cheesa

ACKNOWLEDGMENT

CHEESA: Chemical Engineering Research Articles

Our highest gratitude and appreciation go to the reviewers who have reviewed the submitted manuscripts and provided suggestions to us. The reviewers who contributed to this issue are,

1. Prof. Dr. Teuku Nanda Saifullah Sulaiman
2. Prof. Johnner P. Sitompul, Ph.D
3. Prof. Husni Husin
4. Prof. Dr. Poedji Loekitowati Hariani
5. Prof. Dr. Yantus A.B. Neolaka
6. Muammar Fawwaz, Ph.D
7. Ronny Purwadi, Ph.D
8. Dr. Eng. Dewi Agustina Iryani
9. Dr. Salfauqi Nurman
10. Dr. Maryudi
11. Dr. Zuhdi Ma'sum
12. Dr. Rahmat Basuki
13. Dr. Agus Budianto
14. Dr. apt. Rahmi Annisa
15. Rokiy Alfanaar
16. Wahyu Prasetyo Utomo

with the seriousness and thoroughness of the reviewers, help us to improve a quality and maintain the quality of writing in the CHEESA: Chemical Engineering Research Articles Volume 7 No 1, June 2024.

Our thanks also go to the various parties who have helped, so that this edition can be published online according to the specified time.

Editorial
CHEESA

Volume 7 No 1, 2024

ISSN 2614-8757 (Print), ISSN 2615-2347 (Online)

Available online at: http://e-journal.unipma.ac.id/index.php/cheesa

TABLE OF CONTENTS

CHEESA: Chemical Engineering Research Articles

CHEESA is a journal that becomes a media of study for chemical and chemical engineering. This journal serves as a media for publication of research in chemistry and chemical engineering aimed at academics, practitioners and community at large. Articles that were published in the CHEESA Journal have gone through editing according to established rules without changing the original manuscript.

Research Articles

Review Articles

Volume 7 No 1, 2024

ISSN 2614-8757 (Print), ISSN 2615-2347 (Online) Available online at: http://e-journal.unipma.ac.id/index.php/cheesa

CHEESA: Chemical Engineering Research Articles
ISSN 2614-8757 (Print), ISSN 2615-2347 (Online)
Available online at: http://e-journal.unipma.ac.id/index.php/cheesa

Research Article

Pinch-Exergy Approach to Enhance Sulphitation Process Efficiency in Sugar Manufacturing

Pendekatan Pinch-Eksergi sebagai Peningkatan Efisiensi Proses Sulfitasi di Pabrik Gula

Indra Riadi[1)], Johnner Sitompul[1*)], Hyung Woo Lee[2)]

[1)]Institut Teknologi Bandung, Department of Chemical Engineering, Indonesia
[2)]Research Institute of Sustainable Technology & Innovation (RISTI)
4F, 51, Yeok Sam-ro 17-gil, Gangnam-gu, Seoul, Korea, Rep.

Article History
Submitted: 17th September 2023; Revised: 20th March 2024; Accepted: 27th March 2024;
Available online: 22th April 2024; Published Regularly: June 2024

doi: 10.25273/cheesa.v7i1.17831.1-14

*Corresponding Author.
Email: sitompul@itb.ac.id

Abstract

This study aimed to enhance the thermal efficiency of the sulphitation process in the boiling house of sugar plants using a combined approach of pinch and exergy analyses. Pinch analysis is a reliable method for optimizing the design of energy recovery systems. However, the primary limitations arise from its exclusive focus on heat transfer processes. On the other hand, exergy balance provides valuable insight into the consumption of supplied exergy by individual process units, serving as a quantitative measure of inefficiency. The boiling house was evaluated and modified using pinch-exergy analysis with Sulphitation Process capacity production of 8000 TCD. The results showed a potential reduction in exergy destruction by approximately 10.25 MW. The optimization effort led to reductions of 18.18 and 14.70% in the use of hot and cold external utility, respectively.

Keywords: boiling house; exergy analysis; heat exchanger network; pinch analysis; process integration; sugar plant

Abstrak

Pada penelitian ini, kombinasi analisis pinch dan eksergi diaplikasikan pada proses Sulfitasi di unit boiling house pabrik gula sebagai peningkatan efisiensi energi. Analisis pinch dikembangkan sebagai alat perhitungan yang digunakan untuk optimasi desain dengan menghemat energi. Namun, salah satu batasan pinch analysis adalah teknik yang digunakan sebatas penghematan energi saja yaitu perpindahan panas. Neraca eksergi digunakan pada sistem untuk mengetahui seberapa besar eksergi yang dipindahkan ke sistem yang telah terkonsumsi oleh unit proses. Kehilangan eksergi merupakan menginformasi seberapa besar proses yang inefisien. Tujuan dari penelitian ini adalah evaluasi dan modifikasi jaringan panas dengan menggunakan metode pinch-exergy pada proses sulfitasi dengan kapasitas giling 8000 TCD. Evaluasi dan modifikasi jaringan penukar panas menghasilkan pengurangan nilai kehilangan eksergi sebesar 10,25 MW. Terlebih lagi, jumlah utilitas panas eksternal dan jumlah utilitas dingin eksternal dapat dikurangi sebesar 18,18% dan 14,70% secara berturut-turut.

***Kata kunci**: analisis eksergi; analisis pinch; boiling house; jaringan penukar panas; pabrik gula; proses integrasi*

1. Introduction

The focus of this investigation centers on sugar plants, where the predominant method used for converting sugarcane into sugar is the sulphitation process. A significant component of the sulphitation process is the Multiple Effect Evaporation (MEE) system, which needs a large amount of heat. However, the integration of MEE includes using the steam generated from an effect in other facilities [1]. Considering the amount of energy in the sugar factory, some efforts are made to minimize its requirements. Energy optimization can be performed using several methods, including exergy and pinch analyses [2].

Pinch analysis has proven effective in optimizing energy in various industries by constructing a better heat exchanger network to reduce the utility of heating and cooling media [3]. This analysis offers the benefit of extracting information through visual aids such as composite curves, grand composite curves, and grid diagrams [4]. The desired energy target is determined prior to constructing the heat exchanger network [5]. Several studies have used pinch analysis in industrial energy management. For instance, Westphalen et al investigated a triple-effect evaporator system in a sugar factory, showing a potential reduction in heating utility consumption by up to 23% [6]. Singh et.al [7] applied pinch analysis to optimize energy usage in the Malelane Mill sugar factory, achieving a decrease in steam on cane (SOC) from 67% to 56.2% - 56.8% with a payback period of 1.11 - 1.19 years. Additionally, Riadi et.al [8] reported a 30% potential energy savings in MEE using Low-Pressure Steam (LPS) at 0.9 – 1.1 kg/cm^2.G.

The application of pinch technology to increase energy efficiency has shown satisfactory results. A detailed examination focuses on energy optimization through a thermodynamic analysis based on the exergy concept. Exergy analysis is a method used for energy optimization and evaluation within a system. Applying exergy balance across the entire plant provides insights into the available potential energy and the extent to which exergy supplied to the system has been used by the various process units [9]. Loss of exergy or irreversibility provides a general quantitative measure of process inefficiency [10]. Individual analyses can be conducted to pinpoint the specific unit responsible for the highest exergy loss contribution [11] and show the optimization potential of the system [12]. Particularly in systems using a workload, such as refrigeration [13], the primary aim is to determine the minimum work required to achieve a specific desired outcome [14]. The design of the Heat Exchanger Network (HEN) for the sulphitation process is presented in Figure 1, while the exergetic efficiency of the boiling sulphitation process component for base case design is shown in Table 1. Pinch analysis of the process has shown energy inefficiency in the current configuration of the HEN design.

In this study, the initial step entails describing the operation of a boiling house in a typical sulphitation process. Subsequently, exergy equations were formulated for each component within the boiling house process for the base case design. Exergy analysis was conducted to compute both exergetic efficiency and destruction for each individual component within the boiling house process for the base case design. The combined use of

exergy destruction and exergetic efficiency serve as effective tools for assessing energy performance [15], facilitating the identification of sources within the system requiring optimization. Additionally, a method was outlined for determining the minimum heat requirement for a boiling house. The objective of this study includes providing suggestions for decreasing SOC while discussing the reason for deviation from the reversible process. Both pinch and exergy analysis methods were used for improving exergetic efficiency.

The process flow diagram of the boiling house sulphitation process in a sugar plant, operating at a capacity of 8000 TCD is shown in Figure 1. In this study, raw juice from a mill station was heated up to 75°C by 2 primary heaters (JH1-1 and JH1-2) for the defecation and sulphitation process, using vapor bled from 3rd and 2nd effect evaporators, respectively. Subsequently, the temperature of sulphitated juice was raised to 105°C using two secondary heaters (JH2-1 and JH2-2). This heating was accomplished through vapor extracted from the 2nd and the 1st effect evaporators, respectively, before transferring the juice to the clarifier. Prior to being introduced into the 1st effect evaporator, the clear juice (with a concentration of 11.9% brix) from the clarifier was raised to a temperature of 105°C. This process was achieved through vapor extracted from the 1st effect evaporator, facilitated by the tertiary heater (JH3). MEE (EV-1, EV-2, EV3, EV-4, and EV-5) were operated at low-pressure steam 1 kg/cm^2.G, with the 5th effect evaporator operating at 0.14 kg/cm^2.a. Thick juice as a product should have 64 %brix being fed to crystallization station. In this station, all Vacuum Pans (VPA, VPC, and VPD) were heated by 1st effect evaporator and at vacuum condition of 0.14 kg/cm^2.a. Massecuite A, Massecuite C, and Massecuite D were the products obtained from Vacuum Pan A, C, and D, respectively, with approximate concentrations of 94%, 96%, and 98%, correspondingly.

2. Research Methods

The commercial simulator Aspen Plus version 11 from Aspen Technology was used to generate simulated data. The selected fluid package for process simulation was NRTL. Thermodynamics properties such as water activity, osmotic coefficient, vapor pressure, boiling point temperature, freezing point, and solubility were described in 3 binaries systems, namely D-fructose, water, and sucrose [16] [17].

In the Aspen Plus model of the sulphitation process within the boiling house, D-fructose was used as a representation for all non-sucrose sugar, while sucrose specifically denotes sucrose sugar. In this study, exergy calculation and analysis were conducted in Aspen Plus and Excel. It is important to note that exergy analysis should be preceded by mass and energy balances of the system.

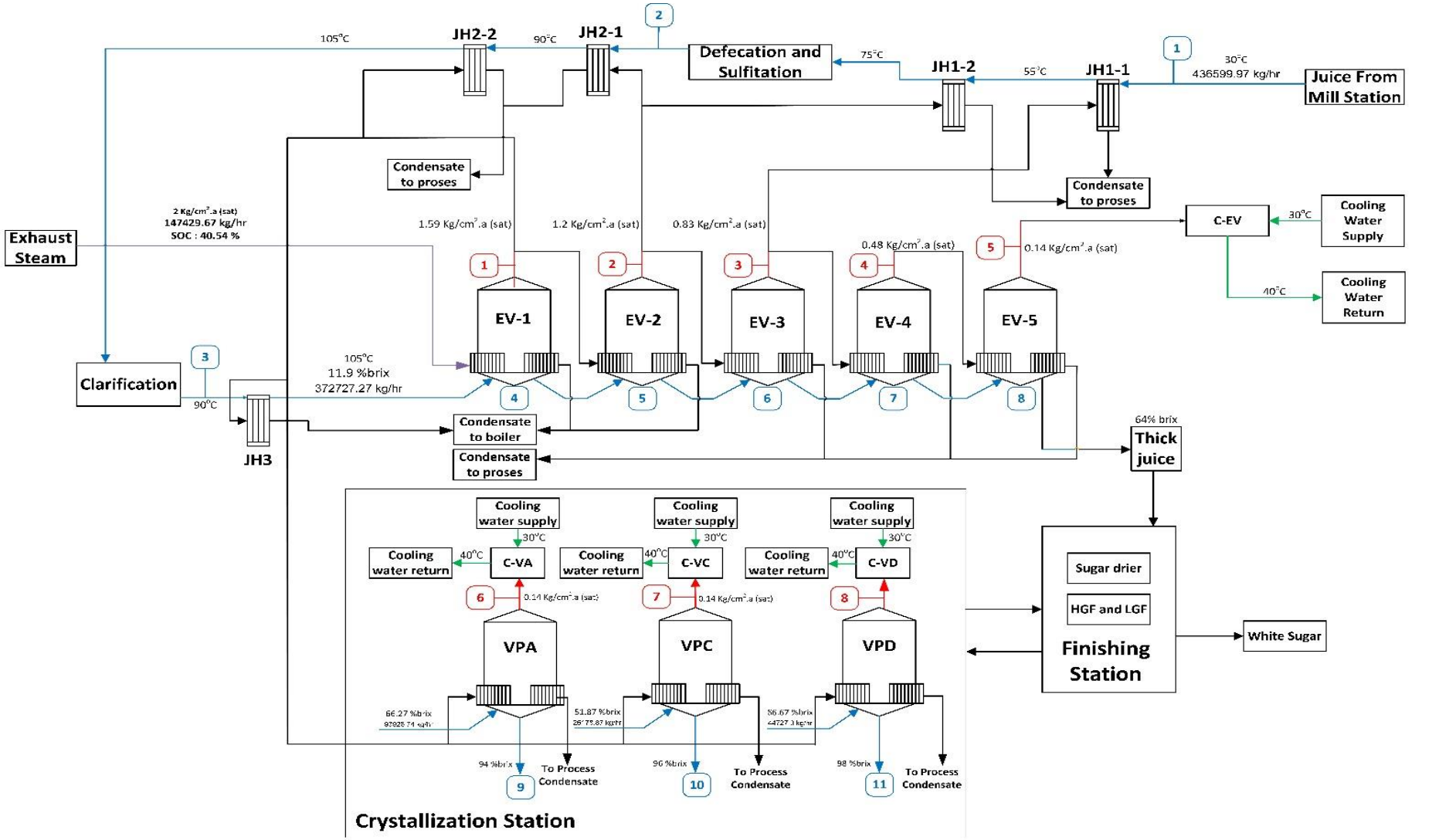

Figure 1. Boiling house sulphitation process in sugar plant base case design

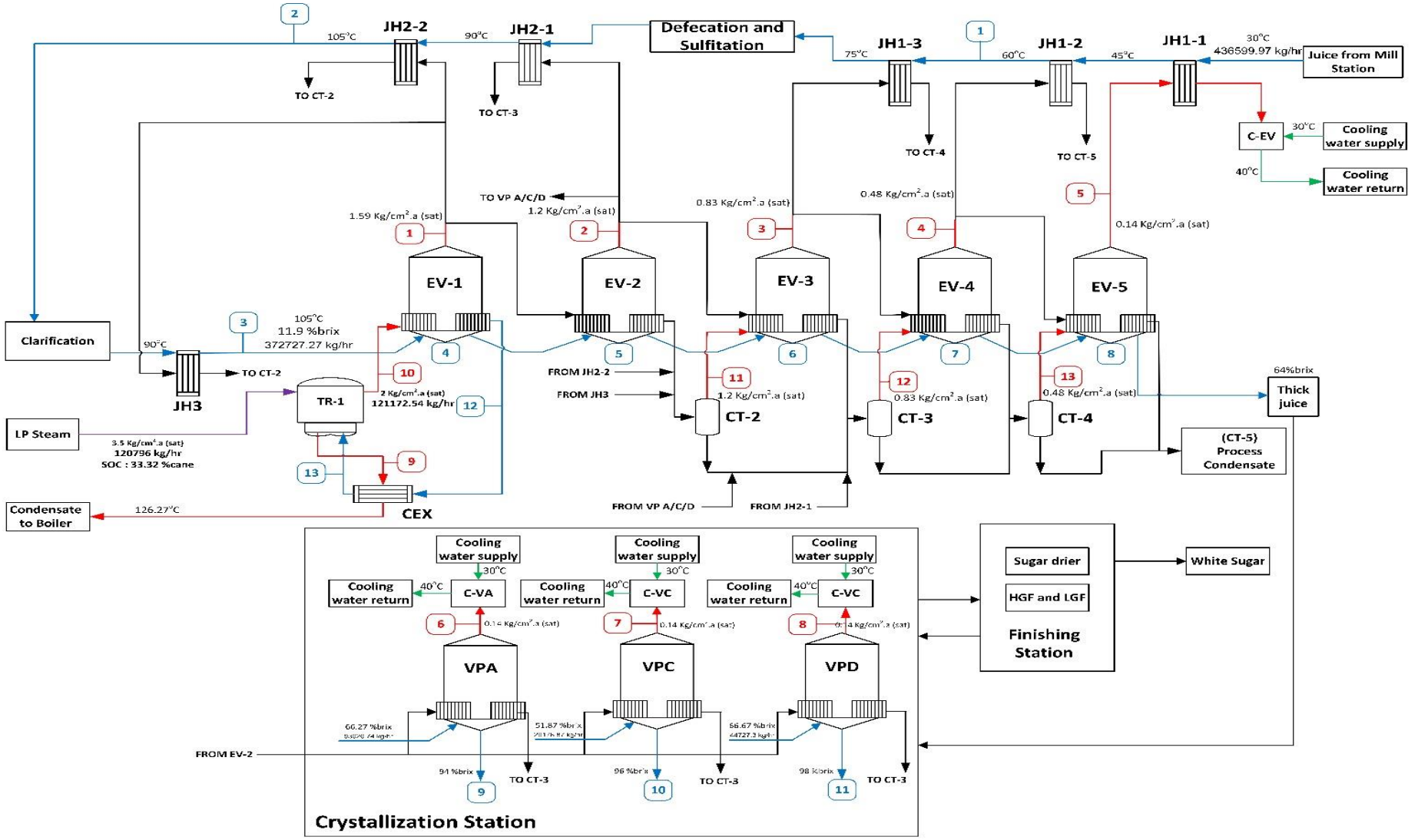

Figure 2. Optimized boiling house sulphitation process in sugar plant

Table 1. Exergetic efficiency of boiling house sulphitation process components for base case design

HE	Stream		T (ºC)		Q	m	H (kJ/kg)		S (kJ/kg.K)		Ex	η
			In	Out	(kJ/hr)	(kg/hr)	In	Out	In	Out	(kJ/hr)	
JH1-1	Shell (h)	Bleed EV3	95.70	94.52	40955782	18000	13288.63	15563.95	1.97	8.16	5395020.98	86.83
	Tube (c)	Raw Juice	30.00	55.01		436600	14138.83	14045.02	8.21	7.91		
JH1-2	Shell (h)	Bleed EV-2	105.69	104.83	33709284	15000	3270.22	15517.50	2.09	8.04	2963629.32	91.21
	Tube (c)	Raw Juice	55.01	75.01		436600	14045.02	13967.81	7.91	7.69		
JH2-1	Shell (h)	Bleed EV-2	105.69	104.83	26068513	11600	13270.22	15517.50	2.09	8.04	1053870.37	95.96
	Tube (c)	Sulphited Juice	75.01	90.08		436600	13967.81	13908.10	7.69	7.52		
JH2-2	Shell (h)	Bleed EV-1	113.75	113.16	26576780	11950	13255.34	15479.34	2.18	7.94	511038.65	98.08
	Tube (c)	Sulphited Juice	90.08	105.04		436600	13908.10	13847.23	7.52	7.36		
JH3	Shell (h)	Bleed EV-1	113.75	113.16	22707023	10210	13255.34	15479.34	2.18	7.94	437443.84	98.07
	Tube (c)	Clear Juice	90.06	105.01		372727	13954.38	13893.46	7.55	7.38		
EV1	Shell (h)	LPS	120.27	120.27	324948733	147500	13243.92	15446.96	2.26	7.86	4136360.39	98.73
	Tube (c)	EV1 Juice	105.01	113.75		372727	13893.46	13021.64	7.38	5.13		
EV2	Shell (h)	Bleed EV1	113.75	113.16	131150628	58970	13255.34	15479.34	2.18	7.94	2038603.67	98.45
	Tube (c)	EV2 Juice	105.40	105.69		232546	12880.77	12316.79	6.90	5.42		
EV3	Shell (h)	Bleed EV2	105.69	104.83	78900049	35109	13270.22	15517.50	2.09	8.04	1573943.28	98.01
	Tube (c)	EV3 Juice	95.34	95.70		170837	11972.40	11510.56	6.61	5.36		
EV4	Shell (h)	Bleed EV3	105.69	104.83	44201670	19426	13288.63	15563.95	1.97	8.16	1303214.59	97.05
	Tube (c)	EV4 Juice	95.34	95.70		133411	11011.75	10680.43	6.30	5.37		
EV5	Shell (h)	Bleed EV4	81.82	80.33	50267042	21738	13314.43	15626.80	1.79	8.34	3381584.00	93.27
	Tube (c)	EV5 Juice	53.87	54.72		111672	10167.69	9717.56	6.06	4.68		
VPA	Shell (h)	Bleed EV1	113.75	113.16	66497551	29900	13255.34	15479.34	2.18	7.94	8612196.69	87.05
	Tube (c)	VPA syrup	54.94	67.10		93926	8479.05	7771.07	5.54	3.40		
VPC	Shell (h)	Bleed EV1	113.75	113.16	29023179	13050	13255.34	15479.34	2.18	7.94	3832074.14	86.80
	Tube (c)	VPC syrup	53.98	73.53		26178	9781.85	8673.20	5.96	2.60		
VPD	Shell (h)	Bleed EV1	113.75	113.16	35806374	16100	13255.34	15479.34	2.18	7.94	4372845.70	87.79
	Tube (c)	VPD syrup	55.31	87.21		44727	7742.63	6942.08	4.94	2.54		
C-EV	Shell (h)	vapor EV5	54.72	52.55	59125099	24827	13364.61	15746.02	1.37	8.69	2882715.46	95.12
	Tube (c)	Cooling water	30.00	39.81		1450000	15843.68	15802.90	8.99	8.86		
C-VA	Shell (h)	vapor VPA	67.10	52.55	66661914	27765	13317.98	15718.91	1.30	8.67	3266870.56	95.10
	Tube (c)	Cooling water	30.00	39.83		1630000	15843.68	15802.78	8.99	8.85		
C-VC	Shell (h)	vapor VPC	73.53	52.56	29120995	12098	13267.43	15674.39	1.26	8.65	1436289.52	95.07
	Tube (c)	Cooling water	30.00	39.86		710000	15843.68	15802.66	8.99	8.85		
C-VD	Shell (h)	vapor VPD	87.21	52.58	35049029	14539	13101.94	15512.62	1.17	8.56	1774459.14	94.94
	Tube (c)	Cooling water	30.00	39.80		860000	15843.68	15802.92	8.99	8.86		

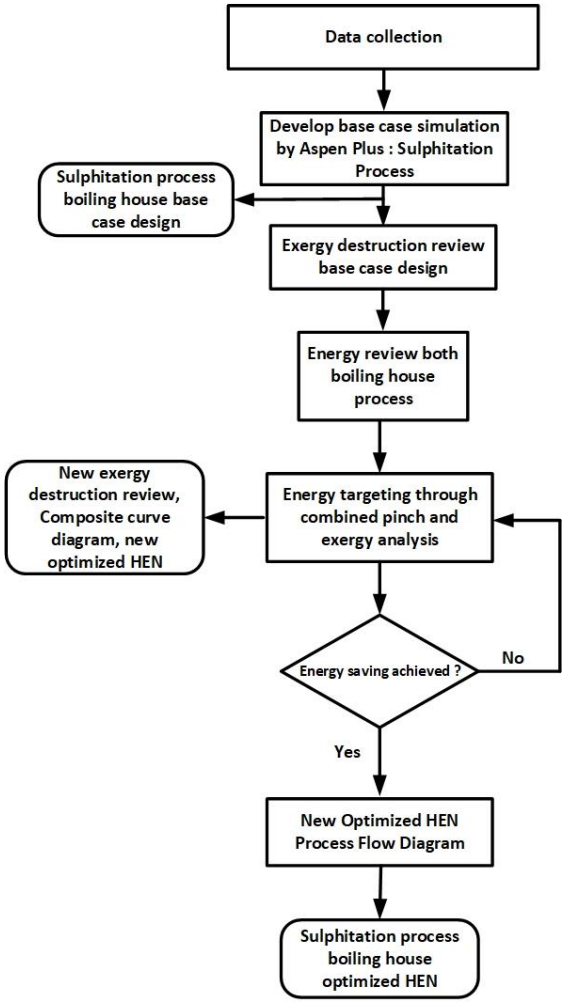

Figure 3. Flowchart of works methodology

Aspen stream results were exported to Excel. Energy optimization of HEN was conducted with the help of Aspen Energy Analyzer v.11. Figure 3 provides a full description of the study approach. The process commenced by collecting the required data to create a simulation of the base case design for a boiling house in a sugar plant. This data comprised specifications for the juice and syrup inputs and outputs, flow details for the shell and tube sides of all heat exchangers (HE), and operating conditions. The next step included the computation of exergetic efficiency from the base case design of the HEN. These exergetic efficiency calculations were conducted to determine the extent of exergy destruction before any optimization.

The basic concept revolves around the application of the first law of thermodynamics. The law states that while energy cannot be created or destroyed, it can change forms. This principle finds application in heat exchangers, devices designed to transfer heat from a higher to lower temperature fluid. In this process, the hot stream serves as the heat source, elevating the temperature of the cold stream. The complete transfer of energy from the hot to cold stream is impeded by the second law of thermodynamics. According to the law, entropy (ΔS) consistently increases ($\Delta S > 0$). Consequently, a portion of the energy is inevitably lost, leading to an increase in entropy [18]. This rise is a fundamental characteristic defining irreversibility in the thermodynamic process. The concept of exergy represents the maximum useful work obtainable from a system [19]. The loss of work during the process is termed lost work, denoted as W_{lost}. It is defined as the difference between the ideal work (W_ideal) achievable for the same change of state and the actual work (W_s) performed during the change of state [19]. The system can be expressed as equation (1).

In terms of rates, equation (1) can be transformed into equation (2). The actual work was calculated using the energy balance, equation (3), while the ideal work rate was obtained using equation (4). Substituting equations (3) and (4) into equation (2) produced equation (5). For single surroundings temperature (T_σ), the steady-state entropy balance was expressed by equation (6), and multiplying by T_σ, yielded equation (7). Since the right side of equation (5) and (7) were identical, the

equation was simplified as given by equation (8).

The lost work from equation (5) can be transformed into equation (9). After obtaining the W_{lost} value, the calculation for $\%W_{lost}$ can be expressed in equation (10), which is the proportion of the W_{lost} value to heat exchanger heating load.

$$W_{lost} \equiv W_s - W_{ideal} \quad \text{.....(1)}$$

$$\dot{W}_{lost} \equiv \dot{W}_s - \dot{W}_{ideal} \quad \text{.....(2)}$$

$$\dot{W}_s = \Delta\left[\left(H + \frac{1}{2}u^2 + zg\right)\dot{m}\right]_{fs} - \dot{Q} \quad \text{.....(3)}$$

$$\dot{W}_{ideal} = \Delta\left[\left(H + \frac{1}{2}u^2 + zg\right)\dot{m}\right]_{fs} - T_\sigma\Delta(S\dot{m})_{fs} \quad \text{....(4)}$$

$$\dot{W}_{lost} = T_\sigma\Delta(S\dot{m})_{fs} - \dot{Q} \quad \text{.....(5)}$$

$$\dot{S}_G = \Delta(S\dot{m})_{fs} - \frac{\dot{Q}}{T_\sigma} \quad \text{.....(6)}$$

$$T_\sigma\dot{S}_G = T_\sigma\Delta(S\dot{m})_{fs} - \dot{Q} \quad \text{.....(7)}$$

$$\dot{W}_{lost} = T_\sigma\dot{S}_G \quad \text{.....(8)}$$

$$\dot{W}_{lost} = T_\sigma\{\dot{m}_H(\Delta S)_H + \dot{m}_C(\Delta S)_C\} \quad \text{.....(9)}$$

$$\%W_{lost} = \frac{W_{lost}}{\dot{Q}}x100 \quad \text{..... (10)}$$

4. Results and Discussion

Exergy destruction and efficiency were provided along with the schematic of the component. Furthermore, the flow streams based on the states in Figure 1 are shown in Table 1. An exergy analysis of the boiling house sulphitation process in a sugar plant was conducted in the present study to evaluate the amount of exergy destruction and efficiency in each component. Across all components of the boiling house, a discernible level of irreversibility was observed. According to exergy analysis, heat exchangers, namely JH1-1 (86.83%), VPA (87.05%), VPC (86.80%), and VPD (87.79%) had the lowest efficiency levels.

To minimize exergy destruction, the temperature differences (ΔT_H and ΔT_C) need to be approximately equal in value [20]. It is important to note that pinch analysis does not consider exergy destruction review. The typical design of a heat exchanger network is shown in Figure I. According to the schematic diagram, hot and cold streams were only separated by pinch points. Therefore, the heat exchanger network exclusively obeys the 3 pinch rules [21]. By applying principles aimed at minimizing exergy destruction, the temperature interval lines dividing hot and cold streams in the grid diagram need to be increased.

Table 2. Details of base case design utility requirements

Variable	Value
Hot external utilities	
Low-Pressure Steam	90.26 MW 147.5 TPH SOC: 40.5%
Cold external utilities	
Cooling water	52.76 MW 4650 TPH

The base case design of the heat exchanger comprises a total of 15 units divided into 3 stations. The first (purification process), second (evaporation process), and third stations (crystallization process) consist of 5 JHs, 5 evaporators, and 3 vacuum pans, respectively. As shown in Figure 1, the source of hot and cold external utilities in base case design was derived from Low-Pressure Steam operating at conditions of 2 Kg/cm^2.a at saturated condition and cooling water operating at 30^{o}C respectively. Details of base case design utility requirements have been summarized in Table 2.

In Figure 2, the simulation of the optimized heat exchanger network for the boiling house sulphitation process is presented. The results showed that there are several modification processes in the base case and optimized heat exchanger

network. Tables 3 and 4 show hot and cold stream data for the optimized heat exchanger network of the boiling house sulphitation process in a sugar plant. The number of these streams was increased due to suggestions of some practical ways to improve exergetic efficiency and SOC.

The temperature difference and heat exchange load in heat transfer contribute primarily to exergy destruction. As shown in Table 1, the lowest exergetic efficiency belongs to JH1-1 (86.83%), VPA (87.05%), VPC (86.80%), and VPD (87.79%). Some practical recommendations exist for enhancing exergetic efficiency of the sulphitation process in a boiling house. These included the reduction of the temperature difference between the hot and cold streams and considering alterations in the type and configuration of the boiling house system.

Raw juice was heated up to 75°C using 3 juice heaters, namely JH1-1, JH1-2, and JH1-3. The primary heater was heated using vapor bleed 5th evaporator, vapor bleed 4th evaporator, and vapor bleed 5th evaporator, respectively. Subsequently, VPA, VPC, and VPD were heated by vapor bleed 2nd evaporator. In the optimized heat exchanger network, flash condensate from the preceding effect was used to heat the *n-th* effect evaporator.

Table 3. Hot stream data of optimized boiling house sulphitation process in sugar plant

No Stream	Stream	$\dot{m}$ (10^3 kg/hr)	T_{in} (°C)	T_{out} (°C)	Enthalpy (10^6 kJ/hr)
1	Raw juice	436.59	30.00	75.00	74.64
2	Sulph juice	436.59	75.00	105.00	52.58
3	Clear Juice	372.72	90.06	105.00	22.68
4	EV1 Juice	372.72	105.00	113.68	266.94
5	EV2 Juice	258.62	105.33	105.74	204.43
6	EV3 Juice	163.86	95.39	95.68	60.15
7	EV4 Juice	134.82	81.43	81.86	50.53
8	EV5 Juice	110.31	53.90	54.72	46.91
9	VPA syrup	93.92	54.94	67.13	66.52
10	VPC syrup	26.17	53.98	73.40	29.00
11	VPD syrup	44.72	55.31	86.65	35.72
12	Cond. EV1	121.17	120.27	120.27	7.44
13	Cond. ret	121.17	120.27	120.28	259.49

Table 4. Cold stream data of optimized boiling house sulphitation process in sugar plant

No stream	Stream	$\dot{m}$ (10^3 kg/hr)	T_{in} (°C)	T_{out} (°C)	Enthalpy (10^6 kJ/hr)
1	EV1 vap	114.10	113.68	113.16	253.75
2	EV2 vap	94.75	105.68	104.83	212.95
3	EV3 vap	29.04	95.46	94.52	66.08
4	EV4 vap	24.51	81.36	80.33	56.68
5	EV5 vap	23.35	54.72	52.55	55.61
6	VPA vap	27.77	67.13	52.55	66.68
7	VPC vap	12.09	73.40	52.56	29.11
8	VPD vap	14.51	86.65	52.58	34.99
9	BFW	120.79	138.93	126.27	7.45
10	FCEV1	1.96	104.83	104.83	4.41
11	FCEV2	4.31	94.52	94.52	9.82
12	FCEV3	6.53	80.33	80.33	15.08

The condensate from the first effect is taken directly back to the boilers. This is because it comprised the highest-quality condensate available for boiler feed, originating from the condensed exhaust steam/low-pressure steam. The transformer (TR-1) facilitated the use of exhaust steam/low-pressure steam (3.5 kg/cm2.a at the saturated condition) as the heating medium for condensation from evaporator 1. Condensate from Vacuum Pans and Juice Heaters was added to the combined stream to augment the process.

Rein et.al [22] reported several advantages of applying a condensate flash arrangement. Firstly, it led to the improvement of SOC due to the addition of vapor to the evaporator. Secondly, the loss incurred when condensate was simply taken to the storage, was eliminated. Thirdly, the condensate that was not directed to the boiler was subjected to a flash-down process to match the pressure within the final effect evaporator. With a temperature of approximately 80°C, this condensate is ideally suited for use in either the imbibition process or within the process area.

The composite curve of the boiling house sulphitation process is shown in Figure 4. Table 5 presents the data of heat exchange and exergetic efficiency for an optimized network, using a minimum temperature approach ΔT_{min} = 6ºC. The composite curve provides the overall sources and sink temperature profile of the process. Several other benefits include the integration of process, HEN, and boiling house process simultaneously [23].

The optimization result shows a significant decrease in the consumption of hot external utilities, by 18.18% from the initial heating of 90.26 MW to 72.08 MW. Similarly, the consumption of cold external utilities decreased by 14.7% from the initial cooling of 52.76 MW to 44.99 MW. Heat optimization results have succeeded in obtaining a Maximum Energy Recovery (MER) of 254.88 MW.

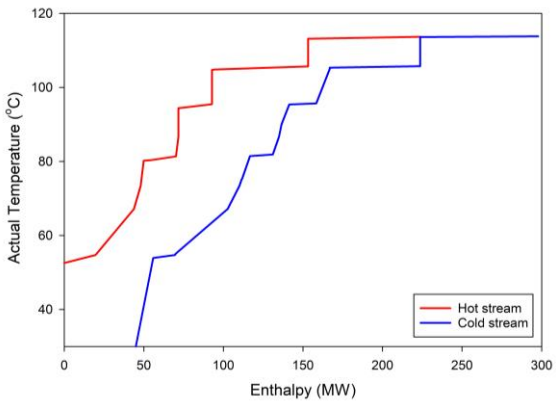

Figure 4. Actual composite curve

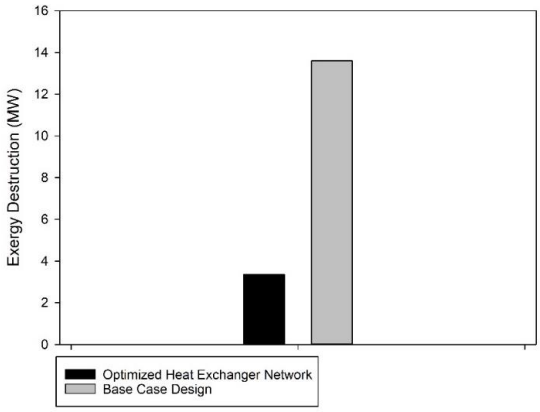

Figure 5. Comparison exergy destruction

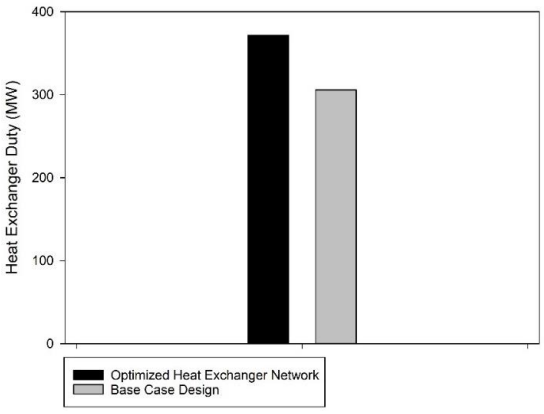

Figure 6. Comparison heat exchanger duty

Exergy analysis between base case design and optimization heat exchanger network has been presented in Tables 1 and 5. As shown in Figures 5 and 6, the

optimization of energy within the heat exchanger network led to a successive decrease in exergy destruction by 10.25 MW. However, there was a corresponding increase in heat exchanger duty by 66.19 MW. This analysis suggests that post-optimization, there is a greater capacity for heat supply transfer to the cold flow. As heat duty rises, the W_{lost} of HEN drops. This shows that, while the amount of heat supplied increases, the heat lost during heat transfer process in HE decreases. As a result, HEN energy developed in this study is capable of producing more efficient heat transfer between hot and cold streams.

4. Conclusion

In conclusion, the study presented the methodology and results of applying both exergy and pinch analysis on an industrial scale, with the main focus on the boiling house sulphitation process. A total of 3 practical ways, incorporating pinch and exergy analysis methods, were used to improve the overall exergetic efficiency of the sulphitation process. First, Raw juice was heated up to 75°C using 3 juice heaters (JH's), adopting vapor bleed 5th evaporator, vapor bleed 4th evaporator, and vapor bleed 5th evaporator, as heating media, respectively. Second, VPA, VPC, and VPD were heated using a vapor bleed 2nd evaporator. Third, in an optimized heat exchanger network, flash condensate from the preceding effect was used to heat the *n-th* effect evaporator.

From the optimization result, the amount of hot external utilities was successfully reduced by 18.18% from the initial heating of 90.26 MW to 72.08 MW. Additionally, the amount of cold external utilities was successfully reduced by 14.7% from the initial cooling of 52.76 MW to 44.99 MW. Following energy optimization conducted on the heat exchanger network, the value of exergy destruction was reduced by 10.25 MW, while heat exchanger duty increased by 66.19 MW.

Nomenclature

E	Exergy flow (KJ/hr)
H	Specific enthalpy (KJ/Kg)
Q	Heat transfer (KJ/hr)
S	Entropy (KJ/Kg.K)
T	Temperature (oC)
η	Exergetic efficiency (%)
ṁ	Flowrate (Kg/hr)
Ėx	Exergy rate (KJ/hr)

Subscripts

In	inlet state
Out	outlet state
O	dead state

Abbreviation used for blocks in flow diagrams

VP	Vacuum Pan
JH	Juice Heater
EV	Evaporator
C	Condenser

Table 5. Exergetic efficiency of optimized boiling house sulphitation process components

HE	Stream		T (ºC)		Q (kJ/hr)	m (kg/hr)	H (kJ/kg)		S (kJ/kg.K)		E (kJ/hr)	η
			In	Out			In	Out	In	Out		
JH1-1	Shell (h)	Bleed EV5	54.72	52.55	24418154.64	23351.12	3192.09	3441.85	0.33	1.10	248650.95	98.98
	Tube (c)	Raw Juice	30.00	45.00		436599.80	3377.00	3363.64	1.96	1.92		
JH1-2	Shell (h)	Bleed EV4	81.86	80.33	24856914.69	10749.26	3180.07	3732.38	0.43	1.99	410376.59	98.35
	Tube (c)	Raw juice	45.00	60.00		436599.80	3363.64	3350.04	1.92	1.88		
JH1-3	Shell (h)	Bleed EV3	95.68	94.52	25368340.97	11149.51	3173.95	3717.39	0.47	1.95	356507.64	98.59
	Tube (c)	Raw juice	60.00	75.00		436599.80	3350.04	3336.17	1.88	1.84		
JH2-1	Shell (h)	Bleed EV2	105.74	104.83	25957501.45	11550.14	3169.49	3706.27	0.50	1.92	251359.21	99.03
	Tube (c)	Sulphited juice	75.00	90.00		436599.80	3336.17	3321.97	1.84	1.80		
JH2-2	Shell (h)	Bleed EV1	113.68	113.16	26630755.82	11974.94	3166.05	3697.21	0.52	1.90	123243.67	99.54
	Tube (c)	Sulphited juice	90.00	105.00		436599.80	3321.97	3307.40	1.80	1.76		
JH3	Shell (h)	Bleed EV1	113.68	113.16	22689303.05	10202.60	3166.05	3697.21	0.52	1.90	104474.74	99.54
	Tube (c)	Clear Juice	90.06	105.00		372727.13	3332.95	3318.41	1.80	1.76		
EV1	Shell (h)	LPS	120.27	120.27	266948220.00	121172.54	3163.26	3689.44	0.54	1.88	810265.50	99.70
	Tube (c)	EV1 juice	105.00	113.68		372727.13	3318.41	3147.34	1.76	1.32		
EV2	Shell (h)	Bleed EV1	113.68	113.16	204429074.18	91924.77	3166.05	3697.21	0.52	1.90	762160.45	99.63
	Tube (c)	EV2 juice	105.33	105.74		258624.82	3139.09	2950.30	1.67	1.18		
EV3	Shell (h)	Bleed EV2	105.68	104.83	60148439.45	26765.19	3169.55	3706.30	0.50	1.92	285819.47	99.52
	Tube (c)	EV3 juice	95.39	95.68		163868.42	2823.55	2735.88	1.56	1.33		
EV4	Shell (h)	Bleed EV3	95.46	94.52	50530965.94	22212.30	3174.14	3717.49	0.47	1.95	355746.07	99.30
	Tube (c)	EV4 Juice	81.43	81.86		134824.06	2641.51	2551.99	1.51	1.26		
EV5	Shell (h)	Bleed EV4	81.36	80.33	46910345.68	20293.35	3180.46	3732.58	0.43	1.99	753108.77	98.39
	Tube (c)	EV5 Juice	53.90	54.72		110312.32	2412.43	2310.86	1.44	1.13		
VPA	Shell (h)	Bleed EV2	105.74	104.83	66524618.64	29601.02	3169.49	3706.27	0.50	1.92	1787410.44	97.31
	Tube (c)	VPA syrup	54.94	67.13		93926.74	2025.19	1856.02	1.32	0.81		
VPC	Shell (h)	Bleed EV2	105.74	104.83	29005489.71	12906.38	3169.49	3706.27	0.50	1.92	797054.24	97.25
	Tube (c)	VPC syrup	53.98	73.40		26178.88	2336.35	2071.72	1.42	0.62		
VPD	Shell (h)	Bleed EV2	105.74	104.83	35723692.41	15895.74	3169.49	3706.27	0.50	1.92	898133.78	97.49
	Tube (c)	VPD syrup	55.31	86.65		44727.30	1849.30	1658.53	1.18	0.61		
C-EV	Shell (h)	Bleed EV5	52.55	52.55	31190078.83	23351.12	3441.85	3760.88	1.10	2.07	365270.71	98.83
	Tube (c)	Cooling water	30.00	39.62		779695.35	3784.20	3774.64	2.15	2.12		
C-VA	Shell (h)	Bleed VPA	67.13	52.55	66686606.96	27774.85	3180.92	3754.38	0.31	2.07	781789.74	98.83
	Tube (c)	Cooling water	30.00	39.79		1638735.42	3784.20	3774.48	2.15	2.12		
C-VC	Shell (h)	Bleed VPC	73.40	52.56	29105512.34	12092.91	3169.09	3743.95	0.30	2.07	343640.92	98.82
	Tube (c)	Cooling water	30.00	39.79		715171.59	3784.20	3774.48	2.15	2.12		
C-VD	Shell (h)	Bleed VPD	86.65	52.58	34989103.74	14514.25	3131.20	3706.98	0.28	2.04	422759.64	98.79
	Tube (c)	Cooling water	30.00	39.79		859622.58	3784.20	3774.48	2.15	2.12		
TR-01	Shell (h)	Cond EV1	120.27	120.28	259499995.75	121172.54	3674.76	3163.25	1.84	0.54	2127154.81	99.18
	Tube (c)	Exhaust Steam	138.93	138.93		120796.19	3154.78	3667.88	0.58	1.83		
CEX	Shell (h)	Boiler Feed	138.93	126.27	7449531.04	120796.19	3667.88	3682.61	1.83	1.86	88414.04	98.81
	Tube (c)	Cond EV1	120.27	120.27		121172.54	3689.44	3674.76	1.88	1.84		

References

[1] Higa, M., Freitas, A. J., Bannwart, A. C., & Zemp, R. J. (2009). Thermal integration of multiple effect evaporator in a sugar plant. *Applied Thermal Engineering*, 29(2–3), 515–522. doi: 10.1016/j.applthermaleng.2008.03.009

[2] Sa, D. (2023). Economic Analysis of Separation Unit of Methanol to Propylene Production Based on Optimization of Refrigeration Cycles Using Pinch and Exergy Analysis. *International Journal of Refrigeration*, 146, 108–117. doi: 10.1016/j.ijrefrig.2022.09.029

[3] Truls Gundersen, David Olsson Berstad, & Audun Aspelund. (2009). Extending pinch analysis and process integration into pressure and fluid phase considerations. *Chemical Engineering Transactions*, 18, 33–38. doi: 10.3303/CET0918003

[4] Ramanath, T., Foo, D. C. Y., Tan, R. R., & Tan, J. (2023). Integrated enterprise input-output and carbon emission pinch analysis for carbon intensity reduction in edible oil refinery. *Chemical Engineering Research and Design*, 193, 826–842. doi: 10.1016/j.cherd.2023.03.045

[5] Kemp, I. C. (2007). *Pinch analysis and process integration: a user guide on process integration for the efficient use of energy* (2nd ed.). Amsterdam ; Boston: Butterworth-Heinemann.

[6] Westphalen, D. L., & Wolf Maciel, M. R. (2000). Optimization of bleed streams in evaporation systems based on pinch analysis: new approach. *Computer Aided Chemical Engineering*, 8, 997–1002. Elsevier. doi: 10.1016/S1570-7946(00)80168-6

[7] Singh, I., Riley, R., & Seillier, D. (1997). Using pinch technology to optimise evaporator and vapour bleed configuration at the malelane mill. *Proc S Afr Sug Technol Ass*, 71(207–216).

[8] Riadi, I., & Puji Utomo, D. (2022). The Effect of Operating Condition on Low Pressure Steam (LPS) in Sugar Factory by Pinch Analysis. *UNISTEK*, 9(1), 68–82. doi: 10.33592/unistek.v9i1.1786

[9] Gaggioli, R. (1998). Available Energy and Exergy. *Int.J. Applied Thermodynamics*, 1(1–4), 1–8.

[10] Wan, T., Bai, B., & Zhou, W. (2023). Exergy destruction analysis of a power generation system utilizing the cold energy of LNG. *Heliyon*, e19393. doi: 10.1016/j.heliyon.2023.e19393

[11] Kotas, T. (1995). *The Exergy Method of Thermal Plant Analysis*. Krieger Publishing Company.

[12] Ghorbani, B., Salehi, G. R., Ghaemmaleki, H., Amidpour, M., & Hamedi, M. H. (2012). Simulation and optimization of refrigeration cycle in NGL recovery plants with exergy-pinch analysis. *Journal of Natural Gas Science and Engineering*, 7, 35–43. doi: 10.1016/j.jngse.2012.03.003

[13] Pacheco-Cedeño, J. S., Rodríguez-Muñoz, J. L., Ramírez-Minguela, J. J., & Pérez-García, V. (2023). Comparison of an absorption-compression hybrid refrigeration system and the conventional absorption refrigeration system: Exergy analysis. *International Journal of Refrigeration*, S0140700723002177. doi: 10.1016/j.ijrefrig.2023.08.003

[14] Cerci, Y. (2002). The minimum work requirement for distillation processes. *Exergy, An International Journal*, 2(1), 15–23. doi: 10.1016/S1164-0235(01)00036-X

[15] Kumar Dhakar, M., Choudhary, P., & Singh, N. K. (2021). Performance improvement of a sugar mill through EXERGY analysis. *Materials Today: Proceedings*, 46, 11202–11207. doi: 10.1016/j.matpr.2021.02.427

[16] Peres, A. M., & Macedo, E. A. (1996). Thermodynamic properties of sugars in aqueous solutions: correlation and prediction using a modified UNIQUAC model. *Fluid Phase Equilibria*, 123, 71–95.

[17] Kylan, G., Annegret, S., & Maciet, S. (2019). Development and verification of an aspen plus® model of a sugarcane biorefinery. *Proc S Afr Sug Technol Ass*, 92, 254–273.

[18] Mafi, M., Naeynian, S. M. M., & Amidpour, M. (2009). Exergy analysis of multistage cascade low temperature refrigeration systems used in olefin plants. *International Journal of Refrigeration*, 32(2), 279–294. doi: 10.1016/j.ijrefrig.2008.05.008.

[19] Smith, J. M., Van Ness, H. C., Abbot, M. M., & Swihart, M. T. (2018). *Introduction to Chemical Engineering Thermodynamics* (8th ed.). New York: McGraw-Hill Education.

[20] Pambudi, N., Laurensia, R., Wijayanto, D., Perdana, V., Saw, L., & Handogo, R. (2017). Exergy Analysis of Boiler Process Powered by Biogas Fuel in Ethanol Production Plant: A Preliminary Analysis. *Energy Procedia*, 142, 216–223. doi: 10.1016/j.egypro.2017.12.035

[21] Lambert, C., Laulan, B., Decloux, M., Romdhana, H., & Courtois, F. (2018). Simulation of a sugar beet factory using a chemical engineering software (ProSimPlus ®) to perform Pinch and exergy analysis. *Journal of Food Engineering*, 225, 1–11. doi: 10.1016/j.jfoodeng.2018.01.004

[22] Rein, P. (2007). *Cane Sugar Engineering*. Berlin: Verlag Dr. Albert Bartens KG.

[23] Zhang, K., Liu, Z., Huang, S., & Li, Y. (2015). Process integration analysis and improved options for an MEA CO2 capture system based on the pinch analysis. *Applied Thermal Engineering*, 85, 214–224. doi: 10.1016/j.applthermaleng.2015.03.073

CHEESA: Chemical Engineering Research Articles
ISSN 2614-8757 (Print), ISSN 2615-2347 (Online)
Available online at: http://e-journal.unipma.ac.id/index.php/cheesa

Research Article

The Antibacterial Potential of Ethyl Acetate Fraction from *Plectranthus amboinicus* Leaves and Identification of Active Compounds Using LC-MS

Potensi Antibakteri Fraksi Etil Asetat Daun Jinten (Plectranthus amboinicus) dan Identifikasi Senyawa Aktif Menggunakan LC-MS

Rahma Diyan Martha[1*)], Yunita Diyah Safitri[2)], Nasa Bela Dwi Lestari[1)], Danar[3)], Hesty Parbuntari[4)], Margarita Claudya Maida[5)], Afidatul Muadifah[1)], Choirul Huda[1)]

[1)]*STIKes Karya Putra Bangsa, Department of Pharmacy, Indonesia*
[2)]*STIKes Karya Putra Bangsa, Department of Medical Laboratory Technology, Indonesia*
[3)]*Universitas Negeri Malang, Department of Chemistry, Indonesia*
[4)]*Universitas Negeri Padang, Department of Chemistry, Indonesia*
[5)]*Tokyo Metropolitan University, Department of Applied Chemistry, Jepang*

Article History
Submitted: 08th September 2022; Revised: 10th May 2024; Accepted: 15th May 2024;
Available online: 06th June 2024; Published Regularly: June 2024

doi: 10.25273/cheesa.v7i1.13826.15-23

*Corresponding Author.
Email: rahmadiyan@stikes-kartrasa.ac.id

Abstract

The Indian Borage plant (*Plectranthus amboinicus*) is a traditional medicinal ingredient in Indonesia, containing flavonoids, alkaloids, polyphenols, saponins, and essential oils. Therefore, this study aimed to determine the antibacterial activity of *P. amboinicus* leaves ethyl acetate fraction using the disc diffusion method and identify the composition with LC-MS. The antibacterial activity test was conducted with concentration variations of 15%, 20%, and 25% with Chloramphenicol 500 mg and 5% DMSO as a positive and negative control, respectively. The results showed that the ethyl acetate fraction at a concentration of 20% had the largest inhibition zone diameter, with an average of 30 mm. The LC-MS results identified 115 compounds, and the highest concentration values were found in kaempferol 3-(6"-caffeoylglucoside) and kaempferol 3-glucosyl-(1→2) galactosyl-(1→2)-glucoside, with a composition of 3.26109% and 3.26141%, respectively.

Keywords: Antibacterial activity; Ethyl acetate fraction; LC-MS; *Plectranthus Amboinicus*

Abstrak

Tanaman jinten (Plectranthus amboinicus) merupakan bahan obat tradisional di Indonesia yang mengandung senyawa flavonoid, alkaloid, polifenol, saponin, dan minyak atsiri. Penelitian ini bertujuan untuk mengetahui aktivitas antibakteri fraksi etil asetat daun jinten dengan metode difusi cakram serta komposisi senyawa yang terkandung menggunakan LC-MS. Uji aktivitas antibakteri dilakukan dengan menggunakan variasi konsentrasi 15%, 20%, dan 25%, Kloramfenikol 500 mg sebagai kontrol positif, dan DMSO 5% sebagai kontrol negatif. Hasil dan kesimpulan yang diperoleh pada uji antibakteri metode difusi cakram yakni fraksi etil asetat daun jinten dengan konsentrasi 20% memiliki diameter zona hambat terbesar dengan rata-rata sebesar 30 mm. Hasil dari LC-MS terdapat sebanyak 115 senyawa yang ada di daun jinten. Hasil identifikasi LC-MS senyawa dengan nilai konsentrasi komposisi tertinggi yaitu senyawa kaempferol 3-(6"-caffeoylglucoside) dengan komposisi senyawa 3,26109%, dan kaempferol 3-glucosyl-(1→2) galactosyl-(1→2)-glucoside dengan kompisisi senyawa 3,26141%.

***Kata kunci**: antibakteri; daun jinten; fraksi etil asetat; LC-MS*

1. Introduction

Indonesia is renowned for having the global greatest biodiversity, comprising fauna and flora with great potential as medicines. In general, traditional medicine has various advantages, including affordability, simpler treatment techniques, relative safety without strict supervision, ease of administration without needing medical personnel, and relatively low side effects [1]. With these various advantages, traditional medicine is expected to become an alternative to chemical medicines in the future.

Among the rich flora in Indonesia, Indian Borage (*Plectranthus amboinicus*) has great potential as a traditional herbal medicine. This plant, commonly found in India, Ceylon, and South Africa, is characterized by thick, upright, and oval-shaped leaves [2], known to contain various secondary metabolites, including flavonoids, alkaloids, polyphenols, saponins, and essential oils [3]. The leaves have antibacterial activity capable of killing or inhibiting the growth of bacteria, including *Escherichia coli*. This is due to the flavonoids and polyphenol content which have antioxidant and antibacterial properties [4].

E. coli is a gram-negative bacteria responsible for 85% of urinary tract infection (UTI) cases and 50% of nosocomial infections. The bacteria is also a major cause of diarrhea due to the production of enterotoxins that bind to the mucosa of the small intestine [5]. Effective antibacterial agents are needed to target infectious and non-infectious organisms [6]. An effective traditional medicinal material that can be used is *P. amboinicus* leaves.

Agustianasari et al. [3] reported that the ethyl acetate fraction of *P. amboinicus* seeds had better and more effective antibacterial properties compared to water and n-hexane against *Bacillus* and *E. coli* bacteria. Therefore, this study aimed to determine the antibacterial activity of *P. amboinicus* leaves ethyl acetate fraction using the disc diffusion method and analyze the compound composition with LC-MS.

2. Research Methods

2.1 Tools and Materials

The tools used include Ultra-Performance Liquid Chromatography-Mass Spectrometry (UPLC-MS) from Shimadzu, a set of maceration tools, micropipettes, a rotary evaporator, and an autoclave. The materials used include fresh *P. amboinicus* leaves, distilled water, 70% ethanol, n-hexane, ethyl acetate, Nutrient Broth (NB), Nutrient Agar (NA), *E. coli* bacteria, DMSO (Dimethyl sulfoxide), Chloramphenicol, $FeCl_3$, Dragendorff reagent, Mayer's reagent, NaCl, Mg, and HCl.

2.2 Preparation of Simplisia

The simplisia from *P. amboinicus* leaves was prepared by thoroughly washing the leaves and cutting them to uniform thickness. The leaves were then air-dried away from direct sunlight. Depending on the weather, this drying process typically took 48 hours. After drying, the leaves were sorted to remove any dirt or foreign particles. The next step entailed grinding the simplisia into a powder, which was then sieved using an 80-mesh sieve to ensure uniform consistency. [7].

2.3 Preparation of *P. amboinicus* Leaves Extract

The *P. amboinicus* leaves extract was made using the maceration method with 70% ethanol as the solvent. A total of 500 grams leaves powder was placed in a

maceration vessel, and 1000 mL of 70% ethanol was added. The maceration process lasted 4 to 24 hours with occasional stirring. The obtained extract was filtered using flannel cloth until the solution was clear. Subsequently, the leaves extract was concentrated using an evaporator until a thick extract was obtained [8].

2.4 Phytochemical Screening

2.4.1 Alkaloid Compounds

Tests for alkaloid compounds could be performed using the Dragendorff and the Mayer methods. In the Dragendorff test, 2 mL of extract was added to 1 mL of the reagent, while in the Mayer test, 1 mL of extract was added to 2 N HCl and the reagent. The Mayer test results were indicated by the formation of a white precipitate in the extract, and a positive result for the Dragendorff test was demonstrated by an orange precipitate [9].

2.4.2 Flavonoid Compounds

To test for flavonoid compounds, 2 mL of extract was added to 2 mL of 70% ethanol, stirred, heated, and filtered. The filtrate was then added with Mg and concentrated HCl. A positive result was indicated by the formation of an orange or red precipitate [10].

2.4.3 Saponin Compounds

Saponin compounds were tested by adding 2 mL of extract to hot water and shaking vigorously. The presence of stable foam for 5 minutes after adding 1 drop of 2 N HCl indicated the presence of saponins [10].

2.4.4 Tannin Compounds

P. amboinicus leaves were added to 3 mL of hot distilled water and stirred until homogeneous. After cooling, 5 drops of a 10% NaCl solution were added. Two test tubes were used, one as a blank and one with the filtrate to which 3 drops of $FeCl_3$ reagent were added. The remaining filtrate was added with gelatin. The presence of tannin compounds in the extract was indicated by a color change to blue-black or brownish-gree [11].

2.5 Fractionation

About 5 grams of the extract were dissolved in 25 mL of distilled water, and 25 mL of n-hexane were added. The solution was shaken, and the two fractions were separated. The filtered aqueous phase was further divided by adding 25 mL of ethyl acetate. This process was repeated three times with the same steps for several fraction solutions. The filtrate from the filtration was evaporated using a rotary evaporator.

2.6 Preparation of Media

2.6.1 Nutrient Agar (NA)

The 4 grams of Nutrient Agar (NA) were dissolved in 200 mL of distilled water in an Erlenmeyer flask. The solution was stirred and homogenized using a stirrer while being heated. Subsequently, the solution was sterilized using an autoclave at 121°C for 15 minutes. The NA media was then poured into Petri dishes, incubated at 37°C for 24 hours and the bacteria used were *E. coli.*

2.6.2 Nutrient Broth (NB)

The 0.3 grams of Nutrient Broth were dissolved in 30 mL of distilled water and homogenized. Subsequently, 6 mL of the media solution was poured into each reaction tube. Using an autoclave, the media was sterilized at 121°C for +60 minutes [12].

2.7 Preparation of Test Solutions

2.7.1 Test Solution of *P. amboinicus* Leaves Fraction

Test solutions of the ethyl acetate fraction at concentrations of 15%, 20%, and 25% were prepared by weighing 1.5 grams, 2 grams, and 2.5 grams, respectively, and dissolving in 10 mL of 5% DMSO.

2.7.2 Positive Control Solution

The positive control used was Chloramphenicol 500 mg tablet, which was ground into a fine powder. Subsequently, the powder was weighed and dissolved in 50 mL of 5% DMSO in a volumetric flask. The resulting Chloramphenicol solution had a concentration of 50 µg/50 µL.

2.7.3 Negative Control Solution

5% DMSO was used as the negative control. It was prepared by dissolving 5 mL of DMSO in distilled water up to 100 mL.

2.7.4 Bacterial Suspension

Bacteria were cultured in NA media for 24 hours at 37°C. The suspension was prepared by transferring the culture into a 0.9% NaCl solution, and the turbidity level was visually standardized using a McFarland 0.5 standard. About 100 µL of the suspension was pipetted and added to 10 mL of NB to obtain a colony count of 1-2 x 10^6 CFU/mL.

2.8 Antibacterial Activity Test

2.8.1 Disc Diffusion Method

A volume of 10 mL of NA media was poured into Petri dishes/plates and allowed to solidify. *E. coli* bacteria cultures were taken using a pipette from NB media into previously sterilized plates, adding 200 µL. The culture was then spread evenly using a sterile cotton swab. Discs soaked in test solutions were transferred onto the NA media containing *E. coli* in an aseptic manner and then incubated at 37 °C for 24 hours. [12].

2.8.2 Measurement of Inhibition Zone

The clear zones formed around the discs, commonly referred to as inhibition zones, were measured using calipers. The strength of the bacterial inhibition zones was determined based on the classification in Table 1.

Table 1. Classification of Bacterial Inhibition Zones

Diameter (mm)	Strength of Inhibition Zone
≤ 5	Weak
6-10	Moderate
11-20	Strong
≥ 21	Very Strong

2.9 Compound Identification with LC-MS

The process of identifying compounds with LC-MS started with sample preparation. A total of 1 L precipitated sample was injected into the Shimadzu LC-MS-8040 instrument. The analysis was performed using UPLC-MS equipped with a binary pump. LC was connected to a Quadrupole Time of Flight (QTOF) mass spectrometer using Electrospray Ionization (ESI) as the ionization source. Furthermore, the mass spectrometry (MS) system used was the QTOF system in positive ionization mode. The ESI parameters included a capillary temperature of 350 degrees Celsius and an atomizer gas flow rate of 60 mL/HR, with a voltage source of 5.0V. Full scanning was performed in the m/z range of 100-5000 with a source temperature of 100 degrees Celsius. For the UPLC column, a Shimadzu Shim Pack FC-ODS with dimensions of 2mm x 150mm and 3µm particles was used. The eluent consisted of 90% methanol and water, with a 0.5 mL/minute flow rate. The

identification results showed all types of compounds contained in the *P. amboinicus* leaves extract, along with the percentage of each.

2.10 Statistical Analysis

Data from the antibacterial activity test of *P. amboinicus* leaves fractions against *E. coli* bacteria were analyzed using One-Way ANOVA to observe the differences in the average diameter of inhibition zones for each test sample using Statistical Product and Service Solution (SPSS 23) software. A p-value <0.05 indicated that variation in the concentration of *P. amboinicus* leaves ethyl acetate fraction affected the growth of *E. coli* bacteria.

3. Results and Discussion

3.1 Phytochemical Screening

The purpose of phytochemical screening was to provide an overview of the compounds contained in *P. amboinicus* leaves. Table 2 shows the results of compounds including alkaloids, flavonoids, saponins, and tannins. Flavonoids damage bacteria cell membranes by forming protein complex compounds. Saponins decrease the surface tension of bacteria cell walls, leading to cell damage and death, while tannins coagulate proteins, having a similar effect to phenolic compounds [13].

3.2 Antibacterial Activity and Measurement of Inhibition Zones

Antibacterial agents are substances that can kill or inhibit bacterial growth. The clear zones around the growing bacteria indicate that the active compounds in the test substance can inhibit growth.

Chloramphenicol was used as a positive control due to its potentially strong antibacterial activity. This study compared the effectiveness of the test compounds in inhibiting bacteria bacterial growth with a widely tested standard. The 5% DMSO was used as a negative control due to its ability to dissolve almost all compounds, whether polar or non-polar and because it was not bactericidal. This ensures that any antibacterial activity observed can be attributed solely to the *P. amboinicus* leaves ethyl acetate fraction, free from solvent interference. Consequently, the results obtained from this study can be considered pure and accurate [14].

Table 2. Results of Phytochemical Screening

Compound	Reagent	Test Result	
Alkaloid	Extract + Dragendorff reagent	Orange	(+)
Flavonoid	Extract + DMSO + Dragendorff reagent	Orange	(+)
Saponin	Extract + HCl 2N	Presence of foam	(+)
Tannin	Extract + distilled water + 10% sodium chloride + $FeCl_3$	Brownish-green	(+)

Description: (+) indicates the presence of the compound, and (-) indicates the absence of the compound.

Table 3. Diameter of Antibacterial Inhibition Zones of *P. amboinicus* Leaves Ethyl Acetate Fraction

Treatment	Diameter of Inhibition Zone (mm)				Description	p-value
	I	II	III	Mean		
15%	25	20	31	25,33	Very Strong	
20%	25	45	20	30	Very Strong	
25%	20	23	25	22,67	Very Strong	0,000
K +	45	50	43	46	Very Strong	
K -	00	00	00	00	-	

Figure 1 shows the formation of clear zones in all 3 variations of the ethyl acetate fraction from *P. amboinicus* leaves. Table 3 presents the average diameter of the three concentration variations in inhibition zones. Based on the results, all three variations of the ethyl acetate fraction had strong inhibitory activity, suggesting antibacterial activity. Several factors can influence antibacterial activity testing, including the content of antibacterial compounds, the number and type of bacteria inhibited, as well as the concentration of leaves extract [15].

The One-Way ANOVA test results showed a p-value <0.05, indicating that variations in the ethyl acetate fraction from *P. amboinicus* leaves significantly affected the growth of *E. coli* bacteria. A total of 5 data groups were compared namely concentrations of 20%, 15%, and 25%, as well as positive and negative controls. Each group has an average value for *E. coli* bacteria growth. As shown in Table 4, subsets indicate which groups have average values without significant differences. Different subsets imply significant differences between these groups.

Based on the result, the ethyl acetate fraction with a concentration of 20% had an average value close to the positive control and was in the same subset, indicating a fairly good antibacterial effect. Meanwhile, fractions with concentrations of 15% and 25%, as well as the negative control, were in different subsets, indicating significant differences in antibacterial activity.

Table 4. Tukey Test Subset Data

Concentration (%)	Average bacterial growth value	Subset
15	25.3333	2
20	30.0000	3
25	22.6667	2
+	46.0000	3
-	0.0000	1

3.3 LC-MS Identification

LC-MS identification was conducted at the Muhammadiyah University of Malang. The purpose of conducting LC-MS is to analyze organic, inorganic, and biological compounds in a complex sample commonly found in the environmental origin. The principle is based on the separation of analytes in line with the polarity level of compounds. LC-MS consists of a stationary phase column and a specific solution for the mobile phase. Compounds are separated according to polarity levels and respective speeds to reach the detector, leading to different retention times and observed spectra of separated peaks [13].

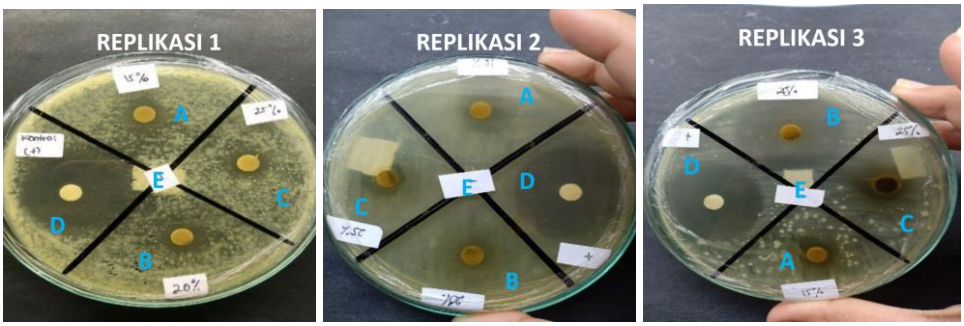

Figure 1. Results of Antibacterial Activity Test (Note: A = Ethyl Acetate Fraction 15%; B = Ethyl Acetate Fraction 20%; C = Ethyl Acetate Fraction 25%; D = Positive Control; E = Negative Control)

Figure 2 shows the chromatogram results of the LC-MS test for *P. amboinicus* leaves ethyl acetate fraction. Based on the LC-MS results, peaks ranged from low to high, with 115 compounds. The highest peak was number 101, identified with the largest composition of 3.26109%, and named kaempferol 3-(6”-caffeoylglucoside) (Figure 3.). Meanwhile, the compound identified at peak number 113 had a composition of 3.26141% and was named kaempferol 3-glucosyl-(1→2) galactosyl-(1→2)-glucoside (Figure 4.). Kaempferol 3-(6”-caffeoyl glucoside) compound has a molecular weight (m/z) of 610.1323, with the chemical formula $C_{30}H_{26}O_{14}$, and kaempferol 3-glucosyl-(1→2) galactosyl-(1→2)-glucoside has a molecular weight (m/z) of 772.2062 with the chemical formula $C_{33}H_{40}O_{21}$.

Both compounds, belonging to the flavonoid group, are suspected to be the most important in the ethyl acetate fraction of *P. amboinicus* leaves regarding antibacterial activity [16]. Flavonoids, as antibacterial agents, inhibit the function of the cytoplasmic membrane, nucleic acid function, and energy metabolism of bacteria. These compounds also inhibit RNA synthesis within the DNA cell, disrupt metabolism within bacteria, and damage cell membranes, releasing intracellular compounds from the bacteria [13].

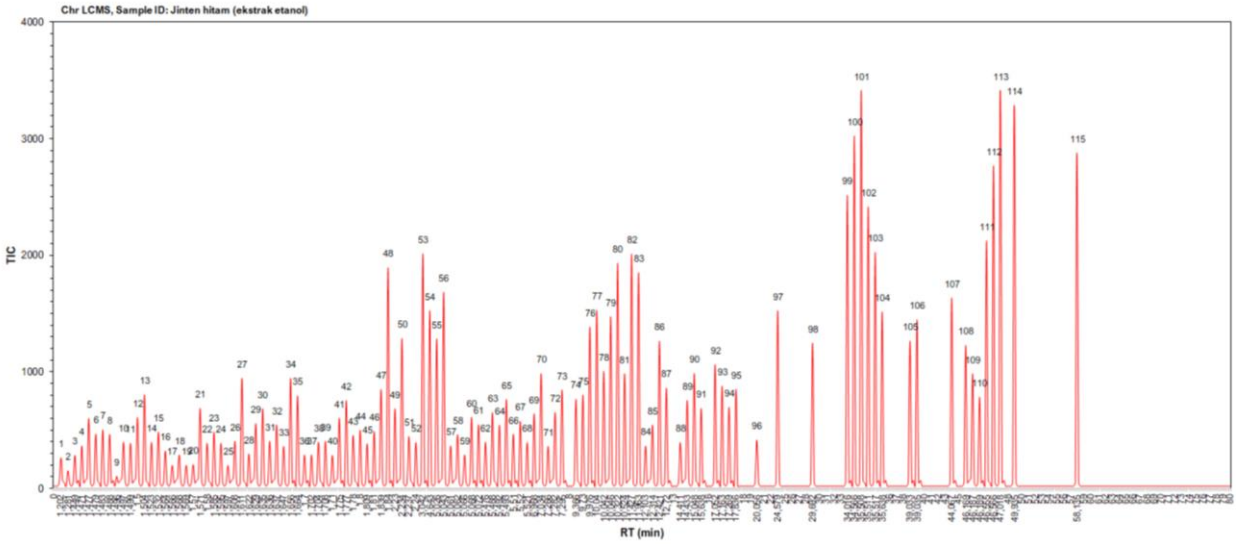

Figure 2. Chromatogram results from LC-MS (Liquid Chromatography-Mass Spectrometry)

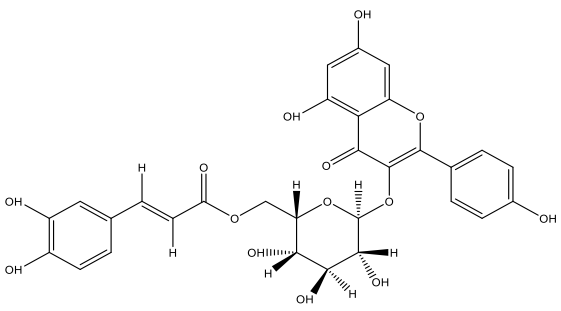

Figure 3. Structure of compound kaempferol 3-(6”-caffeoylglucoside)

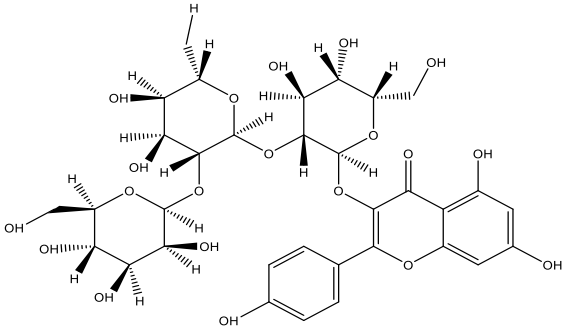

Figure 4. Structure of compound kaempferol 3-glucosyl-(1→2) galactosyl-(1→2)-glucoside

4. Conclusion

The ethyl acetate fraction of *P. amboinicus* leaves showed antibacterial activity against *E. coli*. The 20% fraction concentration demonstrated had optimum inhibitory zone against *E. coli* with a value of 30 mm. A total of 115 compounds were identified in *P. amboinicus* leaves, with the largest composition being 3.26109% for the compound kaempferol 3-(6''-caffeoylglucoside) and 3.26141% for kaempferol 3-glucosyl-(1→2) galactosyl-(1→2)-glucoside. Based on the results, further studies are needed using other methods, such as Soxhlet extraction and antibacterial testing against gram-positive bacteria. Additionally, the isolation of secondary metabolites using Thin Layer Chromatography (TLC) could provide rapid and accessible information about the quantity and types of compounds present in the sample without requiring specialized instruments for detection.

References

[1] Alaydrus, S. (2020). Tingkat Pengetahuan Masyarakat Terhadap Pembuatan Dan Penggunaan Obat Tradisional Di Desa Sunju Rt Ii Kecamatan Marawola Kabupaten Sigi Provinsi Sulawesi Tengah. *Jurnal farmasi UIN Alauddin Makassar*, 8(2), 46–53. Retrieved from http://journal.uin-alauddin.ac.id/index.php/jurnal_farmasi/article/view/11729

[2] Yuniarachmah, A., Roviq, M., & Nihayati, E. (2019). Respon Pertumbuhan dan Kandungan Flavonoid Tanaman Bangun-Bangun (Plectranthus amboinicus Lour.) pada Berbagai Kerapatan Naungan dan Dosis Pupuk Nitrogen Response of Growth and Flavonoid Content of Plectranthus amboinicus Lour at Various Shade Density and. *Jurnal Produksi Tanaman*, 7(12), 2206–2214.

[3] Agustianasari, I., Mulqie, L., & Choesrina, R. (2016). Uji Aktivitas Antibakteri Ekstrak dan Fraksi Biji Jinten Hitam (Nigella sativa L .) terhadap Bakteri Bacillus subtilis dan Escherichia coli Test Antibacterial Extract Activity and Biji Jinten Hitam Fraction (Nigella sativa L .) Divisi : Magnoliophyta Ke. *Prosiding Farmasi*, 682–690.

[4] Munawaroh, S., & Prima Astuti, H. (2010). Ekstraksi Minyak Daun Jeruk Purut dengan Pelaruit Etanol dan n-Heksan. *Jurnal Kompetensi Teknik*, 1–23.

[5] Suryati, N., Bahar, E., & Ilmiawati, I. (2018). Uji Efektivitas Antibakteri Ekstrak Aloe vera Terhadap Pertumbuhan Escherichia coli Secara In Vitro. *Jurnal Kesehatan Andalas*, 6(3), 518-522. doi: 10.25077/jka.v6i3.732

[6] Ratnawati, D. (2011). Preliminary Test of Determination of Alkoloid and Steroid Compounds and Bioassay on Some Vegetable Plant Extract. *Jurnal Gradien*, 7(7), 692–696.

[7] Shahdadi, F., Mirzaei, H.O., & Garmakhany, A. . (2015). Study of phenolic compound and antioxidant activy of date fruit as a function of ripering stages and drying proceess. *Journal of Food Science and Tehnology*, 52, 1814–1819.

[8] Zalfiatri, Y., Hamzah, F., & Simbolon, M. T. (2018). Pembuatan Sabun Transparan Dengan Penambahan Ekstrak Batang Pepaya Sebagai Antibakteri. *Chempublish Journal*, 3(2), 57–68. doi: 10.22437/chp.v3i2.5713

[9] Wardhani, R. R. A. A. K., Akhyar, O., & Prasiska, E. (2018). Analisis skrining fitokimia, kadar total fenol-flavonoid dan aktivitas antioksidan ekstrak etanol kulit kayu tanaman galam rawa gambut (Melaleuca cajuputi roxb). *Al Ulum: Jurnal Sains Dan Teknologi*, 4(1), 39. doi: 10.31602/ajst.v4i1.1589

[10] Harborne, J. B. (2006). *Metode Fitokimia Penentuan Cara Modern Menganalisis Tumbuhan*. ITB.

[11] Ukoha, P.O., Cemaluk, E.A.C., Nnamdi, O. L., & Madus, E. P. (2011). Tannins and other phytochemical of the samannea saman pods and their antimicrobial activities. *African Journal of Pure and Applied Chemistry*, 5(8), 237–244.

[12] Kabense R., Ginting E.V., Wullur S., Kawung J.N., Losung F., & Tombokan. J. L. (2019). Penapisan Bakteri Proteolitik yang Bersimbiosis dengan Alga Gracillaria sp. *Jurnal Ilmiah Platax, Fakultas Perikanan dan Kelautan*, 7(2), 413-418.

[13] Fatimah, F., Martha, R. D., & Kusumawati, A. (2020). Deteksi dan Identifikasi Senyawa Flavonoid Ekstrak Etanol Kulit Batang Tanaman Majapahit (Crescentia cujete) dengan LCMS. *CHEESA: Chemical Engineering Research Articles*, 3(2), 88-98. doi: 10.25273/cheesa.v3i2.7688.88-98

[14] Fatimah, F., Martha, R. D., & Danar, D. (2022). Analisis toksisitas dan potensi antikanker ekstrak metanol daun Majapahit (Crescentia cujete) dengan metode Brine Shrimp Lethality Test. *Jurnal Penelitian Saintek*, 27(1), 24-30.

[15] Hatupea. (1994). *Metode Fitokimia*. ITB Press: Bandung.

[16] Wardhani R.R.A.A.K., Akhyar O., & Prasiska. E. (2018). Analisis Skrining Fitokimia, Kadar Total Fenol-Flavonoid dan Aktivitas Antioksidan Ekstrak Etanol Kulit Kayu Tanaman Galam Rawa Gambut(Melaleucea cajuputi roxb). *Al Ulum Sains dan Teknologi*, 4(1).

CHEESA: Chemical Engineering Research Articles
ISSN 2614-8757 (Print), ISSN 2615-2347 (Online)
Available online at: http://e-journal.unipma.ac.id/index.php/cheesa

Research Article

Activated Carbon/MnO_2 Composite as Uranium Adsorbent in Solution

Komposit Karbon Aktif/MnO_2 sebagai Adsorben Uranium dalam Larutan

Nita Anjarsari[1)], Titin Anita Zaharah[1*)], Endah Sayekti[1)], Bohari Mohd. Yamin[2)]
[1)]Universitas Tanjungpura, Department of Chemistry, Pontianak, Kalimantan Barat 78124, Indonesia
[2)]University Kebangsaan Malaysia, Department of Chemistry, Faculty of Science and Technology, Bangi 43600, Selangor, Malaysia

Article History
Submitted: 09th September 2022; Revised: 31th May 2024; Accepted: 03rd June 2024; Available online: 22th July 2024; Published Regularly: June 2024

doi: 10.25273/cheesa.v7i1.13863.24-35

*Corresponding Author.
Email: titin.anita.zaharah@chemistry.untan.ac.id

Abstract

This research aimed to make an adsorbent from activated carbon/MnO_2 (AC/MnO_2) composite and examine its characteristics, adsorption capacity, and mechanism for uranyl ions. Carbon was made from Oil Palm Empty Fruit Bunches (OPEFB) through sodium acetate's carbonization and activation processes. The AC/MnO_2 composite was made using the in-situ deposition method, namely by oxidizing Mn^{2+} compounds to Mn^{4+} under alkaline conditions at a temperature of ±80°C. An FTIR spectrophotometer was used to characterize the adsorbent, and a UV-Vis spectrophotometer was used to determine the content of uranyl. The results of FTIR analysis showed that MnO_2 in Mn-O and Mn-O-Mn absorption was bound to activated carbon. It was also discovered that AC/MnO_2 adsorbent reduced uranium content in solution in the form of uranyl ion for adsorbent mass of 2.5 grams and a contact time of 60 minutes, leading to adsorption percentages of 65.5%. The adsorption mechanism followed the Langmuir adsorption isotherm equation by forming a single layer. Meanwhile, the adsorption kinetics followed pseudo-second-order with a value of k = 6.7 g/mg.min.

Keywords: activated carbon; adsorbent; MnO_2; oil palm empty fruit bunch; uranyl ion

Abstrak

Penelitian ini bertujuan untuk membuat adsorben komposit karbon aktif/MnO_2 serta mempelajari karakteristik, kemampuan adsorpsi dan mekanisme adsorpsinya terhadap ion uranil. Karbon dibuat dari tandan kosong kelapa sawit melalui proses karbonisasi dan diaktivasi dengan natrium asetat. Komposit karbon aktif/MnO_2 dibuat dengan teknik pengendapan in-situ, yaitu dengan mengoksidasi senyawa Mn^{2+} menjadi Mn^{4+} dalam kondisi basa pada suhu ±80 °C. Karakterisasi adsorben dilakukan menggunakan spektrofotometer FTIR. Konsentrasi uranil dianalisis menggunakan spektrofotometer UV-Vis. Hasil analisis FTIR diperoleh serapan Mn-O dan Mn-O-Mn, yang mengindikasikan MnO_2 telah berhasil terikat pada karbon aktif. Adsorben karbon aktif/MnO_2 mampu menurunkan kadar uranium dalam larutan dalam bentuk ion uranilnya dengan menggunakan massa adsorben sebanyak 2,5 gram dan waktu kontak 60 menit diperoleh persentase adsorpsi 65,5%. Mekanisme adsorpsi mengikuti persamaan isoterm adsorpsi Langmuir dengan membentuk lapisan monolayer. Kinetika adsorpsi mengikuti pseudo orde dua dengan nilai k = 6,7 g/mg.min.

Kata kunci: *adsorben; ion uranil; karbon aktif; MnO_2; tandan kosong kelapa sawit*

1. Introduction

Liquid waste containing uranyl compounds is generated from industries using uranium, with the possibility of entering the environment through various activities [1]. Although several methods have been applied to remove uranium from wastewater [2], only adsorption using activated carbon proved to be relatively cheap and easy to implement. The use of organic materials as carbon sources is profitable due to its cost-effectiveness and accessibility such as oil palm empty fruit bunches (OPEFB). Additionally, the high lignocellulose content in OPEFB has the potential to produce carbon [3] through carbonization and is activated by immersing in sodium acetate solution [4]. This activated carbon is often applied as an adsorbent, which has been modified with metal oxides such as MnO_2 [5].

MnO_2 is a group of metal oxides with a strong affinity for heavy metals [6]. The direct application of MnO_2 as an adsorbent has the weakness of relatively low stability [7]. Therefore, activated carbon with relatively high stability and an easy composite can be used as a matrix or buffer for MnO_2 [8].

Previous research on uranium removal in wastewater has been carried out using phytoremediation technology, ion exchange, solvent extraction, chemical precipitation-crystallization, and film separation [2]. Despite widespread application, these methods are less effective and uneconomical for handling large amounts of waste containing small quantities of uranyl ionic substances [2]. Therefore, using activated carbon composite adsorbent from OPEFB is more economical and easier to obtain with easy-to-apply work procedures.

In this research, activated carbon adsorbent was made from OPEFB composited with MnO_2 to form an AC/MnO_2 adsorbent composite. The process started by mixing activated carbon with MnO_2 (AC/MnO_2) using an in-situ deposition method. Subsequently, Mn^{2+} was oxidized from $MnSO_4$ to Mn^{4+}, namely MnO_2 using $KMnO_4$ oxidizer in an alkaline environment with NaOH. MnO_2 composite on activated carbon formed Mn-O bonds, which would absorb uranyl ions in solution for the formation of coordination bonds [9].

The reduction of the uranium content of uranyl compounds in solution was carried out using an AC/MnO_2 composite adsorbent. The test parameters examined were adsorbent mass and time variations, including type of adsorption isotherm and kinetics. The AC/MnO_2 adsorbent was characterized using a Fourier-Transform Infrared (FTIR) spectrophotometer.

2. Research Methods

2.1 Tools and Materials

The equipments used were a 100 mesh sieve, laboratory glassware, desiccator, Fourier Transform Infrared (FTIR) SHIMADZU 820 IPC, oven, vortex, shaker, UV-Vis spectrophotometer (Shimadzu 2810-UV-Vis), and furnace. The materials used in this experiment were aquademin, CH_3COONa, HCl, $H_2C_2O_4.2H_2O$, HNO_3, H_2SO_4, $KMnO_4$, $MnSO_4.H_2O$, NaOH, NH_4SCN, $SnCl_2$, OPEFB obtained from PT Patiware in Bengkayang and $UO_2(CH_3COO)_2.2H_2O$.

2.2 Carbonization of OPEFB

OPEFB was cut into small pieces measuring ±5 cm and strung. Subsequently, it was soaked in hot water for 10 minutes, drained, and the fibers

were dried in the sun [10]. The dried OPEFB fiber obtained was weighed and put into the furnace. The carbonization process was carried out at a temperature of ±350°C for 1 hour under closed conditions [11]. The results obtained were weighed, crushed, and sieved using a 100-mesh sieve [12].

2.3 Carbon Activation

Activation was carried out by mixing 72 g of carbon into 250 mL of 1 N CH_3COONa, followed by stirring for 1 hour and heating at a temperature of ±120°C. Activated carbon obtained was filtered, washed using distilled water [13], dried in an oven at a temperature of ±105°C for 2 hours, and weighed.

2.4 Activated Carbon (AC) Composite with MnO_2

The procedure for making activated carbon composite with MnO_2 was carried out using an in-situ deposition lens with a mass ratio of KA:MnO_2 (1 : 1.2) [9]. In this research, 20 g of activated carbon was mixed with 0.552 M MnO_2 made from a mixture of $MnSO_4$ and $KMnO_4$. 28 g of $MnSO_4$ and 18 g of $KMnO_4$ were dissolved in 500 mL of aquademin. The Solution was mixed with 10 g of NaOH and stirred at a temperature of ±80°C. The mixture was allowed to cool to room temperature, filtered, washed with distilled water, left to dry for 24 hours. This was followed by calcination at ±250°C for 3 hours, and the concentration of the separated filtrate was determined using permanganometric titration.

2.5 Standardization of $KMnO_4$ Solution

The 25 mL of distilled water was put into a container of 1.25 mL of 8 N H_2SO_4 solution and heated to ±70°C. This was followed by the addition of 2.5 mL of 0.1 N $H_2C_2O_4$ and titrated with a 0.1 N $KMnO_4$ 0,1 N until the solution changed color from clear to pink. The titration was carried out in duplicate and the volume was recorded [14].

2.6 Permanganometric Titration of the Filtrate

Oxalic acid weighed ±0.15 g and was dissolved in 50 mL of distilled water in an Erlenmeyer. Approximately 5 mL of filtrate was added and heated to a temperature of ±60°C to ±70°C. Subsequently, 5 mL of 4 N H_2SO_4 was added and diluted to 100 mL with distilled water. The solution was titrated with 0.1 N $KMnO_4$ until it turned pink. This procedure was carried out in duplicate [15].

2.7 Determination of Water Content (SNI 06-3730-1995)

Empty porcelain cups were dried in an oven at ±105°C for 30 minutes, cooled in a desiccator, and weighed (W_0). Porcelain cups were used to weigh samples of activated carbon and AC/MnO_2 composite, consisting of 1 g (W_1). This showed the water content of activated carbon and the AC/MnO_2 composite. A porcelain cup containing the sample was placed in an oven at a temperature of ±105°C for 2 hours, cooled in a desiccator and weighed (W_2). Equation (1) is a formula for calculating water content.

$$\text{Water Content} = \frac{W_1 - W_2}{W_1 - W_0} \times 100\% \quad \textbf{....(1)}$$

2.8 Preparation of Uranium Solution

A total of 0.4464 g of uranyl acetate compound was weighed and 10 mL of 2.5 N HNO_3 solution was added until dissolved. This was followed by dilution

with aquamine in a 250 mL measuring flask, achieving uranium concentration of 1000 ppm. A total of 10 mL of a 1000 ppm uranyl acetate solution was pipetted and diluted in a 100 mL volumetric flask using a 0.05 N HNO_3 solution. The uranium content in this solution was 100 ppm [16].

2.9 Calibration Curve Determination

A total of 10, 25, 50, and 75 mL of 100 ppm uranyl acetate solution were taken into a 100 mL volumetric flask (uranyl acetate solution concentration 10, 25, 50, and 75 ppm). Approximately 5 drops of concentrated HCl, 15 mL of aquadenim, 8 mL of 4 M NH_4SCN 4 M, and 2 mL of 5% $SnCl_2$ 5%, were added to each measuring flask and diluted with aquadenim to the limit mark. The Solution was stirred until homogeneous and left for 30 minutes to allow the formation of a perfect yellow color [16]. Measurement was carried out with a UV-Vis spectrophotometer at a wavelength of 306 nm.

2.10 Determination of AC/MnO_2 Mass

The 4 black glass bottles were each filled with 50 mL of 100 ppm uranyl acetate solution. Subsequently, 1 g of adsorbent was added to each bottle, 1.5g, 2 g, and 2.5 g, stirred with a shaker at 225 rpm for 60 minutes and left for 1 night [17]. The mixture obtained was filtered with filter paper. 5 mL of each filtrate obtained was taken, followed by the addition of 5 drops of concentrated HCl, 15 mL of aquademin, 8 mL of 4 M NH_4SCN, and 2 mL of 5% $SnCl_2$ 5%, which were diluted with aquademin to the limit mark. The solution was stirred until homogeneous and left for 30 minutes to allow the formation of a perfect yellow color [16]. This was followed by measuring the solution with a UV-Vis spectrophotometer at a wavelength of 306 nm.

2.11 Determination of Adsorbent Contact Time

There are 3 black glass bottles filled with 50 mL of 100 ppm uranyl acetate solution. This was followed by the addition of 2.5 g of adsorbent to each bottle and stirred with a shaker at a speed of 225 rpm with a time variation of 40, 50, and 60 minutes [18]. The mixture obtained was filtered with filter paper. 5 mL of each filtrate obtained was taken, followed by the addition of 5 drops of concentrated HCl, 15 mL of aquademin, 8 mL of 4 M NH_4SCN 4 M, and 2 mL of 5% $SnCl_2$, which were diluted with aquademin to the limit mark. Solution was stirred until homogeneous and left for 30 minutes to allow the formation of a perfect yellow color [16]. This was followed by measuring solution with a UV-Vis spectrophotometer at a wavelength of 306 nm.

The determination of the Langmuir adsorption isotherm model was carried out by plotting the x curve as Qe and y as Qe/Ce. The data obtained was calculated using Equation 1. The determination of the Freundlich isotherm plots the x curve as Log Ce and y as Log Qe. The Data was calculated using equation (2) and (3).

$$Qe/Ce = kQo - kQe \quad \textbf{(2)}$$

$$Log\ Qe = Log\ kF + 1/n\ Log\ Ce \quad \textbf{(3)}$$

where:
Ce : equilibrium concentration of adsorbate (mg/L)
Qe : the amount of adsorbate in adsorbent at equilibrium (mg/g)
Qo : adsorption capacity (mg/g)
K : Langmuir isotherm constant
kF : Freundlich isotherm constant
n : Adsorption intensity

The adsorption kinetics model was determined to identify the rate of adsorbent absorption over a certain period. The first and second-order pseudo models were selected with the assumption that the adsorption of uranyl ions by the AC/MnO_2 composite is reversible. The first-order pseudo model was calculated using equation 4, while the second-order pseudo model used equation 5.

$$\log (qe-qt) = \log qe-(k_1/2{,}303)t \quad \text{.....(4)}$$

$$t/qt = (1/k_2\, qe^2) + t/qe \quad \text{..... (5)}$$

where:

qt : the amount of adsorbate adsorbed by adsorbent at time t (mg/g)
qe : the amount of adsorbate adsorbed at equilibrium (mg/g)
k1 : pseudo rate constant 1(min^{-1})
k2 : pseudo rate constant 2 (g min^{-1} mg^{-1})

3. Results and Discussion

3.1 Carbonization of OPEFB

The Preparation of OPEFB was carried out by reducing its size and distribution to expand its surface and increase heat transfer during the carbonization process. Soaking in hot water removed impurities and oil from the fiber, thereby preventing heat inhibition during the carbonization process. In this research, drying was performed by sun-drying OPEFB to remove any remaining water in the fibers.

Carbonization was carried out in a furnace at a temperature of ±350°C for 1 hour to degrade lignocellulose and volatile substances such as CO, CO_2, CH_4, and H_2. The final product obtained was carbon in the form of charcoal, with a by-product, namely tar. In carbonization process, water and remaining oil evaporated as well as the decomposition of wood components into liquid smoke [11], leaving carbon (C) in the raw material. The results of OPEFB carbonization produced black charcoal with a brittle and light texture. The charcoal was crushed and sieved using a 100-mesh sieve to obtain a uniform size. The carbon yield from OPEFB obtained was 72%.

3.2 Carbon Activation

The process of carbon activation was carried out using sodium acetate to decompose tar and expand carbon pores by removing impurities [4]. The immersion process ensured the interaction and penetration of the sodium acetate solution into the carbon material. Heating was performed to accelerate the penetration process and open carbon pores [13].

The remaining salt attached to the charcoal surface was replaced by –OH groups when carbon was washed using distilled water, increasing in activated groups [19] through ion exchange reactions. The filtered filtrate was yellow due to the dissolution of most inorganic minerals, non-carbon compounds, and tar remaining in carbon pores. The activated carbon was dried at ±105°C for 2 hours to evaporate the remaining water. The yield of activated carbon obtained after the activation process was 98.1%.

Figure 1. (a) Carbon before activation, (b) Activated carbon

The by-products of the activation process were acetic acid and sodium hydroxide, causing physical and chemical changes to carbon. Visually, the activated carbon obtained had a smoother texture,

and the color was slightly blacker than before activation, as shown in Figure 1.

3.3 AC/MnO_2 Composite

AC/MnO_2 composite was made by mixing activated carbon into MnO_2 solution using an in situ deposition method in a reaction mixture. During this process, the reaction between the oxidizing and reducing agents produced an exothermic reaction. The synthesis of MnO_2 occurred due to the oxidation reaction of Mn^{2+} from $MnSO_4.H_2O$ to Mn^{4+} using the $KMnO_4$ oxidizer in alkaline conditions with NaOH to form a brown MnO_2 precipitate [20]. Heating to a temperature of ±80°C caused the release of water or hydroxide hydration. This led to the formation of the manganese oxide composite in the activated carbon structure [21]. The filtered composite was rinsed with distilled water to dissolve the remaining impurities, allowed to dry for 24 hours, and calcined at ±250°C for 2 hours.

The calcination process was carried out to obtain high-purity oxide powder by releasing gases in the form of carbonates or hydroxides and decomposing compounds such as salts or dihydrates. H_2O and OH were released in the temperature range of ±100°C to ±300°C [22].

Figure 2 shows the reaction between activated carbon from OPEFB and manganese dioxide. Due to the presence of a hydroxy group (-OH) MnO_2, interaction can occur within activated carbon from OPEFB by forming Mn-O bonds on the surface [10]. The resulting activated carbon layered with MnO_2 has a blackish-brown color, as shown in Figure 3.

3.4 Permanganometric Titration

Permanganometric titration was conducted to determine the remaining concentration of MnO_2 in the filtrate. Initially, the $KMnO_4$ solution was standardized due to instability. In permanganometric titration, MnO_4^- ions acted as a potent oxidizing agent, while $C_2O_4^{2-}$ ion in oxalic acid was used as a reductor. In this research, back titration was carried out by mixing the filtrate with excess oxalic acid and titrated using $KMnO_4$ solution. The titration was conducted in an acidic environment for the optimal reaction of MnO_4^- ions, and $KMnO_4$ would experience a reduction to produce colorless Mn^{2+} ions. The reaction between $KMnO_4$ and oxalic acid tended to be slow at room temperature, resulting in difficulty in determining the endpoint of the titration. Therefore, heating was carried out before titration to accelerate the reaction, with $KMnO_4$ serving as an auto-indicator. The color change in permanganometric titration was colorless to pink [23], using 0.2 mL as the average volume of titrant. This titration was performed to show that the MnO_2 concentration obtained decreased from 0.5524 M to 0.0001 M.

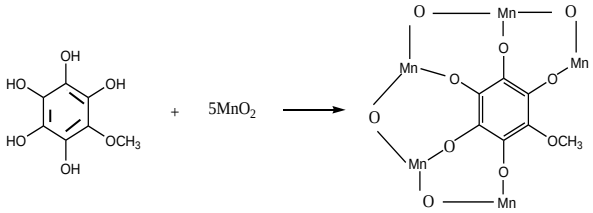

Figure 2. Prediction of the reaction between activated carbon and MnO_2 [10]

Figure 3. Activated carbon after being layered with MnO_2 (AC/MnO_2)

3.5 Characterization of Activated Carbon and AC/MnO_2 Composite

Water content analysis was performed to determine the hygroscopic properties and quality of the adsorbent based on the percentage of water content obtained [24]. Moreover, less water content in the adsorbent contributes to improved absorption. This is because water molecules do not cover the pores, thereby increasing their capacity on the activated side [25]. Based on the results obtained in Table 1, the water content of activated carbon and AC/MnO_2 composite was still within the standard, with a value below 15% as stated in SNI 06-3730-1995.

Table 1. Results of water content analysis

Sample	Water Content (%)
Water content	8.0
AC/MnO_2	1.3

The activate carbon and AC/MnO_2 composites were characterized using FTIR to determine the functional groups and bonds contained in the adsorbent, as shown in Table 2. The results of activated carbon analysis using FTIR in Figure 4, showed absorption at wave number 3448.7cm^{-1} which indicated the presence of Stretching vibrations of O-H. The wave number at 1708 cm^{-1} showed the presence of a C=O double bond [16], while 1585.4 cm^{-1} indicated an aromatic C=C bond [26].

The results of AC/MnO_2 analysis using FTIR showed that the absorption at wave number 3394.7 cm^{-1} was the stretching vibration of O-H. At 1618.2 cm^{-1}, the presence of C=O bond vibrations was shown, while 1570 cm^{-1} indicated C=C aromatic bonds [9],[25]. In the AC/MnO_2 composite, absorption wave numbers of 542 cm^{-1}, 584.4 cm^{-1}, and 746.4 cm-h showed the presence of Mn-O bonds and stretching vibrations of Mn-O-Mn bonds. According to Ying et al. [9] and Wang et al. [27], the absorption of stretching vibrations of Mn-O-Mn and Mn-O bonds was shown at wave numbers 500 cm^{-1} to 800 cm^{-1}.

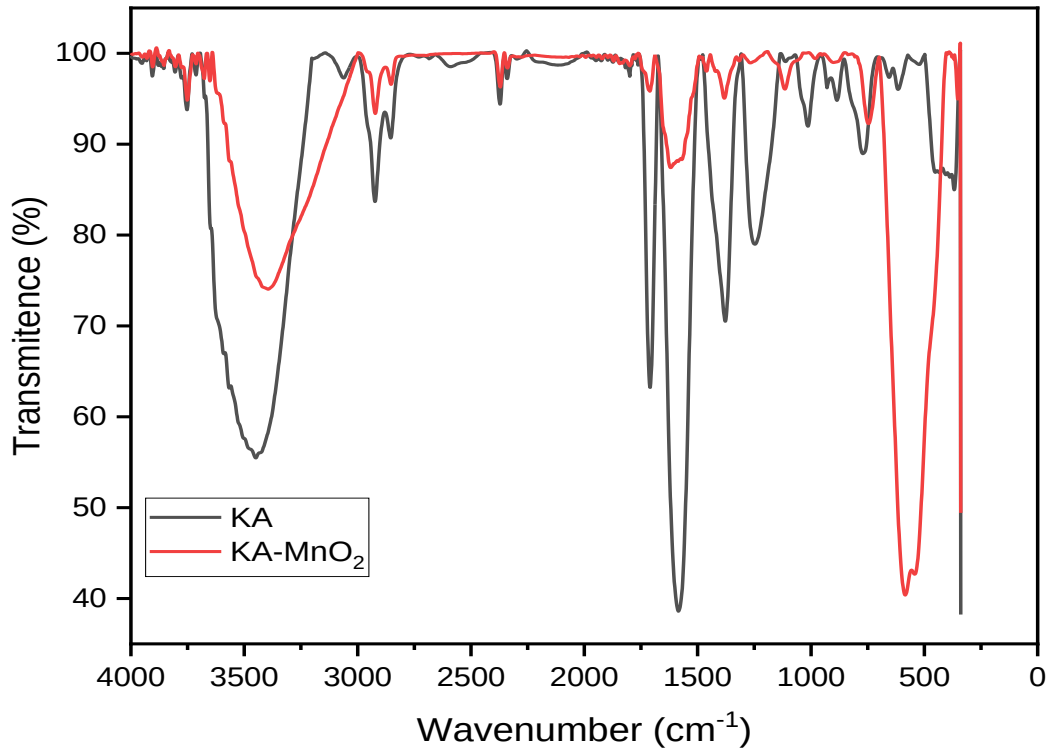

Figure 4. FTIR spectrum from activated carbon characterization

Table 2. FTIR characterization results

	Wavelength number (cm^{-1})		
Activated Carbon (AC)	3448.7 O-H	1708 C=O C=C	1585.4 C=C aromatic
AC/MnO_2	3394.7 O-H	1618.2 1570 C-O C=C aromatic	542 584.4 746.4 Mn-O-Mn Mn-O

3.6 Calibration Curve

Calibration curve shows the relationship between absorbance (Y) and concentration (X), obtaining an equation expressed as Y = aX ± b. In this research, a 100 ppm uranyl acetate solution was made into 10, 25, 50, and 75 ppm in acidic conditions using concentrated HCl. The function of th solution was to avoid the decomposition of the NH_4SCN and $SnCl_2$ solution, to form a yellow uranyl thiocyanate compound complex [16]. The linear equation of the curve obtained from a concentration of 10, 25, 50, and 75 ppm was y = 0.013x + 0.822 with a value of R^2 = 0.989, as shown in Figure 5.

3.7 Effect of AC/MnO_2 Adsorbent Mass

Based on the results in Figure 7, the highest percentage effectiveness of adsorption of uranyl ions was at a mass variation of 2.5 g adsorbent with an adsorption percentage of 65.5%. The amount of mass used affected the adsorbate absorption process due to the availability of activated sites on adsorbent, which could bind the adsorbate effectively. The adsorption mechanism occurred in activated carbon pores. An interaction was also observed between uranyl ion and the AC/MnO_2 adsorbent. Specifically, the positively charged uranyl ion was adsorbed with the negatively charged AC/MnO_2 adsorbent. Uranyl ion was bound by two oxygen atoms in manganese dioxide through a Mn-O bond, forming a coordination bond in activated carbon pore [10]. The structure predictions in Figure 6 were made based on the illustrations of Wang et al. [27] and Ying et al. [9].

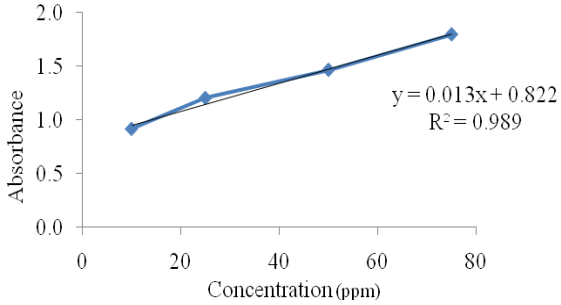

Figure 5. Calibration curve

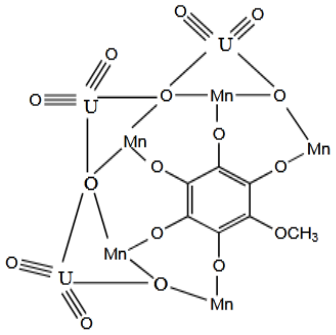

Figure 6. Prediction of the Chemical Structure of AC/MnO_2 with Uranyl Ions $(UO_2)^{2+}$.

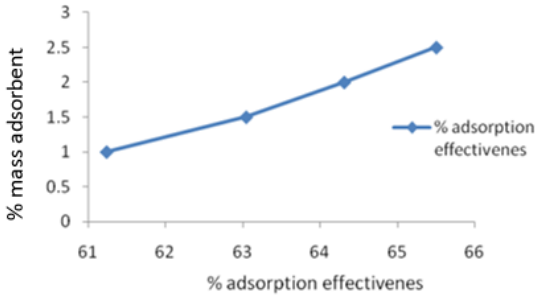

Figure 7. The curve of the influence of adsorbent mass on the % effectiveness of uranyl adsorption

3.8 Effect of AC/MnO_2 Adsorbent Contact Time

Based on the results in Figure 8, the highest percentage effectiveness of uranyl ion adsorption occurred when using a contact time of 60 minutes with an adsorption percentage of 40.6%. The time spent interacting between adsorbent and the adsorbate caused bonds to form between the AC/MnO_2 composite and uranyl. This led to a decrease in the concentration of uranyl in solution after adsorption, while percentage effectiveness increased.

3.9 Determination of the Adsorptions Isotherm and Kinetics Models

The adsorption isotherm model was examined to determine the adsorption mechanism that formed. In this research, the adsorption isotherms used in the solid-liquid phase were the Langmuir and the Freundlich, with the curve results presented in Figures 9 and 10. The adsorption isotherm of uranyl ions using the AC/MnO_2 adsorbent was based on the concentration of the sample solution absorbed by adsorbent. In this context, the Langmuir isotherm type was obtained as shown by the R^2 value, which was close to one (0.999) with a positive constant (K_L), 0.023 L/mg.

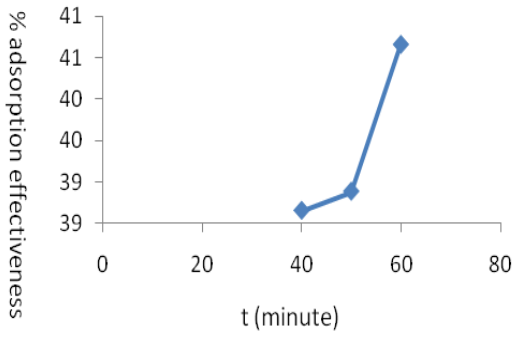

Figure 8 The effect of adsorbent contact time on the % effectiveness of uranyl adsorption.

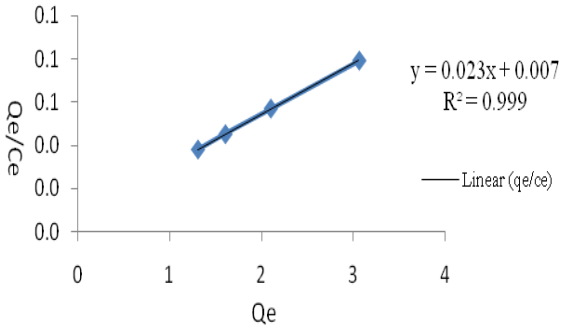

Figure 9. Langmuir isotherm model curve for uranyl adsorption.

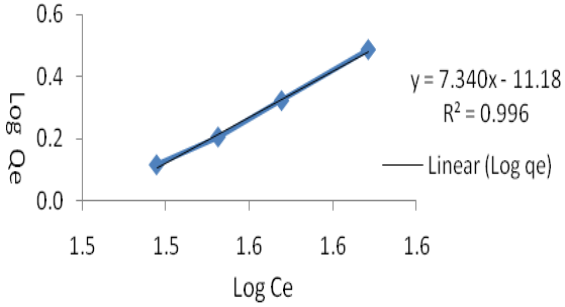

Figure 10. Freundlich isotherm model curve for uranyl adsorption

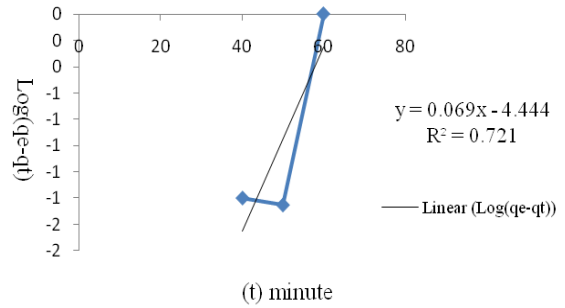

Figure 11. Pseudo-first order uranyl adsorption kinetics curve

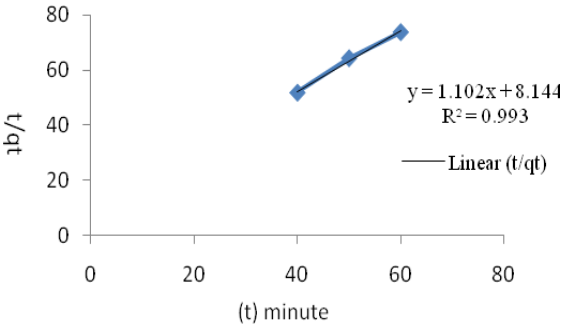

Figure 12. Pseudo-second order uranyl adsorption kinetics curve

Uranyl adsorption process with AC/MnO_2 adsorbent from OPEFB in this research followed the Langmuir isotherm equation. Linearity in the Langmuir isotherm equation shows that chemical adsorption occurs. Uranyl ions bound to the AC/MnO_2 adsorbent form a monolayer.

A mass transfer is observed from the adsorbate as well as a sharing of electrons between the AC/MnO_2 adsorbent and uranyl ions. Therefore, the adsorption mechanism includes physicochemical interactions. Generally, adsorption kinetics state the speed of the adsorbate absorption process by the adsorbent. It is expressed as a function of concentration versus time to obtain a rate constant value (k). Adsorption kinetics are determined based on pseudo-first-order, as in Figure 11, and pseudo-second-order, as in Figure 12.

The appropriate adsorption kinetic model is shown from the R^2 value, which is closest to 1, namely the pseudo-second-order with a value of 0.993 and rate constant (k2) of 6.7 g/mg.minute. This reaction rate constant describes the adsorption equilibrium that occurs when the reactant comes into contact with adsorbent surface and forms a product in the form of uranyl ions, bound to the surface of the AC/MnO_2 adsorbent.

4. Conclusion

In conclusion, this research showed that the formation of AC/MnO_2 adsorbent was due to the presence of hydroxy groups (-OH) on activated carbon from OPEFB. Therefore, MnO_2 could interact by forming Mn-O bonds on the surface of activated carbon. The reduction in uranium content of uranyl compounds in solution using the AC/MnO_2 adsorbent led to an adsorption percentage of 60.5%, with a Langmuir isotherm constant (K_L) value of 0.023 L/mg and using pseudo-second order.

References

[1] Yazid, M. (2014). Peranan Isolat Bakteri Indigenous sebagai Agen Bioremediasi Perairan yang Terkontaminasi Uranium. *Jurnal Iptek Nuklir Ganendra*, 17(1), 35-44, doi:10.17146/gnd.2014.17.1.1300

[2] Xiao-teng, Z., Dong-mei, J., Yi-qun, X., Jun-chang, C., Shuai, H., & Liang-shu, X. (2019). Adsorption of Uranium (VI) from Aqueous Solution by Modified Rice Stem. *Journal of Chemistry*, (1), 1-10, doi: 10.1155/2019/6409504

[3] Richana, N., Lestiana, P., dan Irawadi, T. (2004). Karakterisasi Lignoselulosa dari Limbah Tanaman Pangan dan Pemanfaatannya untuk Pertumbuhan Bakteri RXA III-5 Penghasil Xilanase. Penelitian Pertanian Tanaman Pangan, 23(3), 171-176, Retrieved from http://pangan.litbang.pertanian.go.id/repositori

[4] Taer, E.; Mustika W. S., dan Sugianto. (2016). Pemanfaatan Potensi Tandan Kosong Kelapa Sawit Sebagai Karbon Aktif untuk Pembersih Air Limbah Aktivitas Penambangan Emas. *Jurnal Komunikasi Fisika Indonesia*, 13(13), 852-858, doi: 10.31258/jkfi.13.13.852-858

[5] Gova, A.M., dan Oktasari A. (2019) *Arang Aktif Tandan Kosong Kelapa Sawit Sebagai Adsorben Logam Berat Merkuri (Hg)*. (Skripsi, Universitas Islam Negeri Raden Fatah)

[6] Langenati, R., M Mordiono R., Mustika D., Wasito B., dan Ridwan. (2012). Pengaruh Jenis Adsorben dan Konsentrasi Uranium Terhadap Pemungutan Uranium dari Larutan Uranil Nitrat. *Jurnal Teknik Bahan Nuklir.*, 8(2), 95-104, http://jurnal.batan.go.id/index.php/jtbn/article/view/812

[7] Chaundhry, A. S., Khan, A. T., dan Ali, I. (2016). Adsorptive Removal of Pb(II) and Zn(II) from Water Onto Manganese Oxide-Coated Sand: Isoterm, Thermodynamic and Kinetic Studies. *Egyptian Journal of basic and Applied Sciences*, 3(3), 287-300, doi: 10.1016/j.ejbas.2016.06.002

[8] Effendi, Devi, B., Nurul, H. L., Asep B., dan Dani, N. (2015) Review: Sintesis Nanoselulosa 1. *Jurnal Integrasi Proses*, 5(2), 61-67, http://jurnal.untirta.ac.id/index.php/jip

[9] Ying, D., Hong, P., Jiali, F., Qinqin, T., Yuhui, L., Youqun, W., Zhibin, Z., Xiaohong, C., & Yunhai, L. (2020). Removal of Uranium Using MnO_2/Orange Peel Biochar Composite Prepared by Activation And In-Situ Deposit in a Single Step. *Biomassa and Bioenergy*, 142, 2-10, doi: 10.1016/j.biombioe.2020.105772

[10] Hustiany, R., dan Rahmi, A. (2019). *Kemasan Aktif Berbasiskan Arang Aktif Tandan Kosong dan Cangkang Kelapa Sawit.* Purwokerto: CV IRDH.

[11] Sopiah, N., Prasetyo, D., dan Aviantara, B.D. (2017). Pengaruh Aktivasi Karbon Aktif dari Tandan Kosong Kelapa Sawit Terhadap Adsorpsi Cadmium Terlarut. *Jurnal Riset Teknologi Pencegahan Pencemaran Industri*, 8(2), 58-66, doi: 10.21771/jrtppi.2017.v8.no.2.p55-66

[12] Irma, K. N., Wahyuni, N., dan Zaharah, T. A. (2015). Adsorpsi Fenol Menggunakan Adsorben Karbon Aktif dengan Metode Kolom. *Jurnal Kimia Khatulistiwa*, 4(1), 24-28, https://jurnal.untan.ac.id/index.php/jkkmipa/article/view/11723

[13] Apriyanti dan Apriyani, M. E. (2018). Analisis Kadar Zat Organik pada Air Sumur Warga Sekitar TPA dengan Metode Titrasi Permanganometri. *ALKIMIA: Jurnal Kimia dan Terapan*, 2(2), 11-14, doi: 10.19109/alkimia.v2i2.2988

[14] Abriani, D. T. (2020). Penetapan Kadar MnO_2 dalam Batu Kawi Secara Permanganometri. https://youtu.be/opLe5K5Sqqs.

[15] Adventini, N., Lestiani, D. D., Muhayatun, dan Damastuti, E. (2009). *Penentuan Kadar Uranium pada Serbuk UO_2 dan U_3O_8 Menggunakan Spektrofotometri UV-Vis*. Prosiding Seminar Nasional Sains dan Teknologi Nuklir, Bandung: PTNBR-BATAN.

[16] Selumbung, Y. K. N., dan Langenati, R. (2012). *Pemungutan Uranium Dalam Efluen Proses Menggunakan Komposit Magnetik-Karbon Aktif.* Seminar Nasional VIII SDM. Yogyakarta: Teknologi Nuklir.

[17] Tolumeko, L. C., Sesa E., dan Darwis., D. (2017). Penentuan Waktu Kontak Optimum dan Massa Optimum Arang Aktif Kulit Kakao Sebagai Adsorben Ion Timbal (Pb). *Gravitasi*, 16(1), 27-32, doi: 10.22487/gravitasi.v16i1.9466

[18] Arif, A. R. (2014). *Adsorpsi Karbon Aktif dari Tempurung Kluwak (Pangium Edule) terhadap Penurunan Fenol*. (Skripsi, Universitas Islam Negeri Alauddin).

[19] Suriadi, A., Shofiyani, A., dan Destiarti, L. (2017). Sintesis dan Karakterisasi Pasir Besi Terlapis Mangan Dioksida serta Aplikasinya untuk Penurunan Kadar Ion Fosfat dalam Air. *Jurnal Kimia Khatulistiwa*, 6(1), 64-72, https://jurnal.untan.ac.id/index.php/jkkmipa/article/view/18550/15646

[20] Istiana, S., Jumaeri & Agung T., P. (2020). Preparasi Arang Aktif Trembesi Magnetit untuk Adsorpsi Senyawa Tannin dalam Limbah Cair. *Indonesian Journal Chemical Science*, 9(1), 18-23, http://journal.unnes.ac.id/sju/index.php/ijs

[21] Lisdawati, A.N. (2015). Pengaruh Variasi Suhu dan Waktu Kalsinasi pada Pembentukan Fasa ZrO_2. *Tesis*, Institut Teknologi Sepuluh November

[22] Putra, F. A., dan Sugiarso R. D. (2016). Perbandingan Metode Analisis Permanganometri dan Serimetri dalam Penentuan Kadar Besi (II). *Skripsi*, Institut Teknologi Sepuluh November).

[23] Sahara, E., Wahyu, D., S., dan I., Putu, A., S., M. (2017). Pembuatan dan Karakterisasi Arang Aktif dari Batang Tanaman Gumitir yang Diaktivasi dengan H_3PO_4, *Jurnal Kimia*,11(1), 1-9, doi: 10.24843/JCHEM.2017v11.io1.po1

[24] Sa'diyah, K., Suharti H. K., Hendrawati, N., Pratamasari, F.A., dan Rahayu, M.O. (2021). Pemanfaatan Serbuk Gergaji Kayu sebagai Karbon Aktif melalui Proses Pirolisis dan Aktivasi Kimia. *CHEESA: Chemical Engineering Research Articles*, 4(1), 91-99, doi: 10.25273/cheesa.v4i2.8589.91-99

[25] Efiyanti, L., Wati, S. A., dan Maslahat, M. (2019). Pembuatan dan Analisis Karbon Aktif dari Cangkang Buah Karet dengan Proses Kimia dan Fisika. *Jurnal Ilmu Kehutanan*, 14(1), 94-108, doi: 10.22146/jik.57479

[26] Wang, Z., Zhong, M., dan Chen, L. (2015). Coal-Based Granular Activated Carbon Loaded with MnO_2 as an Efficient Adsorbent for Removing Formaldehyde from Aqueous Solution. *Desalination and Water Treatment.* 57(28), 13225-13235, doi:10.1080/19443994.2015.1057533

[27] Wang, Z., Lee, S-W., Catalano, J. G., Lazema-Pacheco, J. S., Bargar, J. R., Tebo, M. B., & Giammar, D. E. (2012). Adsorption of Uranium (VI) to Manganese Oxides: X-ray Absorption Spectroscopy and Surface Complexation Modeling. *Environmental Science & Technology*, 42(2), 850-858, doi:10.1021/es304454g

CHEESA: Chemical Engineering Research Articles
ISSN 2614-8757 (Print), ISSN 2615-2347 (Online)
Available online at: http://e-journal.unipma.ac.id/index.php/cheesa

Research Article

Optimization of Particle Size and Addition of Vinasse Waste to Improve Characteristics of Rice Husk Charcoal Briquettes

Optimasi Ukuran Partikel dan Penambahan Limbah Vinasse dalam Meningkatkan Karakterstik Briket Sekam Padi

Sintha Soraya Santi[1*)], Tsania Putri Azzahra[1)], Dian Rizka Salfana[1)], Timotius Pasang[2)]
[1)]Universitas Pembangunan Nasional "Veteran" East Java, Department of Chemical Engineering, Faculty of Engineering and Science, Surabaya, 60294, Indonesia
[2)]Western Michigan University, Engineering Design, Manufacturing, & Management System, Kalamazoo, Michigan, MI 49008, United States of America

Article History
Submitted: 28th March 2024; Revised: 06th August 2024; Accepted: 06th August 2024;
Available online: 21th August 2024; Published Regularly: June 2024

doi: 10.25273/cheesa.v7i1.19575.36-46

*Corresponding Author.
Email: sintha.tk@upnjatim.ac.id

Abstract

Biobriquettes are a biomass fuel with high calorific value. This study aims to determine the optimal conditions for the particle size of husk charcoal and the addition of vinasse waste as an independent variable, using the Response Surface Methodology and the Central Composite Design (CCD) method on Design Expert 13 software. The sample mixed with tapioca starch (8:1), which acts as an adhesive, and add vinasse waste in 3, 6, 9, and 12 mL amounts. Carbonization process, which is then mashed and sieved according to particle sizes of 20, 30, 40, 50, and 60 mesh. Then, the sample is mixed with tapioca starch as adhesive with the ratio of charcoal and adhesive 8:1 as well as vinasse waste in volumes of 3, 6, 9, and 12 mL. The resulting briquette samples were tested in the form of water content, ash content, and calorific value tests. The optimum conditions that have a significant effect on the response variable are the combination of particle size variables of 35.152 mesh and the volume of vinasse waste of 6.049 mL. The moisture content obtained was 6.696%., The ash content was 5.450%, and the calorific value was 5003.399 cal/g with a desirability value of 0.927 in the quadratic model.

Keywords: biobriquettes; optimization; Response Surface Methodology; rice husk briquettes

Abstrak

Biobriket merupakan salah satu bahan bakar biomassa yang memiliki nilai kalor yang tinggi. Penelitian ini bertujuan untuk mengetahui kondisi optimal pada ukuran partikel arang sekam dan penambahan limbah vinasse sebagai variabel bebas dengan menggunakan Response Surface Methodology metode Central Composite Design (CCD) pada perangkat lunak Design Expert 13. Proses pembuatan briket arang sekam padi dilakukan dengan proses karbonisasi yang kemudian dihaluskan dan diayak sesuai dengan ukuran partikel yaitu 20, 30, 40, 50, dan 60 mesh. Kemudian, sampel dicampur dengan tepung tapioka sebagai perekat dengan perbandingan arang dan perekat 8:1 serta limbah vinasse dengan volume 3, 6, 9, dan 12 mL. Sampel briket yang dihasilkan dilakukan pengujian berupa uji kadar air, kadar abu, dan nilai kalor. Kondisi optimum yang berpengaruh signifikan terhadap variabel respon adalah kombinasi variabel ukuran partikel 35,152 mesh dan volume limbah vinasse 6,049 mL. Kadar air yang diperoleh sebesar 6,696%, kadar abu sebesar 5,450%, dan nilai kalor sebesar 5003,399 kal/g dengan nilai desirability sebesar 0,927 pada model kuadratik.

***Kata kunci**: biobriket; briket sekam padi; optimasi; Response Surface Methodology*

1. Introduction

With the growing times, alternative gas fuels are needed to reduce the increasing consumption of LPG. One alternative that can be used is the utilization of biomass as a more environmentally friendly fuel with raw materials that generally come from industrial and agricultural waste.

Charcoal briquettes, a product derived from biomass utilization, represent an alternative fuel that is both easy to produce and implement [1]. They are made by mixing fibrous waste with adhesives to bind charcoal particles together, ensuring the briquettes are durable and resistant to breakage [2]. In the process, low-density biomass is processed into a high-density, energy-concentrated fuel [3]. The biomass feedstock is selected based on its high content of the main organic compound, cellulose. Rice husk is often utilized as a fuel because rice husk is composed of cellulose fibrous tissue that contains a lot of very hard silica [4]. Generally, rice husk contains about 31% cellulose and 16% silica [5]. The quality of the briquettes depends on the physicochemical properties of the biomass (particle size and surface area), as well as parameters such as compression rate, residence time, temperature, pressure, and the adhesive used [6].

Vinasse is the liquid waste that remains after the ethanol distillation process. Vinasse can be used to produce organic adhesives (lignosulfonates) which have many applications in various industries [7]. Vinasse also has a high content of salts, organic compounds, and inorganic compounds such as carbohydrates, proteins, nitrogen, sulfur, minerals, phosphorus, and other heavy metals. Vinasse has 3.1% carbon. Due to their, carbon content, vinasse can be applied as an ingredient in the manufacture of briquettes because they can improve physical properties, be able to accelerate the ignition of briquettes, and produce a high enough briquette combustion temperature [8].

Briquettes have several quality parameters including moisture content, ash content, and calorific value. High moisture content in briquettes reduce their quality, a problem exacerbated by smaller charcoal particle sizes, which tend to retain moisture due to smaller pore sizes, making drying more difficult. According to SNI 01-6235-2000, the standard moisture content of briquettes should not exceed 8%. Lower ash content indicates higher-quality briquettes, as they burn more efficiently without turning into ash during combustion. According to SNI 01-6235-2000, the maximum ash content is 8% [9]. Calorific value is another crucial indicator of briquette quality, influenced by moisture content, ash content, carbon content, and volatile matter. According to SNI 01-6235-2000, the minimum calorific value of briquettes is 5000 calories per gram.

In previous studies, experience may decrease in quality, but they can evenly distribute heat, ensuring complete combustion [10]. However, there has been limited research on optimizing the addition of vinasse waste in order to improve the quality of briquettes. Optimization in the research can be achieved through the Response Surface Methodology (RSM) method, an experimental approach necessary to understand how various factors affect the response. The aim is to identify the conditions that yield the optimal response.

Experimental designs include Full Factorial 3-Level Design (FFD), Box-

Behnken Design (BBD), and Central Composite Design (CCD). CCD in the optimization process to determine the approximate optimal conditions with unknown optimization and optimal location. In CCD, the test points are taken based on the test limit values determined for each research factor. The response data obtained is modeled by the appropriate mathematical model. In CCD, there are several models, namely mean, linear, quadratic, 2-factor interaction (2FI), and cubic [11].

In this study, optimization is needed on the particle size factor and the volume of vinasse waste. This is because the particle size can affect the density of the briquette. Whichever the particle size, can increase the density of the briquette. The higher density value also produced the higher heating value [12]. Then, for optimization of the volume of vinasse waste, the addition of vinasse waste concentration can affect the physical quality of briquettes because vinasse waste contains various organic and inorganic compounds that can provide more even heat and increase combustion temperature [8].

2. Research Methods

This research was conducted through several steps. Starting with the carbonization of rice husks, crushing, screening, mixing with adhesives, and printing. Then the briquette samples were tested for moisture content, ash content, and calorific value, the results of which were optimized using the Response Surface Methodology (RSM) method with Design Expert 13 software to determine the optimum particle size and addition of vinasse waste.

2.1 Tools and Materials

The tools were used in this research include a sieve, an oven, an analytical balance, pipe mold, and a furnace. The materials used in this research include rice husk, vinasse waste, and tapioca flour.

2.2 Research Procedure

The research was conducted in three steps. The first step involves the process of making briquettes, which includes carbonization, briquette formation, printing, and drying. Rice husk is carbonized in a furnace with a temperature of 250^{o}C to obtain rice husk charcoal. The charcoal is then sieved to uniform sizes of 20, 30, 40, 50, and 60 mesh. It is mixed with tapioca glue adhesive in a ratio of 1:8 (tapioca glue to charcoal) and vinasse waste in volumes of 3, 6, 9, and 12 mL. Subsequently, the mixture is printed and dried into briquettes at a temperature of 75^{o}C.

The second step is the process of testing the quality of briquettes, including analyzing moisture content, ash content, and calorific value. The third step is the process of processing data analysis results to obtain optimal results using RSM Design Expert 13.

2.3 Briquettes Analysis

The analysis of briquettes consisted of moisture content analysis, ash content analysis, and calorific value analysis. Moisture content shows the value of moisture content tends to increase with the smaller particle size of charcoal briquettes. This is because the smaller the particle size, the smaller the pore size produced, so that during drying, the water in the briquette will be difficult to evaporate [9]. In this research, the analysis of moisture content using ASTM (American Standard

Testing and Material) D 5142 - 02 with the equation (1) [13].

$$\text{Moisture Content}(\%) = \frac{BD - AD}{BD} \times 100\% \quad ..(1)$$

Description:
BD =Weight before drying in the oven (g)
AD =Weight after drying in the oven (g)

Ash content greatly affects the heating value. A low ash content can produce a high heating value. High ash content can reduce the calorific value of the briquettes, which makes the quality of the charcoal briquettes decrease. According to SNI, a good moisture content for briquette products is less than 8% [14]. In this study, the ash content analysis used ASTM D 5142 - 02 with the equation (2) [13].

$$\text{Ash Content}(\%) = \frac{\text{Ash weight}}{\text{Sample weight}} \times 100\% \quad ...(2)$$

Calorific value is the energy that is transferred through a system due to the temperature difference between the system and the environment, which is called heat [15]. The calorific value of fuel is said to be the maximum amount of heat energy released through complete combustion of the fuel itself. The calorific value of fuel can be known with a bomb calorimeter tool. The principle of calculating the total energy in briquettes is the amount of heat produced when one briquette is completely oxidized in a bomb calorimeter. Based on SNI. 01-6235-2000, charcoal briquettes are said to be of quality if the calorific value in briquettes is more than 5000 cal/g [16].

After the analysis, the data is processed into RSM optimization. In this research, optimization is carried out using the RSM method with the CCD type whose parameters can be seen in the Table 1.

3. Results and Discussion

Optimization was carried out with the factors of particle size and volume of vinasse waste on physical properties, namely moisture content, ash content, and calorific value of rice husk charcoal briquettes, as well as responses on the dependent variable from 11 experiments using the Design Expert 13 application. Experimental design in the form of CCD can be seen in Table 2.

Table 1. Parameters of CCD for briquette making process

Level	Factor	
	A: Particle Size	B: Vinasse Waste Volume
Low (-1)	20	0
Moderate (0)	40	6
High (1)	60	12

Table 2. Data experimental with CCD optimization

Run	Particle Size (Mesh)	Vinasse Waste Volume (mL)	Moisture Content (%)	Ash Content (%)	Calorific Value (cal/g)
1	20	0	6.82	5.85	5000.32
2	20	6	6.71	6.57	4764.43
3	20	12	6.78	5.33	4962.66
4	40	0	7.45	6.75	4521.66
5	40	6	6.8	5.39	4989.07
6	40	6	6.58	5.38	4881.67
7	40	6	7.57	6.8	4654.68
8	40	12	7.98	6.89	4593.17
9	60	0	6.98	6.72	4937.95
10	60	6	6.83	5.45	5002.81
11	60	12	6.84	6.41	4845.57

Based on the data analyzed, the briquettes with the highest moisture content were obtained in briquettes with the addition of 12 mL of vinasse waste. This occurs because vinasse waste has a high moisture content. The results of previous research shows that the moisture content in briquettes using vinasse waste is higher than briquettes not using vinasse, but the use of vinasse waste produces briquettes with stronger physical properties because they can dry optimally through drying [17].

Meanwhile, the briquettes with the highest ash content have a 40 mesh particle size variable, where the particle size affects the high ash content of the briquettes. Ash content is directly proportional to particle size, where the smaller particle size causes the briquette to have smaller gaps (pores) between its particles so that the density of the briquette will be greater and will produce more ash in the combustion process of briquette [18]. High ash content decreases the calorific value of the fuel and reduces it flammability, and it contributes to high thermal resistance, leading to reduced heat transfer into the combustion chamber [19].

In this study, the calorific value ranged from 4521.66 - 5002.81 cal/g, where the highest calorific value was found at 60 mesh particle size with the addition of 6 mL vinasse. This is in line with the more moisture content in the briquette, the heat will first evaporate the water so that the calorific value of the briquette is low. The larger mesh size causes the briquette to have large gaps (pores) between its particles so that the briquette water will be easier to evaporate and show the value of the water content of the briquette is low and the high calorific value.

Table 3 shows the response model suggested by Design Expert 13 based on the Analysis of Variance (ANOVA) data on each parameter in the quadratic model. In the quadratic model, the Standard Dev column quadratic model is chosen because it has the smallest value among the other models. Std. Dev shows the standard deviation value, or the square root of the mean square of the error which determines the distribution of the data, so the greater the standard deviation value, the more diverse and can be said to be more inaccurate; conversely, the smaller the standard deviation, the more similar the values on the item or the more accurate [11]. In ANOVA, the quadratic model is considered appropriate if the difference between the values of Adjusted R^2 and Predicted R^2 is less than 0.2. This small difference indicates the absence of noise, leading to accurate estimates. All three responses give a difference of no more than 0.2, so the quadratic model is said to be significant in determining the three responses.

Table 3. Response mathematical model analysis

Response	Math's Model	Std. Dev	R^2	Adj. R^2	Pred. R^2	Adeq. Prec.	PRESS	F-Value	P-Value	Lack of Fit
Moisture	Quadratic	0.084	0.981	0.962	0.845	20.924	0.297	51.54	0.0003	0.052
Ash	Quadratic	0.113	0.985	0.971	0.863	18.994	0.591	66.7	0.0001	0.164
Calorific Value	Quadratic	29.56	0.986	0.971	0.871	21.127	39029.4	68.24	0.0001	0.272

The adequate precision value is used to measure the ratio of signal to noise or interference, which shows a good response because the value obtained is greater than 4. Adequate precision compares the predicted value range at the design points to the average prediction error. Ratios greater than 4 indicate sufficient model discrimination. In this particular case, the value is well above 4 [20]. So, the quadratic model in 3 responses can be said to make sense in making predictions or further experiments.

The R^2 value indicates the proportion of data variability that has a relationship between the predicted data and the experimental data [21]. A high R^2 value (close to 1) indicates that there is a satisfactory fit between the prediction data and the experimental data. The interpretation of the R^2 value in the interval of 0.8 - 1.0 is stated to be the level of relationship between the independent variable and the dependent variable, which is very strong [22]. In the response to moisture content, the high R^2 value shows a high correlation between observation and prediction values, stating that 98.1% (0.981) of the moisture content in briquettes is influenced by the particle size factor and the volume factor of vinasse waste added in the briquetting process. While the remaining 1.9% is influenced by other factors not included in the model.

The PRESS (Predicted Error Sum of Square) value is a value that states the ability of the model to predict observations that are not used in a new experiment. The smaller PRESS value indicates that the prediction results are improving. The lowest PRESS value is shown in the quadratic model, which means that the quadratic model has the best ability to predict the response with the lowest error rate.

In ANOVA analysis, the P-value provides an indication of the significance of a model relative to the F-value. For a given F-value, it can be defined as the probability that a variable did not affect the response. If the P value for the model is less than 0.05, the model is said to be significant, which means that there is a 5% chance that the F value is due to noise. If the P-value is above 0.1 (10%), the model is said to be insignificant [23]. The P-value of the quadratic models in each response is less than 0.05 so that the relationship between variables can be declared significant or affect each other. While the F-value in the quadratic model shows a value greater than the other models, it is also declared significant, and the lack of fit value, which is greater than 0.05 (5%) indicates inaccuracy, so it is declared insignificant. The lack of fit is insignificant, implying that the model is suitable for use. So the quadratic model has a significant effect on the 3 responses.

3.1 Moisture Content with RSM Analysis

Based on the quadratic model, the moisture content response has a significant effect because it has a P-value of 0.0003 (0.03%) not greater than 0.05, which indicates the presence of noise or disturbance of only 0.03%. While the F value of 51.54 forms a model that can state the moisture content response well, and the lack of fit value obtained is 0.0517 (5.17%) which is greater than 0.05 (5%) so the inaccuracy can be declared insignificant, implying that the model is suitable for use. This RSM model can be applied with the RSM equation or model for the moisture content response shown in equation (3).

$$Z = 7.8717 - 0.0817x + 0.01038y - 0.000542xy + 0.001239x^2 - 0.000263y^2 \quad \text{.....(3)}$$

Description :
Z = Moisture Content of Briquettes
x = Particle Size
y = Vinasse Wate Volume

The response surface shape is used to describe the effect of independent variables on the response. The quadratic model equation indicates that the regression line formed is parabolic. The response surface shows the relationship between the two independent variables and their effect on the response moisture content of rice husk charcoal briquettes, which can be seen in Figure 1.

Figure 1 shows the highest color in briquettes with a particle size of 60 mesh with or without the addition of vinasse. The larger particle size causes the briquette to have large gaps (pores) between the particles, so the density is getting low. In the drying process, the briquette water will be easier to evaporate. Figure 1 also shows the relationship between moisture content and the volume of vinasse waste added, which is directly proportional where the more vinasse waste added, the higher the moisture content of the briquette. This is because vinasse waste has a high moisture content. However, under conditions that are considered optimum, between 40 and 50 mesh particle size with the addition of vinasse, the moisture content of the briquettes does not exceed the SNI limit.

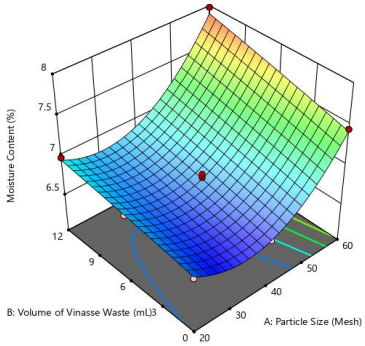

Figure 1. 3D response of moisture content

3.2 Ash Content with RSM Analysis

Based on the quadratic model, the moisture content response has a significant effect because it has a P-value of 0.0001 (0.01%) not greater than 0.05 which indicates the presence of noise or disturbance of only 0.01%. While the F-value of 66.7 forms a model that can state the moisture content response well. The lack of fit value obtained is 0.164 (16.4%), which is greater than 0.05 (5%) so the inaccuracy can be declared insignificant, implying that the model is suitable for use. The RSM model can be applied with the RSM equation or model for the moisture content response shown in equation (4).

$$Z = 9.8606 - 0.2264x - 00359y - 0.000021xy + 0.0029x^2 + 0.004825y^2 \quad \text{.....(4)}$$

Description :
Z = Ash Content of Briquettes
x = Particle Size
y = Vinasse Wate Volume

The response surface shape is used to describe the effect of independent variables on the response. The quadratic model equation indicates that the regression line formed is parabolic. The response surface shows the relationship between two independent variables and their influence on the ash content response of rice husk charcoal briquettes, which can be seen in Figure 2.

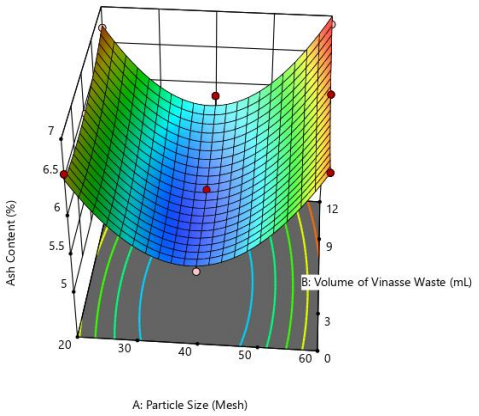

Figure 2. 3D response of ash content

Figure 2 shows the 3D contour plot graph of ash content response with particle size and vinasse volume. It can be seen that the highest color is located in the briquette sample with a particle size of 60 mesh without the addition of vinasse. This shows that the highest ash content value is located in the briquette with a particle size of 60 mesh without the addition of vinasse. According to Thoyeb et al., ash content is directly proportional to particle size; the smaller the particle size, the higher the ash content of the briquettes [18]. The smaller particle size causes the briquette to have smaller gaps (pores) between its particles, resulting in a higher density of the briquette and more ash. In addition, briquettes with low density allow more oxygen flow in the gaps between particles so that combustion can be carried out more completely and produce less ash. Figure 2 shows the relationship between ash content and the volume of vinasse waste added, which is directly proportional, where the more vinasse waste added, the higher the ash content of the briquettes. This is because vinasse waste has a high ash content.

3.3 Calorific Value with RSM Analysis

Based on the quadratic model, the calorific value response has a significant effect because it has a P-value of 0.0001 (0.01%) not greater than 0.05, which indicates the presence of noise or disturbance of only 0.01%. While the F-value of 68.24 forms a model that can state the moisture content response well. The lack of fit value obtained is 0.272 (27.2%), which is greater than 0.05 (5%), so the inaccuracy can be declared insignificant, implying that the model is suitable for use. The RSM model can be applied with the RSM equation, a model for the calorific value response shown in equation (5).

$$Z = 4145.1985 + 41.9399x + 33.566y - 0.2125xy - 0.5893x^2 - 1.2469y^2 \quad \textbf{.....(5)}$$

Description :
Z = Calorific Value of Briquettes
x = Particle Size
y = Vinasse Waste Volume

The response surface shape is used to describe the effect of independent variables on the response. The quadratic model equation indicates that the regression line formed is parabolic. The response surface form shows the relationship between the two independent variables and their influence on the response of the calorific value of rice husk charcoal briquettes, which can be seen in Figure 3.

Figure 3 shows the 3D contour plot graph of the heating value response with the particle size factor and the volume of vinasse waste. It can be seen that the highest color is in briquettes with a particle size of 40 mesh with the addition of vinasse. At the condition that is considered optimum, the calorific value of the briquettes decreases, which is around the particle size of 60 mesh with the addition of vinasse. This is because the smaller particle size causes the briquette to have small gaps (pores) between the particles in the briquette so that it has a high-density value. The briquette's high density value causes its calorific value to be lower. This is consistent with the higher moisture content in the briquette. The heat will first evaporate the water, resulting in a low calorific value. In addition, briquettes with a particle size of 60 mesh have a high density, making it difficult for oxygen to be distributed in the briquettes.

Figure 3 also shows the relationship between the heating value and the volume of vinasse waste added, which is directly proportional, where the more vinasse waste is added, the higher the heating value of the briquettes. This is because there are several contents, such as carbon and oxygen, in vinasse waste, which are quite high. However, in conditions that are considered optimum, the calorific value of the briquettes decreases, around the particle size of 60 mesh with the addition of vinasse.

3.4 Optimization of Process Conditions

Optimization in this study was carried out to determine the value of factors to produce the optimum response value. In optimization, there are several target parameters, including the upper limit, lower limit, and importance of each independent variable. This is needed to get a combination of variables that are within the upper and lower limits to achieve SNI criteria.

Table 4 shows the parameters to determine the combination that will obtain some recommended conditions, with the importance of each parameter shown. The importance value in determining the optimum condition is needed to find out how important each variable is to get the optimum result. The importance of 3 or declared important in the particle size and volume of vinasse waste is given to provide a balanced combination between the two. The importance of 4 or very important is given to the results of the ash content and moisture content parameters given to provide the smallest results or values and not exceed the maximum value of 8. Importance 5 or very-very important is given to the results of the calorific value parameter to provide high results above 5000, where the value of importance 5 is intended because the results of the research data conducted have not fully met the standards (>5000 cal/g).

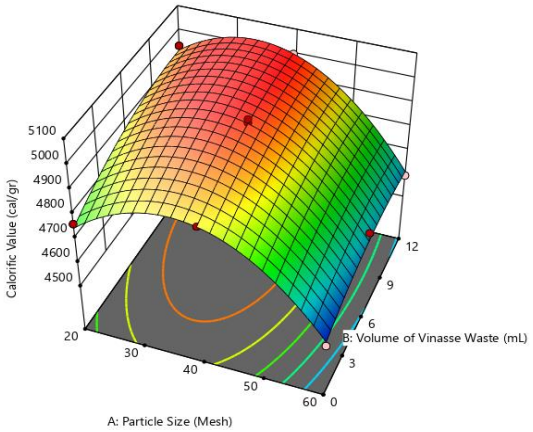

Figure 3. 3D response of calorific value

Table 4. Parameters for determining the optimum condition combination

Variable	Target	Lower Limit	Upper Limit	Importance
A : Particle Size	*is in range*	20	60	+++
B : Vinasse Waste Volume	*is in range*	0	12	+++
Moisture Content	*minimize*	6.58	8	++++
Ash Content	*minimize*	5.33	8	++++
The Calorific Value	*is target = 5050*	4521.66	5100	+++++

Description : *importance 1 (not very important); 2 (somewhat important); 3 (important); 4 (very important); 5 (very - very important)

Table 5. Optimum condition based on RSM

Particle Size (mesh)	Vinasse Waste (mL)	Moisture Content (%)	Ash Content (%)	The Calorific Value (cal/g)	Desirability	
35.152	6.049	6.696	5.450	5003.399	0.927	***Selected***

Furthermore, the optimum condition is determined based on the desirability value. Desirability states how close or fulfilled the response value is to the targeted value so that the selected optimum condition is expected to have a desirability value close to one (1.0). The desirability value becomes an optimization goal that shows the value of optimization accuracy and states the ability of the program to meet the specified parameters.

Table 5 shows the solution for the Design Expert 13 calculation system's general conditions. The optimum point with the best response results was obtained at a combination of particle size of 35.152 mesh with a volume of vinasse waste added of 6.049 mL. Based on this combination of variables, the moisture content was obtained at 6.696%, ash content at 5.45%, and calorific value at 5003.399 cal/g. In addition, the desirability value obtained is 0.927, which shows that the optimum point obtained based on the program is very good because it is close to the value of 1. Hidayat et al., [24] shows that the desirability value of 1 indicates the perfect case. Where the desirability value is a characteristic used to explain how well the optimal solution given is by the objectives of the response.

4. Conclusion

Response Surface Methodology (RSM) provides a model to predict the response of moisture content, ash content, and heating value, namely the quadratic model. Particle size influences the results of the analysis of moisture content and ash content, and vinasse waste can increase the heating value. The results of RSM optimization provide a combination of optimal conditions from the process of making briquettes from rice husks with the addition of vinasse waste, which is located at a size of 35.152 mesh and a volume of vinasse waste of 6.049 mL, which produces a moisture content of 6.696%, an ash content of 5.45%, and 5003.399 cal/g with a desirability of 0.927.

References

[1] Razuan, R., Finney, K. N., Chen, Q., Sharifi, V. N., & Swithenbank, J. (2011). Pelletised fuel production from palm kernel cake. *Fuel Processing Technology*, 92(3), 609–615. doi: 10.1016/j.fuproc.2010.11.018

[2] Vegatama, M. R., & Sarungu, S. (2022). Pengaruh Variasi Jenis Perekat Organik terhadap Nilai Kalor Biobriket Serbuk Kayu. *Jurnal Pendidikan Tambusai*, 6(2), 13256–13262.

[3] Liu, Z., Quek, A., Kent Hoekman, S., & Balasubramanian, R. (2013). Production of solid biochar fuel from waste biomass by hydrothermal carbonization. *Fuel*, 103, 943–949. doi: 10.1016/j.fuel.2012.07.069

[4] Irianto, K. (2015). Pengelolaan Limbah Pertanian. *Warmadewa*, 24(2), 91.

[5] Sipahutar, D. (2017). Teknologi Briket Sekam Padi. *Balai Pengkajian Teknologi Pertanian (BPTP)* (Vol. 0761).

[6] Oladosu, K. O., Babalola, S. A., Kareem, M. W., Ajimotokan, H. A., Kolawole, M. Y., Issa, W. A., … Ponle, E. A. (2023). Optimization of fuel briquette made from bi-composite biomass for domestic heating applications. *Scientific African*, 21(July), e01824. doi: 10.1016/j.sciaf.2023.e01824

[7] Otoo, M., & Drechsel, P. (2018). *Resource Recovery From Waste*. New York.

[8] Porol, J. T. C., Claur, W. A., & Antonio, A. Z. C. (2019). Performance Evaluation of Charcoal Briquettes Derived from Sugarcane Tops Using Vinasse as Binder. *2019 IEEE 11th International Conference on Humanoid, Nanotechnology, Information Technology, Communication and Control, Environment, and Management, HNICEM 2019*. doi: 10.1109/HNICEM48295.2019.9073606

[9] Hidayati, N. R., Trisnawati, A., Sudarni, D. H. A., Setiawan, M. A., & Wahyuningsih, S. (2021). Teknologi Pemanfaatan Limbah. *Cv. Ae Media Grafika*, 5–24.

[10] Jaswella, R. W. A., Sudding, & Ramdani. (2022). Pengaruh Ukuran Partikel terhadap Kualitas Briket Arang Tempurung Kelapa. *Jurnal Chemica*, 23(1), 7–19.

[11] Myers, R., Montgomery, D., & Anderson-Cook, C. (2009). *Response Surface Methodology*. (J. Wiley & S. inc, Eds.) (3rd Editio.). Canada.

[12] Anizar, H., Sribudiani, E., & Somadona, S. (2020). Pengaruh Bahan Perekat Tapioka Dan Sagu Terhadap Kualitas Briket Arang Kulit Buah Nipah. *Perennial*, 16(1), 11–17.

[13] Basuki, H. W., Yuniarti, Y., & Fatriani, F. (2020). Analisa sifat fisik dan kimia briket arang dari campuran tandan kosong aren (Arenga pinnata Merr) dan cangkang kemiri (Aleurites trisperma). *Jurnal Sylva Scienteae*, 3(4), 626. doi: 10.20527/jss.v3i4.2346

[14] AK Wijaya, Agnesia, A., Yulianti, N. L., & Gunadnya, I. B. (2021). Karakteristik Briket Biomassa dari Variasi Bahan Baku Dan Persentase Perekat yang Berbeda. *JURNAL BETA (BIOSISTEM DAN TEKNIK PERTANIAN*, 9(2), 1–10.

[15] Ridhuan, K., & Suranto, Jo. (2016). Perbandingan pembakaran pirolisis dan karbonisasi pada biomassa kulit durian terhadap nilai kalori. *TURBO:Jurnal Teknik Mesin Univ. Muhammadiyah Metro*, 5(1), 50–56.

[16] Almu, M. A., Syahrul, & Padang, Y. A. (2014). Analisa Nilai Kalor dan Laju Pembakaran pada Briket Campuran Biji Nyamplung (Calophyllm Inophyllum) dan Abu Sekam Padi. *Journal of Materials Processing Technology*, 4(2), 117–122.

[17] Dharma, U. S., Rajabiah, N., & Setyadi, C. (2017). Biobriket Dengan Perekat Berbahan Baku Tetes Tebu. *Jurnal Teknik Mesin Univ. Muhammadiyah Metro*, 6(1), 92–102.

[18] Thoyeb, E., Hamzah, F. H., Zalfiatri, Y., Jurusan, M., Pertanian, T., Pertanian, F., & Riau, U. (2021). Perbedaan Ukuran Partikel Terhadap Kualitas Briket Arang Batang Pisang. *Jom Faperta*, 8, 4–8.

[19] Kipngetich, P., Kiplimo, R., Tanui, J. K., & Chisale, P. (2023). Effects of carbonization on the combustion of rice husks briquettes in a fixed bed. *Cleaner Engineering and Technology*, 13(February), 100608. doi: 10.1016/j.clet.2023.100608

[20] Noordin, M. Y., Venkatesh, V. C., Sharif, S., Elting, S., & Abdullah, A. (2004). Application of response surface methodology in describing the performance of coated carbide tools when turning AISI 1045 steel. *Journal of Materials Processing Technology*, 145(1), 46–58. doi: 10.1016/S0924-0136(03)00861-6

[21] Chicco, D., Warrens, M. J., & Jurman, G. (2021). The coefficient of determination R-squared is more informative than SMAPE, MAE, MAPE, MSE and RMSE in regression analysis evaluation. *PeerJ Computer Science*, 7, 1–24. doi: 10.7717/PEERJ-CS.623

[22] Sanny, B., & Dewi, R. (2020). Pengaruh Net Interest Margin (NIM) Terhadap Return on Asset (ROA) Pada. *Jurnal E-Bis (Ekonomi Bisnis*, 4(1), 78–87. doi: https://doi.org/ 10.37339/jurnal e-bis.v4i1.239

[23] Pambi, R. L. L., & Musonge, P. (2016). Application of response surface methodology (RSM) in the treatment of final effluent from the sugar industry using Chitosan. *Water Pollution XIII*, 1(Wp), 209–219. doi: 10.2495/wp160191

[24] Hidayat, I. R., Zuhrotun, A., & Sopyan, I. (2021). Design-expert Software sebagai Alat Optimasi Formulasi Sediaan Farmasi. *Majalah Farmasetika*, 6(1), 99–120.

CHEESA: Chemical Engineering Research Articles
ISSN 2614-8757 (Print), ISSN 2615-2347 (Online)
Available online at: http://e-journal.unipma.ac.id/index.php/cheesa

Research Article

Comparative Study of Maceration and Ultrasonic Techniques in Coffee Oil Extraction Based on Energy Evaluation and Mass Transfer Value

Studi Perbandingan Teknik Maserasi dan Ultrasonik pada Ekstraksi Minyak Kopi Berdasarkan Evaluasi Energi dan Nilai Transfer Massa

Mega Mustikaningrum[1*)], Mohamad Endy Yulianto[2)], Laras Prasakti[3,4)]
[1)]*Universitas Muhammadiyah Gresik, Chemical Engineering Department, Gresik, East Java, 61121, Indonesia*
[2)]*Universitas Diponegoro, Industrial Chemical Engineering Department, Semarang, Central Java, 50275, Indonesia*
[3)]*Universitas Gadjah Mada, Chemical Engineering Department, Sleman, Yogyakarta, 55281, Indonesia*
[4)]*RWTH Aachen University, IME Process Metallurgy & Metal Recycling, 52062, Aachen, Germany*

Article History
Submitted: 12th February 2024; Revised: 31th July 2024; Accepted: 15th August 2024; Available online: 24th August 2024; Published Regularly: June 2024

doi: 10.25273/cheesa.v7i1.19326.47-56

*Corresponding Author.
Email: megamustikaningrum@umg.ac.id

Abstract

Coffee is a significant commodity trend, with numerous coffee shops rapidly established in Indonesia. The development of this industry has led to an increased discharge of coffee grounds into the environment. The discarded grounds contain oil which can be optimized using various methods and serve as a raw material for biodiesel. Therefore, this study aimed to compare the maceration and ultrasonic methods of extracting coffee grounds. The comparison focused on yield, mass transfer value (diffusivity), and extraction speed constant based on the proposed mathematical model. The results showed a yield of 12.1% and 16%, for the maceration and ultrasonic methods, respectively. Diffusivity value was registered at 9.99 x 10^{-11} m^2/min and 9.8 x 10^{-10} m^2/min, while extraction speed constant values were discovered to be 0.2 m/min and 1.798 m/min, respectively. Additionally, the energy evaluation of ultrasonic extraction produced a Gibbs energy value of -3765.72 Joules.

Keywords: coffee grounds; extraction; Gibbs energy; maceration; mass transfer; ultrasonics

Abstrak

Kopi menjadi trend komoditi terbaru saat ini dengan maraknya coffee shop yang didirikan di Indonesia. Dengan berkembangnya industri ini, buangan ampas kopi ke lingkungan semakin bertambah. Buangan ampas kopi memiliki kandungan minyak kopi yang dapat dimanfaatkan salah satunya menjadi bahan baku biodiesel. Berbagai metode telah dilakukan untuk melakukan optimalisasi terhadap minyak kopi yang dihasilkan. Pada penelitian ini bertujuan untuk membandingkan dua metode ekstraksi ampas kopi yaitu metode maserasi dan ultrasonik. Perbandingan dilihat dari yield yang dihasilkan, nilai transfer massa dan konstanta kecepatan ekstraksi berdasarkan pengajuan model matematika. Yield minyak kopi hasil maserasi sebesar 12,1 % dan 16 % untuk metode ultrasonik. Nilai difusivitas untuk ekstraksi maserasi sebesar 9,99 x 10^{-10} m^2/min dan untuk ultrasonik sebesar 9.8 x 10^{-09} m^2/min. Untuk nilai konstanta kecepatan esktraksi untuk metode maserasi dan ultrasonik didapatkan sebesar 17,98 dan 200 m/min. Berdasarkan evaluasi energi pada ekstraksi ultrasonik didapatkan nilai energi Gibbs sebesar -3765,72 Joules.

***Kata kunci**: ampas kopi; ekstraksi; energi Gibbs; maserasi; ultrasonik; transfer massa*

1. Introduction

Coffee is a popular beverage that has become a trend and a staple lifestyle of urban communities. According to the Indonesian Central Statistics Agency, Indonesia is the third largest producer of this commodity worldwide [1]. Data from the Association of Indonesian Coffee Exporters (AICE) recorded a significant increase in coffee consumption across the country [2], reflecting the abundant availability of grounds. The increase in consumption has reached an average of 7% per year and 5 million 60-kilogram bags in 2020 - 2021. This led to the generation of substantial waste disposed into the environment.

On average, a ton of fresh coffee beans produces approximately 650 kg of grounds. The instant coffee industry accounts for approximately 50% of global ground production, leading to an annual quantity of coffee grounds of estimated 6 million tons [3]. This suggested that the availability of coffee grounds is quite abundant. Depending on the variety, the organic residue that comes from coffee grounds after the brewing process, commonly referred to as spent coffee grounds (SCG) has an oil content ranging from 10-15% by weight (%wt) [4]. Grounds discarded into the environment produce methane gas, which significantly contributes to climate change [5],[6].

Coffee oil presents a viable alternative as a raw material for biodiesel production due to the decreasing availability of fuel [7]. Every year, approximately 8 million tons of coffee are produced globally, and an estimated 1.3 billion L of biodiesel is derived from the oil, leading to increased fuel supply [8]. Despite this potential, Indonesia has yet to fully develop the benefits of coffee oil [9].

Various methods have been used to isolate coffee oil from grounds, including maceration [10][11], soxhletation method [12][13], supercritical liquid extraction [14], microwave-assisted extraction [15][16], and more recently ultrasonic extraction [17][18]. The diffusivity value of coffee oil in the maceration and ultrasonic methods, influenced by temperature and activation energy, was compared. The comparison included calculating the diffusivity of oil extraction under varying temperatures for both methods. This diffusivity value represents the rate of mass transfer of solute from high concentration to low concentration [19].

Studies on the development of a mathematical model for coffee oil extraction are limited. Therefore, data on kinetic and thermodynamic parameters are limited. This study presents kinetic and thermodynamic modeling to determine the constant value of extraction speed (kd), diffusivity (D), extraction equilibrium constant (K), and Gibbs energy. It is important to consider mathematical values such as diffusivity and rate constant which influence the transition rate of coffee oil from solid to liquid. The generated values can be utilized to conduct simulations, eliminating the need for additional data.

This study evaluates the energy feasibility of the extraction processes by analyzing the amount of entropy produced. The analysis showed whether the system occurs spontaneously or certain energy is required to facilitate the extraction process.

2. Research Methods

2.1 Tools and Materials

A complete series of maceration extractor equipment, comprised of three-neck flasks, a return cooler, thermometer, magnetic stirrer, hose, and pump, was

assembled as shown in Figure 1a. The sonicator series (110V/220V Digital Ultrasonic Cleaner 40Khz 50W Sonicator Washing Bath) includes a sonicator instrument and an Erlenmeyer for holding the sample, as detailed in Figure 1b. The raw materials used in this study were coffee grounds sourced from the Gresik area and 70% n-hexane technical solvent from Nirwana Surabaya.

2.2 Research Procedure

2.2.1 Maceration Method

A total of 100 grams of coffee grounds were dissolved in 600 mL of n-hexane solvent. Extraction was performed for 3 hours at a temperature setting of 70-80 ^{o}C using an extractor. An optimization stage included soaking the mixture for 24 hours in a closed glass cup for maceration. After extraction, the solvent was separated using distillation at 80-90 ^{o}C [20] until dripping stopped.

2.2.2 Ultrasonic Method

Approximately 10 grams of coffee grounds that had been prepared were dissolved in 200 mL of n-hexane solvent. Extraction was performed at 50 ^{o}C for 180 minutes in the sonicator. Following oil isolation, the distillation process was conducted to separate the n-hexane solvent from the coffee oil at 80-90 ^{0}C [21]. The distilled were weighed using balance analysis to determine the yield, calculated using equation (1).

$$\text{yield (\%)} = \frac{\text{weight coffee oil}}{\text{sample mass x coffee oil content in coffee grounds}} \text{x } 100\ \% \quad \textbf{..(1)}$$

2.2.3 Kinetic Data Retrieval

After extraction, samples were taken at a certain time range, and the data were analyzed and fitted to find the diffusivity parameter value. The equations and parameter values will be discussed further in a later section. The fitting will be done by minimizing the difference between the collected data and the calculation result.

In section 2.3, mathematical modelling produces partial second-order differential equations to represent the phenomena during the process. The differential equations will be discretized using numerical methods to produce ordinary differential equations (ODE). These equations are then able to be solved using the ode15s function in MatLab ver 2013b software. The results from the solved equations will then be fitted with experimental data using the lanolin function in MatLab to obtain unknown kinetic parameters.

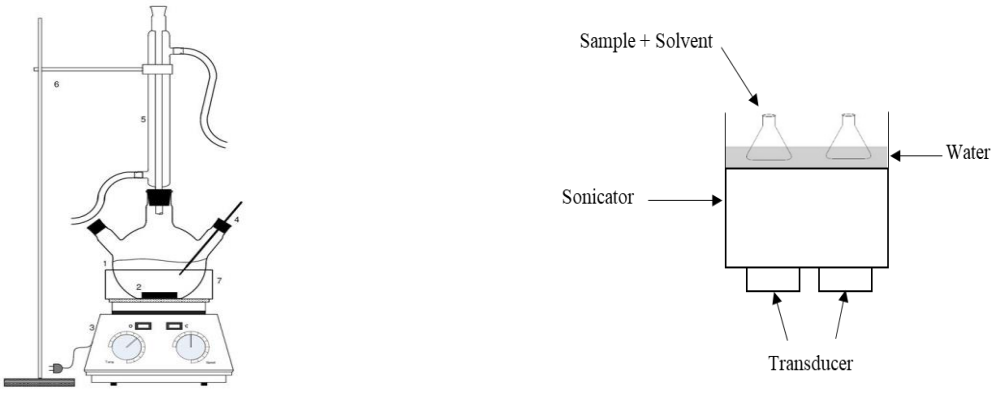

(a) (b)

Figure 1. a) Series of maceration extractor tools, b) Series of ultrasonic extractor tools

2.3 Submission of Kinetic Models

Before developing the modeling, several assumptions were put forward, including that coffee ground particles had a spherical geometric shape with uniform porosity values. The calculations were only conducted on radial gradients without considering the axial direction. The modeling process also neglected temperature changes during extraction and filtration, assuming no variation in particle size and porosity [22]. Additionally, the diffusion equation was solved separately for each component of the bimodal particle size distribution, and the average particle size was used in the results. There were no particle swelling and changes in particle porosity over time.

The mass balance of coffee oil in the solvent is described in equation (2), while the mass balance in the coffee grounds solids is shown in equation (3). In both equations, the notation Ca* represents the concentration of coffee oil in the film layer, a value that cannot be precisely calculated. To address this, a partition equation was adopted as presented in equation (4). Where kd is the extraction speed constant (m/minute), m is the mass of coffee grounds (grams), V is the volume of n-hexane (L), Da is the diffusivity of coffee oil into the solvent (m^2/minute), Ca is the concentration of coffee oil in the solvent (mol/liter), Xa is the concentration of coffee oil in the solids (mol/gram), $\frac{\partial C_a}{\partial t}$ is the concentration of coffee oil in the solvent at any time (mol/liter.minute), $\frac{\partial X_a}{\partial t}$ is the concentration of coffee oil in solids at any time (mol/gram.minute), a is the surface area of coffee grounds calculated quantitatively based on the radius value (m^2), and K is the extraction equilibrium constant [23].

$$\frac{\partial C_a}{\partial t} = D_a \frac{\partial^2 C_a}{\partial r^2} - D_a \frac{2}{r}\frac{\partial C_a}{\partial r} - \frac{kd.a.m}{V}(C_a - C_a^*) \quad \text{.....(2)}$$

$$\frac{\partial X_a}{\partial t} = D_a \frac{\partial^2 X_a}{\partial r^2} - D_a \frac{2}{r}\frac{\partial X_a}{\partial r} + kd.a(C_a - C_a^*) \quad \text{.....(3)}$$

$$X_a = K\,C_a^* \quad \text{.....(4)}$$

To calculate the equation (2), (3), and (4), initial and boundary conditions needed to be established. The initial condition (IC) is expressed mathematically in equation (5). The proposed boundary condition (BC) is represented by equations (6) and (7), with Table 1 showing details of Xao.

At t = 0 → Xa = Xao and Ca=0 .....**(5)**

At r=0 → Xa=Xao; $\frac{\partial C_a}{dt} = 0$.....**(6)**

At r=r → $\frac{\partial X_a}{\partial t} = 0$; Ca=Cao .....**(7)**

Table 1. Calculated parameter values

No.	Variable	Value
1.	Mass (m)	
	Maceration	100 gram
	Ultrasonic	10 gram
2.	Volume (liter)	
	Maceration	100 mL
	Ultrasonic	200 mL
3.	Radius	0.000125 m
4.	Nr (number of iterations)	300
5.	Cao	0 mol/liter
6.	Xao	1889 mol/gram
7.	Surface area per coffee ground mass	0.01 m^2

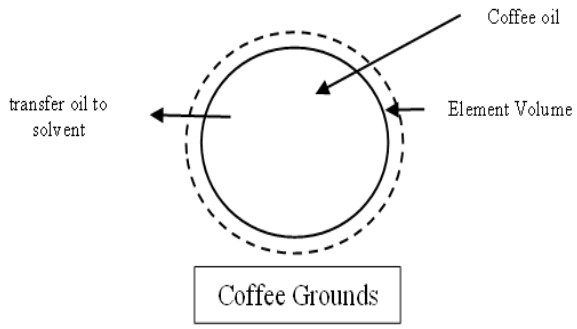

Figure 2. Illustration of the process of transferring oil to solvent

2.4 Energy Evaluation Model

To determine whether a process occurred spontaneously, the entropy factor and Gibbs free energy were considered. The enthalpy parameters (ΔH^o), Gibbs energy (ΔG^o) and entropy (ΔS^o) were calculated using the extraction kinetics equation, and tested at different temperatures.

Furthermore, thermodynamic studies were conducted at temperatures of 30, 40, and 50 °C. The equations for ΔG^o are presented in equation (8) and (9). The values of enthalpy and entropy was determined using linearity from equation (10), with ln K plotted on the y-axis and 1/T on the x-axis. The slope and intercept of the line provided the magnitude of the entropy and enthalpy values.

$$\Delta G^0 = -RT \ln K \quad \text{.....(8)}$$

$$\Delta G^0 = \Delta H^0 - T\,\Delta S^0 \quad \text{.....(9)}$$

$$\ln K = \frac{\Delta S}{R} - \frac{\Delta H}{RT} \quad \text{.....(10)}$$

3. Results and Discussion

3.1 Comparison of Coffee Oil Yields

The extraction process was used to isolate or separate the desired active compound from the raw material. It included stages such as (1) the solvent penetration into the solid matrix, (2) the solute dissolution in the solvent, and (3) the solute diffusion out of the solid matrix. In this case, the effectiveness of extraction depended on several factors such as temperature, the ratio of ingredients, the type of solvent, and the method applied [24].

This study was conducted using two different methods, namely maceration and ultrasonic. Figure 3 presents the differences in coffee oil yield after the extraction process. These differences arise from the distinct principles in the maceration and ultrasonics methods.

The maceration method was conducted at room temperature and it represented the simplest conventional method, where a liquid penetrated the cell walls of a plant and entered a cavity containing the active substance. This substance, present as a concentrated solution, diffused out due to the difference in concentration between the solution and the solute [25]. Based on this principle, maceration extraction usually requires an extended duration.

The yield of coffee oil from coffee grounds ranged from 5.7-16.0% [25]. Based on the results shown in Figure 3, the final yield obtained using the maceration method was 12. 42% wt, while the ultrasonic extraction produced 16% wt. The advantages of the ultrasonic method include faster processing time, and lower extraction power requirements, and the ability to perform extraction at lower temperatures [26]. The results are in line with the study conducted by Hibbert et al., where a coffee oil yield of 11.54% was obtained using the maceration method [15]. Meanwhile, the ultrasonic method produced 14.51% after 30 minutes [18].

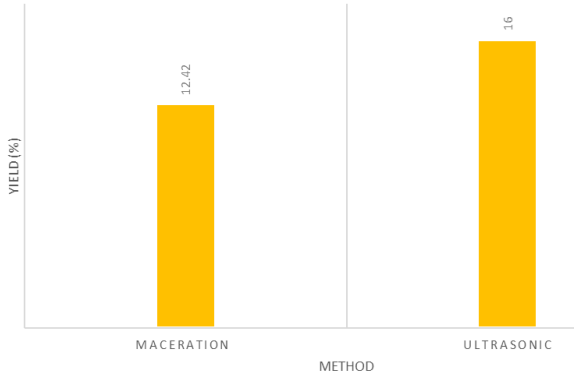

Figure 3. Differences in extraction results from maceration and ultrasonic methods

The ultrasonic method utilizes high-intensity sound waves to disrupt plant tissue through physical forces generated during the cavity mechanism, facilitating the release of coffee oil components into the solvent within a short time and enhancing diffusivity [27]. This phenomenon, known as erosion, causes the surface of the solid matrix to degrade, allowing the solvent to penetrate the plant tissue more effectively, leading to higher yields [28].

Based on mathematical calculations performed using MatLab, the decrease in coffee oil concentration at each time and position was detailed in Figures 4 and 5. These images were generated using the *imagesc* command in MatLab software, which visualized the relationship between the coffee grounds radius (x-axis), time (y-axis), and the concentration of coffee oil in the solid. The projection captured a radius range of 0 to 12 x 10^{-5} m. This visualization was intended to observe the distribution of oil reduction in solid coffee grounds.

Figure 4 explains the distribution of coffee oil at each position and time. In this case, the color gradation described the difference in concentration. Based on observation, towards the surface, the dense matrix of coffee oil was less than on the inside where the radius approached zero. This image was similar to the ultrasonic extraction phenomenon.

Based on the image, the distribution in the coffee matrix area using the ultrasonic method at a radius of 6 x10^{-5} m began to decrease significantly. In the maceration stage, subsidence was initiated at a radius of 8 x10^{-5} m. However, over the same distance range, the magnitude of the reduction in coffee oil concentration using the maceration method was not significant.

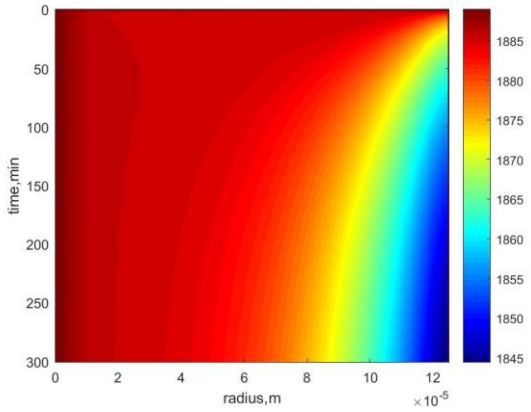

Figure 4. Distribution of coffee oil in a solid matrix using the maceration method

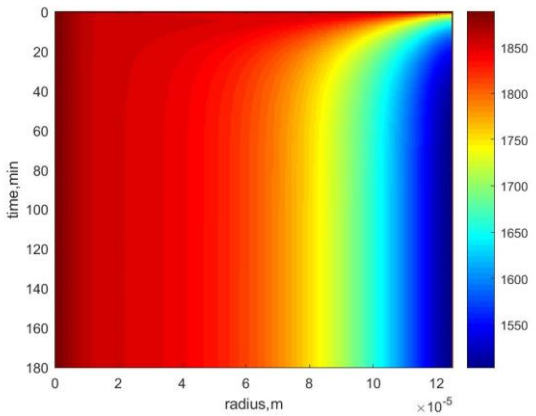

Figure 5. Distribution of coffee oil in a solid matrix using the ultrasonic method

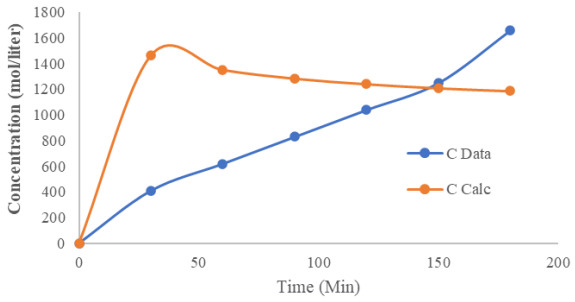

Figure 6. Comparison of research data vs calculations on maceration method

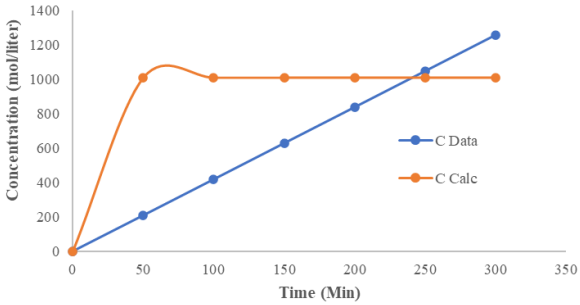

Figure 7. Comparison of research data vs calculations on ultrasonic method

The ultrasonic method can penetrate deeper pores. The result was obtained through data comparison and calculations. Figure 6 shows the comparison results of the maceration extraction method. Based on Figure 7, the final extraction result from the study data was 1659 mol/liter, while the calculated value was 1185.62 mol/liter. For the maceration method, the study data yielded 1259 mol/liter, compared to a calculated value of 1011.14 mol/liter.

Figures 6 and 7 show discrepancies between calculated and study data, which were relatively minor. In this case, the study had not identified an equilibrium point, resulting in a linear representation. This discrepancy explained the intersection of values in the image display, where the extraction process should ideally show a peak followed by a balanced line, as signified by the proposed mathematical model.

3.2 Differences in Diffusivity Results and Extraction Speed

In this study, the diffusivity of coffee oil into the solvent using hexane was quantitatively tested. It was important to acknowledge that the extraction time using the ultrasonic method was faster. The diffusivity value and extraction speed for each method were quantitatively evaluated. The results of the calculations were presented in Table 2, utilizing the parameter values listed in Table 1.

Table 2. Results of mathematical model calculations

Parameter	Extraction Method	
	Maceration	**Ultrasonic**
Diffusivity (m^2/min)	9.99×10^{-12}	9.8×10^{-11}
Extraction speed constant (m/min)	0.2	17.98

Diffusivity is the number of moles transferred per unit area, per unit time, and per unit concentration gradient. A molar flux in diffusion is comprised of two components attributed to mass movement and the relative speed of particles or molecules [29]. The increase in coffee oil diffusion observed using the ultrasonic method arises from the appearance of microacoustics during the extraction process. In this context, microacoustics refers to the effects of radiation pressure, gravity, cavitation, and acoustic pressure [30].

The acceleration of diffusivity and extraction speed was influenced by the presence of cavitation events produced by water bubbles. These bubbles are caused by alternating cycles of compression and rarefaction, which under certain conditions lead to cavitation, a phenomenon where bubbles burst. The phenomenon caused an increase in heat conditions of up to 5000 K and a high pressure of 1000 atm. This hot spot contributes to the acceleration of biochemical reactions, diffusion, and other phenomena [31].

The presence of cavitation caused several combinations of phenomena such as fragmentation, local erosion, pore formation, shear forces, increased absorption, and swelling index in the plant cellular matrix. This cavitation produces shock waves and accelerated collisions between particles that cause fragmentation of cellular structures. This rapid fragmentation dissolved bioactive components by decreasing particle size and increasing surface fluidity, thereby accelerating diffusivity within the solid matrix layer [32].

Ultrasonography, a phenomenon associated with ultrasonic extraction, enhances solvent absorption, thereby

increasing accessibility to bioactive compounds and subsequently raising diffusivity. This situation did not occur when using maceration extraction.

3.3 Ultrasonic Method Energy Evaluation

The purpose of energy evaluation is to determine the energy value produced by the ultrasonic method. This includes calculating the entropy and enthalpy values of the system. Based on Figure 8, the calculated enthalpy value was 28241.83 Joules, and the entropy was 99.09457 Joules/K. Using these values, the Gibbs energy was discovered to be -3765.72 Joules. The negative value signified that the extraction process was spontaneous and feasible [33].

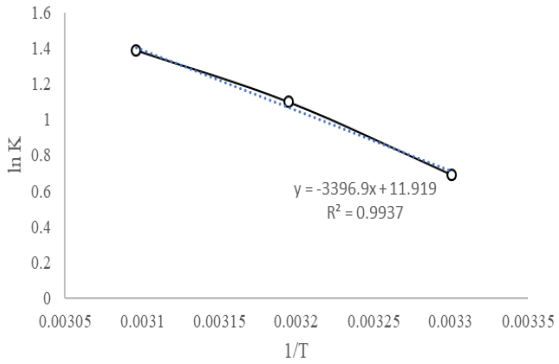

Figure 8. Plotting 1/T vs ln K to find energy parameter

4. Conclusion

In conclusion, the ultrasonic method outperformed maceration, yielding 16%, compared to 12%. The ultrasonic process also had a faster transfer value due to cavitation induced by sound waves, enhancing the diffusivity of coffee oil to the solvent. The Gibbs energy value showed that the process was spontaneous and efficient without requiring additional energy, making it feasible and energy-efficient.

References

[1] BPS. (2022). Statistik Kopi Indonesia. Badan Pusat Statistik, Jakarta

[2] Usman, I and Nanda, A.P.V. (2017). Green business opportunity of coffee ground waste through reverse logistics. *Journal Global Business Advancement,* 10(6), 727-737

[3] Luz, F.C., Volpe, M., Fiori, L., Manni, A., Cordiner, S., Mulone, V., and V. Rocco. (2018). Spent coffee enhanced biomethane potential via an integrated hydrothermal carbonization-anaerobic digestion process. *Bioresources Technology,* 256, 102-109, doi: 10.1016/j.biortech.2018.02.021

[4] Jenkins R.W., Stageman, N.E., Fortune, C.M., and Chuck, C.J. (2014). Effect of the Type of Bean, Processing, and Geographical Location on the Biodiesel Produced from Waste Coffee Grounds. *Energy & Fuels,* 28(2), 1166−1174, doi: 10.1021/ef4022976

[5] Mussatto, S.1., Machado, E.M.S., Martins, S, and Teixeira, J.A. (2011). Production, Composition, and Application of Coffee and Its Industrial Residues. *Food and Bioprocess Technology,* 4(5), 661-672, doi: 10.1007/s11947-011-0565-z

[6] Somnuk, K., Eawlex, P., and Prateepchaikul, G. (2017). Optimization of coffee oil extraction from spent coffee grounds using four solvents and prototype-scale extraction using circulation process. *Agriculture and Natural Resources,* 51(3), 181-189, doi: 10.1016/j.anres.2017.01.003

[7] Al-Hamamre, Z., Foerster, S., Hartmann, F., Kröger, M., and Kaltschmitt, M. (2012). Oil extracted from spent coffee grounds as a renewable source for fatty acid methyl ester manufacturing. *Fuel,*96(1), 70-60, doi: 10.1016/j.fuel.2012.01.023

[8] Campos-Vega, R., Loarca-Piña, G., Vergara-Castañeda, H.A., and Oomah, B.D. (2015). Spent coffee grounds: A review on current research and prospects. *Trends in Food Science & Technology,* 45(1), 24-36, doi: 10.1016/j.tifs.2015.04.012

[9] Fitriaa, M., Mulyawan, R., Sulhatun, A., Muarif, A., and Bahri, S. (2023). Effect of Solvent and Extraction Time Variation on The Coffee Oil Extraction Results. *Journal of Chemistry & Chemistry Education,* 11(1), 26-30, doi: 10.24815/kcd.v11i1.32550

[10] Romadhon, M., and Prasetyo, D. (2021). The Effectiveness of South Sumatra Coffee (Coffea arabica L.) Extract Cream in Burn Wound Recovery od Male White Mice (Mus musculus). *Jurnal Farmasi Sains dan Komunitas,* 18(1), 49-55, doi: 10.24071/jpsc.003018

[11] Gligor, O., Clichici, S., Moldovan, R., Muntean, D., Vlase, A.M., Nadăș, G.C., Matei, I.A., Filip, G.A., Vlase, L., and Crișan, G. (2023). The Effect of Extraction Methods on Phytochemicals and Biological Activities of Green Coffee Beans Extracts. *Plants,* 12(4), 712, doi: 10.3390.plants12040712

[12] Tinoco-Caicedoa, D.L., Mero-Benavides, M., CórdovaMolin, K., and Blanco-Marigorta, A.M. (2013). Oil Extraction from Spent Coffee Grounds: Experimental Studies and Exergoeconomic Analysis. *Chemical Engineering Transactions, 102,* 295-300, doi: 10.3303/CET23102050

[13] Adriyanti, H., Rizkia, G., Syamsuddin, Y., Satriana, S., and Supardan, M.D. (2023). Effect of microwave drying pretreatment before soxhlet extraction of coffee oil. in *The 4th International Conference on Agriculture and Bio-industry*, doi: 10.1088/1755/1183/1/012066

[14] Pattaraprachyakul, W., Sawangkeaw, R., Ngamprasertsith, S., and Suppavorasatit, I. (2023). Optimization of Coffee Oil Extraction from Defective Beans Using a Supercritical Carbon Dioxide Technique: Its Effect on Volatile Aroma Components. *Foods,* 12(13), 2515, doi: 10.3390/foods12132515

[15] Hibbert, S., Welham, K., and Zein, S.H. (2019). An innovative method of extraction of coffee oil using an advanced microwave system: in comparison with conventional Soxhlet extraction method. *SN Applied Science,* 1, 1467, doi: 10.1007/s42452-019-1457-5

[16] Tsukui, A., Júnior, H.S., Oigman, S., Souza, R.d., Bizzo, H., and., Rezende, C. (2014). Microwave-assisted extraction of green coffee oil and quantification of diterpenes by HPLC. *Food Chemistry*, 1(164), 266-271, doi: 10.106/j.foodchem.2014.05.039

[17] Miladi, M., Martins, A.A., Mata, T.M., Vergara, M., Pérez-Infantes, M., Remmani, R., Ruiz-Canales, A., and Núñez-Gómez, D. (2021). Optimization of Ultrasound-Assisted Extraction of Spent Coffee Grounds Oil Using Response Surface Methodology. *Processes,* 9(11), 2085, doi : 10.3390/pr9112085

[18] Goh, B.H.H., Ong, H.C., Chong, C,T., Chen, W.H., Leong, K.Y., Tan, S.X., and Lee, X.J. (2020). Ultrasonic-assisted oil extraction and biodiesel synthesis of Spent Coffee Ground. *Fuel,* 261, 116121, doi: 10.1016/j.fuel.2019.116121

[19] Mustikaningrum, M., and Johar, N. (2023). Penentuan Difusivitas Beta Karoten dalam Berbagai Pelarut pada Ekstraksi Maserasi Labu Kuning. *Jurnal Integrasi Proses,* 22 - 27

[20] M. Mustikaningrum and P. D. Anjarsari, "Analisis Pengaruh Perbedaan Volume Pelarut Heksana pada Parameter Konstanta Kecepatan Ekstraksi Minyak Kopi Robusta. *Jurnal Surya Teknika*, pp. 896-899, 2023.

[21] Muqorrobin M., and Mustikaningrum, M. (2023). Pengaruh Perbedaan Suhu dan Waktu Terhadap Kinetika Ekstraksi Minyak dengan Metode Ultrasonik pada Ampas Kopi. *Jurnal Integrasi dan Lingkungan*, 1(1), 24-29, doi: 10.30587/jipl.v1i1.6416

[22] Beverly, D., Lopez-Quiroga, E., Farr, Melrose, R.J., Henson, S., Bakalis, S., and Fryer, P.J. (2020). Modeling Mass and Heat Transfer in Multiphase Coffee Aroma Extraction. *Industrial & Engineering Chemistry Research*, 59(24), 11099-11112, doi: 10.1021.acs.iecr.0c01153

[23] Mustikaningrum,M., Arista, D., Nyamiati, R.D., and Nanda, D.E. (2023). Evaluasi Nilai Difusifitas Pelarut dan Konstanta Kecepatan Ekstraksi pada Isolasi Piperin Lada Hitam. *Eksergi,* 47-51,

[24] Zhang, Q.W., Lin L.G., and Ye, Y.C. (2018). Techniques for extraction and isolation of natural products: a comprehensive review. *Chinese Medicine,* 13(20), doi: 10.1186/s13020-018-0177-x

[25] Ningsih, A.W., Sukardiman., Syahrani, A, Charisma A.M., and Wahyuni, K.I. (2022). Study of Drying Methods and Extraction Methods on Phenolic Content. in *The 2nd International Conference on Government Education Management and Tourism*, 1(1)

[26] Kumar, K., Srivastav, S., and Sharanagat, V.S. (2020). Ultrasound-assisted extraction (UAE) of bioactive compounds from fruit and vegetable processing by-products: A review. *Ultrasonic Sonochemistry,*105325, doi: 10.1016/j.ultsonch.2020.105325

[27] Ashokkumar, M. (2015). Applications of ultrasound in food and bioprocessing. *Ultrasonics Sonochemistry, 25,* 17-23, doi: 10.1016/j.ultsonch.2014.08.012

[28] Petigny, L., Périno-Issartier, S., Wajsman, J., and Chemat, F. (2013). Batch and Continuous Ultrasound-Assisted Extraction of Boldo Leaves (Peumus boldus Mol.). *International Journal of Molecular Sciences,* 14(3), 5750-5764,doi:10.3390/ijms14035750

[29] Kulkarni, S.J. (2016). Diffusivity: A Review on Research and Studies with Insight into Affecting Parameters. *International Journal of Science and Healthcare Research,* 1(4), 9-14

[30] Lenart, I., and Ausländer, D. (1980). The effect of ultrasound on diffusion through membranes. *Ultrasonics*, 18(5), 216-218, doi:10.1016/0041-624X(80)90123-7

[31] Chemat, F., Rombaut, N., Meullemiestre, A., Turk, M., Perino, S., Fabiano-Tixier, A.S., and Abert-Vian, M. (2017). Review of Green Food Processing techniques. Preservation, transformation, and extraction. *Innovative Food Science & Emerging Technologies,* 41, 357-377, doi: 10.1016/j.ifset.2017.04.016

[32] Roselló-Soto, E., Koubaa, M., Moubarik, A., Lopes, R.P., Saraiva, J.A., Boussetta, N., Grimm, N., and Barba, F.J. (2015). Emerging opportunities for the effective valorization of wastes and by-products generated during olive oil production process: Non-conventional methods for the recovery of high-added value compounds. *Trends in Food Science & Technology*, 296-310

[33] Mustikaningrum, M., Cahyono, R.B., and Yuliansyah, A.T. (2021). Adsorption of Methylene Blue on Nano-Crystal Cellulose of Oil Palm Trunk: Kinetic and Thermodynamic Studies. *Indonesian Journal of Chemistry*, 22(4), 953 - 964, doi: 10.22146/ijc.72156

[34] Mataa, T.M., Martins A.A., and Caetano, N.S. (2017). Bio-refinery approach for spent coffee grounds valorization. *Bioresource Technology,* 1077-1084, doi: 10.1016/j.biotech.2017.09.106

[35] Stylianou, M., Agapiou, A., Omirou,M., Vyrides, I., Ioannides, I.M., Maratheftis, G., and Fasoula, D. (2018). Converting environmental risks to benefits by using spent coffee grounds (SCG) as a valuable resource. *Environmental Science and Pollution Research,* 25(36), 35776-35790, doi: 10.1007/s11356-01802359-6

[36] Mustikaningrum, M., and Anjarsari, P.D. (2023). Analisis Pengaruh Perbedaan Volume Pelarut Heksana pada Parameter Konstanta Kecepatan Ekstraksi Minyak Kopi Robusta. *Jurnal Surya Teknika*, 24-29

[37] Kumar, K., Srivastav, S., and Sharanagat, V.S. (2021). Ultrasound assisted extraction (UAE) of bioactive compounds from fruit and vegetable processing by-products: A review. *Ultrasonics Sonochemistry*, 70, doi:10.1016/j.ultsonch.2020.105325

CHEESA: Chemical Engineering Research Articles
ISSN 2614-8757 (Print), ISSN 2615-2347 (Online)
Available online at: http://e-journal.unipma.ac.id/index.php/cheesa

Review Article

Nanoparticles and Nanoliposomes for Hair Growth Serum

Nanopartikel dan Nanoliposom untuk Serum Pertumbuhan Rambut

Arif Arismunandar[1)], Lutfi Chabib[1*)], Arba Pramundita Ramadani[1)], Arman Suryani[2)], Ezatul Ezleen Kamarulzaman[3)]

[1)]Universitas Islam Indonesia, Master of Pharmaceutical Sciences, Faculty of Mathematics and Natural Sciences, Sleman, Yogyakarta, 55584, Indonesia
[2)]Universitas Islam Sultan Agung, Pharmacy Study Program, Faculty of Pharmacy, Semarang, Central Java, 50112, Indonesia
[3)]Universiti Sains Malaysia, School of Pharmaceutical Sciences, 11800 USM, Penang, Malaysia

Article History
Submitted: 26th May 2024; Revised: 08th August 2024; Accepted: 15th August 2024; Available online: 28th August 2024; Published Regularly: June 2024

doi: 10.25273/cheesa.v7i1.19908.57-66

*Corresponding Author.
Email: lutfi.chabib@uii.ac.id

Abstract

Solubility in penetrating the follicles is the main obstacle in the formulation of hair growth serum preparation with chemicals derived from natural or synthetic materials. Therefore, a delivery system is needed to deliver more chemical compounds into the follicles. Nanoparticles and nanoliposomes are potential chemical compound delivery systems in hair growth serum. Specifically, nanoparticles with a particle size of less than 200 nm can increase the transport of serum chemical compounds into the scalp. The small particle size makes the interaction between atoms and molecules faster and prevents clumping with the repulsive force of dispersed particles. Meanwhile, nanoliposomes with lipids as encapsulation in the delivery of lipophilic or hydrophilic chemical compounds with nanosizes can significantly increase serum diffusion on the scalp.

Keywords: chemical aggregation; dispersion; nanoliposomes, nanoparticles; serum

Abstrak

Kendala utama formulasi serum dari bahan alam maupun sintesis yang dapat menembus folikel adalah kelarutan. Sistem penghantaran diperlukan untuk menghantarkan senyawa kimia lebih banyak masuk ke dalam folikel. Nanopartikel dan nanoliposom adalah sistem penghantaran senyawa kimia potensial pada serum penumbuh rambut. Sediaan nanopartikel memiliki ukuran partikel kurang dari 200 nm akan meningkatkan transport senyawa kimia serum masuk ke dalam kulit kepala. Ukuran partikel yang kecil menjadikan interaksi antar atom dan molekulnya semakin cepat dan dapat menjaga dari agregasi partikel dengan gaya tolak menolak dari partikel terdispersi sehingga dapat menstabilkan diri. Sediaan nanoliposom yang menjadikan lipid sebagai enkapsulasi pada penghantaran senyawa kimia yang bersifat lipofilik maupun hidrofilik dengan ukuran nano dapat meningkatkan secara signifikan difusi serum pada kulit kepala.

***Kata kunci**: agregasi senyawa kimia; dispersi; nanoliposom; nanopartikel; serum*

1. Introduction

The hair growth serum is a cosmetic formulation with great potential [1]. It is formulated with active substances derived from natural ingredients and has advantages such as minimal side effects, abundant availability, and easy extraction [2]. In serum preparations, solubility in penetrating the scalp is usually the main obstacle [3]. Solubility can be increased with the right formulation to deliver more active substances into the follicles and achieve optimal therapeutic effects [4]. To overcome low solubility, serum preparations should be developed into nanoparticles and nanoliposomes [5–7].

Nanoparticles in serum preparations are made with particle sizes below 200 nm [8] using nanotechnology. Several studies showed that nanoparticles have been successfully developed in cosmetic preparations. Pulit-Prociak et al., stated that nanoparticle preparations are safe to use in cosmetics containing nanosilver and nanogold [9]. ZnO particles measuring 1 to 100 µm can be synthesized by adding a capping agent, a compound that plays a role in preventing clumping to avoid colloid destabilization.

Nanoparticles have been successfully formulated into moisturizing creams [10]. Lee et al., formulated a hair growth nanoparticle serum from *Phellinus linteus*, *Cordyceps militaris*, *Polygonum multiflorum*, *Ficus carica*, and *Cocos nucifera oils* containing 4HGF. Poly-γ-glutamic acid (γ-PGA) combined with 4HGF has semipolar properties, interacting with a slow-release system of target ligands and thereby dispersing more substances [11]. Aside from nanoparticles, to improve the delivery system of active substances, serum can also be formulated into nanoliposomes.

Nanoliposomes are the latest technology for the controlled release of bioactive compounds and increasing the stability of the preparations. The application helps increase the delivery of active substances through lipid membranes to enter skin cells. Several publications mentioned that nanoliposomes have been used for cosmetic preparations. Hydroxylated collagen has nonpolar properties, and is insoluble in water, hence, it is difficult to diffuse into the skin, which is semipolar. To increase dispersion into the skin, hydroxylated collagen is synthesized semipolarly with a liposome system [12]. According to Amnuaikit et al., the formulation of hydroxylated collagen in the form of liposomes in serum form can help increase skin penetration, remove unwanted odors, and mask colors by the appropriate lipid bilayer structure. Hameed et al., explained that sunscreens with inorganic materials such as TiO_2 and ZnO_2 metals are better in nanoliposome preparations. TiO_2 and ZnO_2 have thin layer absorption, are nonpolar, insoluble in water, and serve as catalysts. The development of particles to nanosize, and coating with semipolar substances will increase absorption on the skin [13].

This review discusses the potential of nanoparticles and nanoliposomes in hair growth serum preparations. Nanoparticles and nanoliposomes can significantly increase the penetration of active substances contained in serum into the skin, thereby increasing the therapeutic effect. The development of both technologies will have a major impact on the process of delivering active substances to the target.

2. Research Methods

This review was based on literature studies from Google Scholar, Pubmed, and Scopus. The keywords used were nanoparticles, nanoliposomes, serum, solubility, and compound aggregation. A total of 48 studies that discussed nanoparticles or nanoliposomes were retrieved.

3. Serum Preparation

Serum is a cosmetic product that contains active ingredients with high concentrations to provide intensive nutrition to the skin layer. The nature of the active ingredients can be polar, nonpolar, or semipolar. The difference in the chemical properties will provide a difference in the speed of diffusion into the skin which is semipolar. Polar and nonpolar compounds are more difficult to diffuse into the skin. This is due to the difference in electronegativity between the atoms in the active substance of the serum and the skin barrier [14].

Preparations are widely used in the cosmetic industry, one of which is hair growth serum. Specifically, serum preparations are classified as emulsions that have low viscosity [15]. This nature increases the pressure and speed at which the particles rub against each other, leading to rapid delivery of active substances to the skin surface [16]. Another advantage of serum preparations is the high concentration of active substances. This aims to increase the desired therapeutic effect [17, 18].

The formulation of serum preparations used for hair growth should meet several parameters, including organoleptic, adhesive, and spreading power, as well as pH and viscosity [19]. The organoleptic properties of serum must meet the parameters of clarity and softness [20]. The adhesive power that meets the standards must not exceed four seconds. The spreading power does not have a definite value but is considered acceptable between 5-8 [21]. The pH value that enters the skin preparation is 5.5-7.4, while the viscosity is in the range of 2000-4000 cps [22]. Serum preparations that do not meet all of these parameters have the risk of being uncomfortable to use or achieve therapeutic targets.

Several publications stated that effective serum preparations for hair growth are those derived from natural extracts. According to Nabilla et al., apple juice formulated in serum preparations has been shown to increase hair growth in mice. Apple extract contains procyanidin B-2, which binds to metal and becomes a catalyst to accelerate hair follicle growth [23]. According to Collins et al., the combination of candlenut oil and apple extract is also effective in increasing hair growth. Oleic acid in candlenut oil extracted using semipolar solvents can increase diffusion in the skin [24]. In serum preparations, one major obstacle is the solubility of active substances to diffuse into the skin. This obstacle can be overcome by changing serum into nanoparticles and nanoliposomes [25, 26].

4. Nanoparticles

Nanoparticles are colloidal particles that can deliver chemical compounds specifically. Various nanotechnology-based systems include polymer and magnetic nanoparticles, carbon nanotubes, quantum dots, dendrimers, metal nanoparticles, and liposomes [27]. Each type has different advantages. Polymer nanoparticles have advantages due to the ability to effectively standardize particle size. The target of

polymer nanoparticles is the delivery of chemicals to cells [28]. Meanwhile, magnetic nanoparticles can be used as strong carriers and magnetic hyperthermia agents in response to external magnetic fields. Another advantage is that magnetic nanoparticles can act as resonance imaging agents, which allow precise detection of the target location in chemical delivery [29]. Carbon nanotube nanoparticles function in detecting and distinguishing various analytes based on the chemical properties of the substance [30].

The advantages of quantum dot nanoparticles are immunohistochemical analysis, single molecule tracking, and in vivo imaging compared to traditional methods with organic dyes and fluorescent proteins. The unique spectral properties of these nanoparticles offer the opportunity to design systems for multiplex analysis with multicolor imaging to detect multiple targets simultaneously. Conjugation of chemical molecules to quantum dot nanoparticle-based delivery particles allows for real-time monitoring of chemical tracking [31].

Dendrimer nanoparticles can transport large amounts of chemicals to a specific area [32]. Furthermore, metal nanoparticles have the advantage of increasing the delivery of active substances [33]. Liposomes are one type of nanoparticle that functions as a carrier to release controlled and targeted chemicals without degradation [34]. The systematics of nanoparticles in the active substance delivery system are presented in Figure 1.

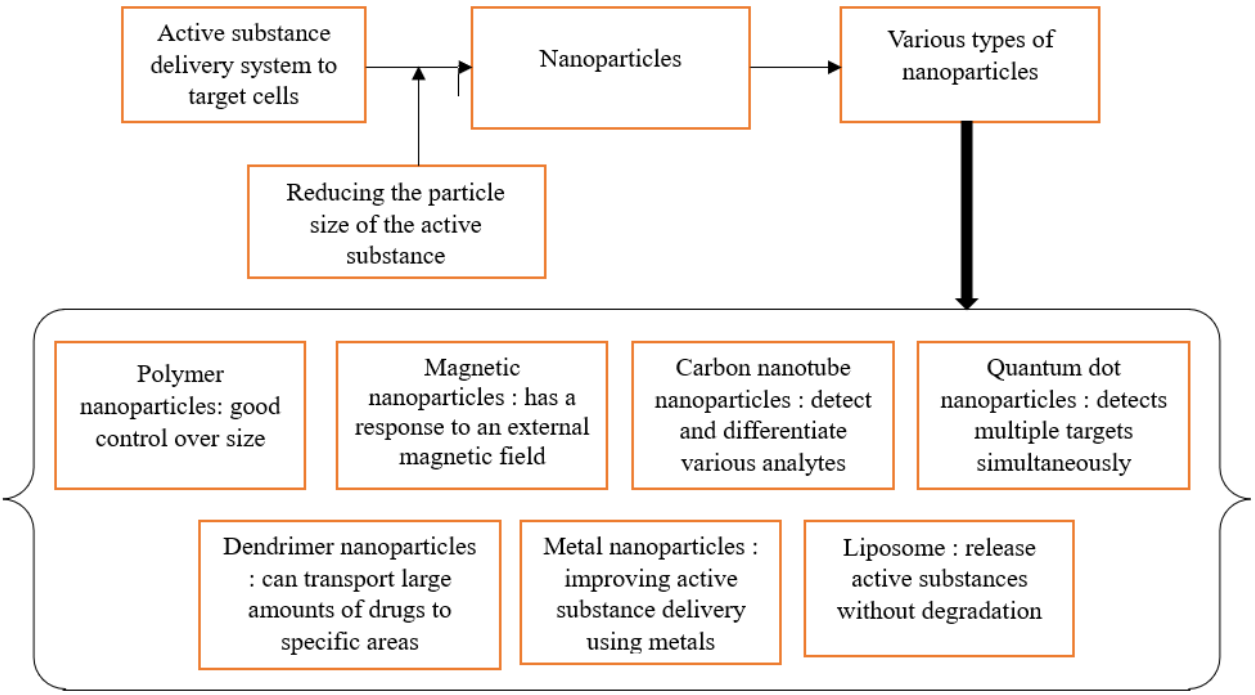

Figure 1. Systematization of Nanoparticle Types in Active Substance Delivery System

5. Nanoliposomes

Nanoliposomes refer to small-sized liposomes and are one of the most frequently examined colloidal delivery systems in food, nutraceutical, drug, and cosmetic studies. This is attributed to the significant capacity to deliver bioactive substances hydrophilically and hydrophobically. Nanoliposomes have been used in several studies and industrial products [35]. The advantages include protecting sensitive chemical compound molecules, stable storage, high loading capacity, increased bioavailability, and sustained release mechanisms. Furthermore, nanoliposomes can deliver lipophilic and hydrophilic materials simultaneously, providing a synergistic effect. Chemical compounds soluble in water and fat can be dispersed into one due to the coating by a lipid barrier [36]. Nanoliposomes are widely formulated for cosmetic preparations.

Several publications mentioned that the use of nanoliposomes for cosmetics can increase the bioavailability of active substances. According to Kocid et al., nanoliposomes successfully increased the levels of active substances in skin care serum derived from soy milk [37]. Saewan et al. added that nanoliposomes increased in vitro and in vivo tests of anti-aging serum from coffee beans [38]. These materials have also been shown to increase the solubility of active substances when applied to serum preparations.

6. Nanoparticles for Hair Growth Serum Preparation

Hair growth serums are widely formulated with nanoparticles technology to achieve the desired target. Several publications on nanoparticles for serum preparations are presented in Table 1.

Table 1. Nanoparticle application for hair growth serum

No	Author	Results	Reference
1	Costa et al., 2021	Three common types of nanoparticles were compared in terms of viability and durability, for example, liposomes, ethosomes, and polymer nanoparticles. Serum enumeration was able to supply, both stable models to more significant follicular areas than nanoparticles.	[39]
2	Tansathien et al., 2021	Niosome serum mucrospicules containing deer antler velvet removal played a basic portion in communicating biomacromolecular protein through the skin and hair follicles, driving practical hair improvement	[40]
3	Takabayashi et al., 2016	The pitiless breadth of the hairs was basically higher after the application of FGF-2&D/P NPs for six months. Objective headways in incline hair were observed in two cases. Nine individuals experienced more significant bounce and hair adaptability	[41]
4	Fernandes et al., 2015	The optimized procedure licenses the course of action of culminating PLA nanoparticles-based points of interest for hair follicle centering. PLA nanoparticles can suitably transport and release lipophilic and hydrophilic compounds into the hair follicles, and the yields obtained are commendable for mechanical purposes.	[42]
5	Kong et al,. 2022	The optimized technique grants the course of action of culminating PLA nanoparticles-based points of interest for hair follicle centering. PLA nanoparticles can reasonably transport and release lipophilic and hydrophilic compounds into the hair follicles, and the yields obtained are commendable for mechanical purposes.	[43]

Table 1 shows that nanoparticles can effectively increase hair growth to overcome alopecia. Through various mechanisms, nanoparticles effectively increase the active serum substances in the follicles, facilitating hair growth. The particle size of the chemical compound is very small and can penetrate the spaces between cells. The ability of nanoparticles to penetrate cell walls is high, both through diffusion and opsonification, as well as the flexibility to be combined. Therefore, nanoparticles are a viable option in the chemical delivery system. The very small particle size enhances rapid delivery of active substances into the follicles through the diffusion system. This preparation does not require significant energy to increase the desired effect.

7. Nanoliposomes for Hair Growth Serum Preparation

Nanoliposomes are nanosized particles coated with a lipid membrane to enhance the transport of more chemicals into the hair follicles. Some publications on nanoliposomes for hair growth serum are presented in Table 2.

Table 2. Nanoliposome application for hair growth serum

No	Author	Results	Reference
1	Tian et al., 2022	Nanoliposomes were stacked with copper peptide, acetyl tetrapeptide-3, and myristoyl pentapeptide-4 (CAM-NLPs) at the same time to achieve a synergistic effect of various bioactive peptides combination for transport efficiency in progressing hair improvement. In rundown, CAM-NLPs are compelling transdermal co-delivery nanocarriers for lessening hair incidents in androgenetic alopecia with hair advancement progression, tall security, and uncommon potential	[44]
2	Zhang et al., 2024	Energized by nanoliposomes and MNs, the exemplified KK-NLPs performed capable skin penetration and moved forward cellular internalization into human dermal papilla cells. Exceptionally, the KK-NLPs-integrated MNs treatment bunch appears basic progressed hair recuperation in vivo, with unclear or predominant accommodating impacts at a much lower estimation than that of minoxidil.	[45]
3	Xu et al., 2018	FGF-2-LIP-SF may be a potential option to prevent hair loss in patients with alopecia areata.	[46]
4	Tanrivedi et al., 2022	Pomegranate peel extract-loaded liposomes were sketched out for hair color security. Organized definitions have an awesome color affirmation on hair strands due to the antioxidant properties of pomegranate peel removal and the film-forming effect of liposomal definitions. Organized liposomal definitions may serve as an incredible elective for lessening coloring repeat and securing hair fibers.	[47]
5	Liu et al., 2024	The nanopreparations had no self-evident skin bothering. The CAR-loaded liposomal definition has potential application for the treatment of AGA.	[48]

Table 2 shows that nanoliposomes can be used to overcome hair loss through serum preparations. Nanoliposomes are effective in delivering chemicals from natural and synthetic materials into hair serum. Furthermore, nanoparticles and nanoliposomes in serum preparations can increase the penetration of chemicals into hair follicles, making both effective for alopecia therapy. The spherical shape of nanoliposomes also makes this preparation easier to diffuse through the intercellular barrier membrane. Chemicals with different levels of polarity when encapsulated in nanoliposomes will have greater solubility. The potential of nanoparticles and nanoliposomes for hair growth serum is presented in Figure 2.

8. Conclusion

In conclusion, nanoparticles and nanoliposomes have great potential to be developed in hair growth serum preparations. Nanoparticles have particle sizes of less than 200 nm which increase the transport of serum chemicals into the scalp. Furthermore, the small particle size makes the interaction between atoms and molecules faster and can prevent clumping with the repulsive force of dispersed particles. Nanoliposomes with lipids as encapsulation in the delivery of nano-sized chemicals can significantly increase serum diffusion on the scalp.

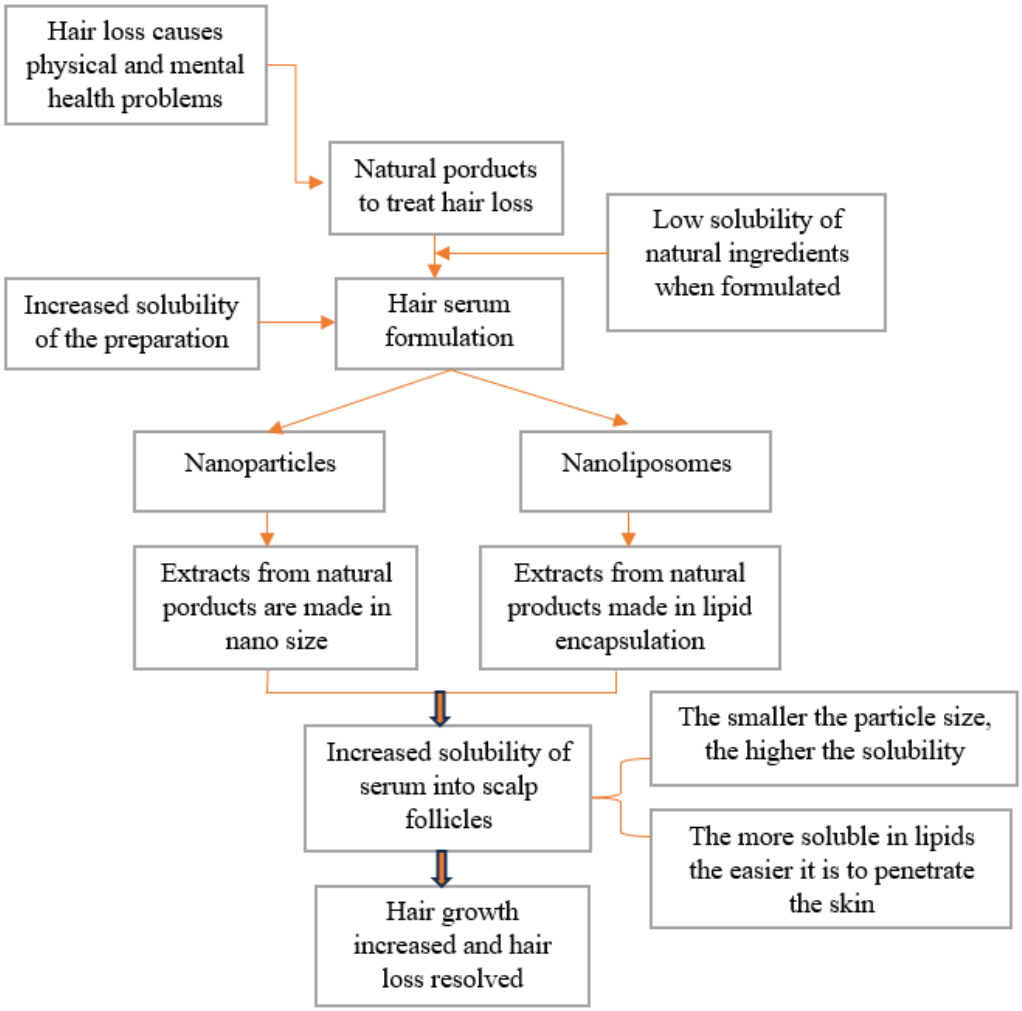

Figure 2. The potential of nanoparticle and nanoliposome preparations for a hair growth serum

References

[1] Majeed, M., Majeed, S., Nagabhushanam, K., Mundkur, L., Neupane, P., & Shah, K. (2020). Clinical study to evaluate the efficacy and safety of a hair serum product in healthy adult male and female volunteers with hair fall. *Clinical, Cosmetic and Investigational Dermatology*, 13, 691–700. doi: 10.2147/CCID.S271013

[2] Bubalo, M. C., Vidović, S., Redovniković, I. R., & Jokić, S. (2018). New perspective in extraction of plant biologically active compounds by green solvents. *Food and Bioproducts Processing*, 109, 52–73. doi: 10.1016/J.FBP.2018.03.001

[3] Vaishampayan, P., & Rane, M. M. (2022). Herbal Nanocosmecuticals: A Review On Cosmeceutical Innovation. *Journal of Cosmetic Dermatology*, 21(11), 5464–5483. doi: 10.1111/JOCD.15238

[4] Patzelt, A., & Lademann, J. (2020). Recent advances in follicular drug delivery of nanoparticles. *Expert Opinion on Drug Delivery*, 17(1), 49–60. doi: 10.1080/17425247.2020.1700226

[5] Alishiri, M., Ebrahimi, S., Shamloo, A., Boroumand, A., & Mofrad, M. R. K. (2021). Drug delivery and adhesion of magnetic nanoparticles coated nanoliposomes and microbubbles to atherosclerotic plaques under magnetic and ultrasound fields. *Engineering Applications of Computational Fluid Mechanics*, 15(1), 1703–1725. doi: 10.1080/19942060.2021.1989042

[6] Eid, K. A. M., & Azzazy, H. M. E. (2014). Sustained broad-spectrum antibacterial effects of nanoliposomes loaded with silver nanoparticles. *Nanomedicine (Lond)*, 9(9), 1301–1310. doi: 10.2217/NNM.13.89

[7] Cheraghi, M., Negahdari, B., Daraee, H., & Eatemadi, A. (2017). Heart Targeted Nanoliposomal/Nanoparticles Drug Delivery: An Updated Review. *Biomedicine & Pharmacotherapy*, 86, 316–323. doi: 10.1016/J.BIOPHA.2016.12.009

[8] Bonifácio, B. V., Silva, D. P. B., Ramos, M. A. D. S., Negri, K. M. S., Bauab, M. T., & Chorilli, M. (2013). Nanotechnology-based drug delivery systems and herbal medicines: A Review. *International Journal of Nanomedicine*, 9(1), 1–15. doi: 10.2147/IJN.S52634

[9] Pulit-Prociak, J., Grabowska, A., Chwastowski, J., Majka, T. M., & Banach, M. (2019). Safety of the application of nanosilver and nanogold in topical cosmetic preparations. *Colloids and Surfaces B: Biointerfaces*, 183, 110416. doi: 10.1016/J.COLSURFB.2019.110416

[10] Mondéjar-López, M., López-Jiménez, A. J., Abad-Jordá, M., Rubio-Moraga, A., Ahrazem, O., Gómez-Gómez, L., & Niza, E. (2021). Biogenic Silver Nanoparticles From Iris Tuberosa As Potential Preservative In Cosmetic Products. *Molecules*, 26(15), 1–12. doi: 10.3390/Molecules26154696

[11] Lee, H. J., Kwon, H. K., Kim, H. S., Kim, M. Il, & Park, H. J. (2019). Hair Growth Promoting Effect Of 4HGF Encapsulated With PGA Nanoparticles (PGA-4HGF) by B-Catenin Activation and its Related Cell Cycle Molecules. *International Journal of Molecular Sciences*, 20(14). doi: 10.3390/Ijms20143447

[12] Amnuaikit, T., Rajagopal, R. S., Nilsuwan, K., & Benjakul, S. (2024). Enhancement of physical appearance, skin permeation, and odor reduction using liposome of hydrolyzed salmon collagen for cosmetic products. *Scientifica*, 2024, 7843660, 14 pages

[13] Rehman, F. U. (2019). Scope of nanotechnology in cosmetics: dermatology and skin care products. *J. Med. Chem. Sci.*, (September 2018). doi: 10.26655/Jmchemsci.2019.6.2

[14] Randad, M., Shrinivas, S., & Bachelor, H. L. D. (2022). Preparation and evaluation of hair serum. *International Journal of Advances in Engineering and Management*, 4(6), 2389.

[15] Hidayah, H., Kusumawati, A. H., Sahevtiyani, S., & Amal, S. (2021). Literature review article: aktivitas antioksidan formulasi serum wajah dari berbagai tanaman. *Journal of Pharmacopolium*, 4(2), 75–80.

[16] Sawiji, R. T., Rumbory, S., Pramita, D. A., Cahyaningrum, W., Fanny, N. P., Dewi, S., … Mahaganesha, F. (2024). Pengaruh variasi konsentrasi gelling agent (xanthan gum dan carbopol) pada sediaan serum dengan bahan aktif retinoic acid. *Acta Holistica Pharmaciana*, 6(1), 1–10. doi: 10.62857/AHP.V6I1.157

[17] Hermawan, A. V., & Susanti, A. (2022). Serum kulit manggis dan beras putih sebagai antiaging dan brightening. *Garina*, 14(1), 43–60. Retrieved from https://garina.org/index.php/journal/article/view/57

[18] Satrianingrum, A., Sari, G. K., & Pistanty, M. A. (2023). Serum Antibacterial Activity Test of Chinese Betel Extract (Peperomia Pellucida) Against Staphylococcus Aureus Bacteria. *Pratama Medika : Jurnal Kesehatan*, 2(1), 66–82. doi: 10.56480/PRATAMAMEDIKA.V2I1.938

[19] Baptista, S., Pereira, J. R., Guerreiro, B. M., Baptista, F., Silva, J. C., & Freitas, F. (2023). Cosmetic emulsion based on the fucose-rich polysaccharide fucopol: bioactive properties and sensorial evaluation. *Colloids and Surfaces B: Biointerfaces*, 225, 113252. doi: 10.1016/J.COLSURFB.2023.113252

[20] Syarifah, A., Budiman, A., & Nazilah, S. A. (2021). Formulation And Antioxidant Activity Of Serum Gel Of Ethyl Acetate Fraction From Musa X Paradisiaca L. *Proceedings of The 4th International Conference On Sustainable Innovation 2020–Health Science and Nursing (Icosihsn 2020)*, 33, 310–315. doi: 10.2991/AHSR.K.210115.066

[21] Wijianto, B., & Pratiwi, L. (2024). Serum of extract onchidium typhae uses hydroxyethyl cellulose and carboxymethyl cellulose natrium base as antioxidant. *Medical Sains : Jurnal Ilmiah Kefarmasian*, 9(1), 363–372. doi: 10.37874/MS.V9I1.1113

[22] Article, O., Noralita, K., Gumilar, B., Yuliani, H., & Dwiastuti, R. (2023). Optimization and physical characterization of quercetin nanoemulgel formula as an antibacterial agent. *International Journal of Applied Pharmaceutics*. doi: 10.22159/Ijap.2023v15i1.46737

[23] Nabilla, C. N., Andriyanto, & Subangkit, M. (2024). View of efek potensial sari buah apel (malus domestica) sebagai penumbuh rambut pada tikus (Rattus Norvegicus). *Jurnal Veteriner dan Biomedis*. 2(1), 29-34. doi: 10.29244/jvetbiomed.2.1.29-34.

[24] Collins, E., Rollando, & Monica, E. (2023). View Of Pembuatan Serum Penumbuh Rambut Kombinasi Minyak Kemiri (Aleurites Moluccanus) Dan Ekstrak Buah Apel (Pyrus Malus L.). *Jurnal Farmasi Ma Chung: Sains Teknologi Dan Klinis Komunitas*. 1(1), 32-41. doi: 10.33479/jfmc.v1i(1).6

[25] Dahiya, M., & Dureja, H. (2018). Recent developments in the formulation of nanoliposomal delivery systems. *Current Nanomaterials*, 3(2), 62–74. doi: 10.2174/2405461503666180821093033

[26] Stark, W. J., Stoessel, P. R., Wohlleben, W., & Hafner, A. (2015). Industrial Applications Of Nanoparticles. *Chemical Society Reviews*, 44(16), 5793–5805. doi: 10.1039/C4CS00362D

[27] Bhatia, S. (2016). Nanoparticles types, classification, characterization, fabrication methods and drug delivery applications. *Natural Polymer Drug Delivery Systems*, 33–93. doi: 10.1007/978-3-319-41129-3_2

[28] Hickey, J. W., Santos, J. L., Williford, J. M., & Mao, H. Q. (2015). Control Of Polymeric Nanoparticle Size To Improve Therapeutic Delivery. *Journal of Controlled Release*, 219, 536–547. doi: 10.1016/J.JCONREL.2015.10.006

[29] Schneider-Futschik, E. K., & Reyes-Ortega, F. (2021). Advantages And Disadvantages Of Using Magnetic Nanoparticles For The Treatment Of Complicated Ocular Disorders. *Pharmaceutics*, 13(8), 1–16. doi: 10.3390/Pharmaceutics13081157

[30] Alim, S., Vejayan, J., Yusoff, M. M., & Kafi, A. K. M. (2018). Recent uses of carbon nanotubes & gold nanoparticles in electrochemistry with application in biosensing: A Review. *Biosensors and Bioelectronics*, 121, 125–136. doi: 10.1016/J.BIOS.2018.08.051

[31] Bilan, R., Nabiev, I., & Sukhanova, A. (2016). Quantum dot-based nanotools for bioimaging, diagnostics, and drug delivery. *Chembiochem*, 17(22), 2103–2114. doi: 10.1002/CBIC.201600357

[32] Carvalho, M. R., Reis, R. L., & Oliveira, J. M. (2020). Dendrimer nanoparticles for colorectal cancer applications. *Journal of Materials Chemistry B*, 8(6), 1128–1138. doi: 10.1039/C9tb02289a

[33] Jamkhande, P. G., Ghule, N. W., Bamer, A. H., & Kalaskar, M. G. (2019). Metal nanoparticles synthesis: an overview on methods of preparation, advantages and disadvantages, and applications. *Journal of Drug Delivery Science and Technology*, 53, 101174. doi: 10.1016/J.JDDST.2019.101174

[34] Miere, F., Fritea, L., Cavalu, S., & Vicaș, S. I. (2020). Formulation, characterization, and advantages of using liposomes in multiple therapies. *Pharmacophore*, 11(3–2020), 1–12. Retrieved from https://pharmacophorejournal.com/article/formulation-characterization-and-

advantages-of-using-liposomes-in-multiple-therapies?html

[35] Demirci, M., Caglar, M. Y., Cakir, B., & Gülseren, I. (2017). Encapsulation By Nanoliposomes. *Nanoencapsulation Technologies for the Food and Nutraceutical Industries*, 74–113. doi: 10.1016/B978-0-12-809436-5.00003-3

[36] Khorasani, S., Danaei, M., & Mozafari, M. R. (2018). Nanoliposome technology for the food and nutraceutical industries. *Trends In Food Science & Technology*, 79, 106–115. doi: 10.1016/J.TIFS.2018.07.009

[37] Kocic, H., Stankovic, M., Tirant, M., Lotti, T., & Arsic, I. (2020). Favorable effect of creams with skimmed donkey milk encapsulated in nanoliposomes on skin physiology. *Dermatologic Therapy*, 33(4), E13511. doi: 10.1111/DTH.13511

[38] Saewan, N., Jimtaisong, A., Panyachariwat, N., & Chaiwut, P. (2023). In Vitro and In Vivo Anti-Aging Effect of Coffee Berry Nanoliposomes. *Molecules*, 28(19). doi: 10.3390/Molecules28196830

[39] Costa, C., Fernandes, B., Guimarães, D., Nogueira, E., Martins, M., Matamá, T., & Cavaco-Paulo, A. (2021). Comparing the delivery to the hair bulb of two fluorescent molecules of distinct hydrophilicities by different nanoparticles and a serum formulation. *International Journal of Pharmaceutics*, 602, 120653. doi: 10.1016/J.IJPHARM.2021.120653

[40] Tansathien, K., Chareanputtakhun, P., Ngawhirunpat, T., Opanasopit, P., & Rangsimawong, W. (2021). Hair growth promoting effect of bioactive extract from deer antler velvet-loaded niosomes and microspicules serum. *International Journal Of Pharmaceutics*, 597, 120352. doi: 10.1016/J.IJPHARM.2021.120352

[41] Takabayashi, Y., Nambu, M., Ishihara, M., Kuwabara, M., Fukuda, K., Nakamura, S., … Kiyosawa, T. (2016). Enhanced effect of fibroblast growth factor-2-containing dalteparin/protamine nanoparticles on hair growth. *Clinical, Cosmetic and Investigational Dermatology*, 9, 127–134. doi: 10.2147/CCID.S108187

[42] Fernandes, B., Silva, R., Ribeiro, A., Matamá, T., Gomes, A. C., & Cavaco-Paulo, A. M. (2015). Improved Poly (D,L-Lactide) Nanoparticles-Based Formulation For Hair Follicle Targeting. *International Journal of Cosmetic Science*, 37(3), 282–290. doi: 10.1111/ICS.12197

[43] Kong, J., Qiang, W., Jiang, J., Hu, X., Chen, Y., Guo, Y. X., … Li, H. (2022). Safflower Oil Body Nanoparticles Deliver HFGF10 To Hair Follicles And Reduce Microinflammation To Accelerate Hair Regeneration in Androgenetic Alopecia. *International Journal of Pharmaceutics*, 616, 121537. doi: 10.1016/J.IJPHARM.2022.121537

[44] Tian, L. W., Luo, D., Chen, D., Zhou, H., Zhang, X. C., Yang, X. L., … Liu, W. (2022). Co-Delivery Of Bioactive Peptides By Nanoliposomes For Promotion of Hair Growth. *Journal of Drug Delivery Science and Technology*, 72, 103381. doi: 10.1016/J.JDDST.2022.103381

[45] Zhang, S., Zhou, H., Chen, X., Zhu, S., Chen, D., Luo, D., … Liu, W. (2024). Microneedle delivery platform integrated with codelivery nanoliposomes for effective and safe androgenetic alopecia treatment. *ACS Applied Materials and Interfaces*, 16(13), 15701–15717. doi: https://doi.org/10.1021/acsami.3c16608

[46] Xu, H. L., Chen, P. P., Wang, L. Fen, Xue, W., & Fu, T. L. (2018). Hair Regenerative Effect Of Silk Fibroin Hydrogel With Incorporation Of FGF-2-Liposome And Its Potential Mechanism In Mice With Testosterone-Induced Alopecia Areata. *Journal of Drug Delivery Science And Technology*, 48, 128–136. doi: 10.1016/J.JDDST.2018.09.006

[47] Tanriverdi, T. S., Gokce, E. H., Filiz, S. B., Kose, F. A., & Ozer, O. (2022). Protection Of Hair Color With Pomegranate Peel Extract-Loaded Liposomal Formulation: Preparation, Characterization, And Ex-Vivo Activity Studies. *Journal of Cosmetic Dermatology*, 21(11), 6292–6301. doi: 10.1111/JOCD.15254

[48] Liu, Z., He, Z., Ai, X., Guo, T., & Feng, N. (2024). Cardamonin-Loaded Liposomal Formulation For Improving Percutaneous Penetration And Follicular Delivery For Androgenetic Alopecia. *Drug Delivery and Translational Research*, 1–17. doi: 10.1007/S13346-024-01519-8/METRICS

Kampus 3 Universitas PGRI Madiun
Jl. Auri No 14-16 Kota Madiun
cheesa@unipma.ac.id

9 772614 875008